Title
A PROPOSAL FOR OBSERVATION AND STOUT OF COHERENT ELECTRON/LASER INTERACTIONS IN SOLIDS

Author
Schmieder, Robert W.

Publication Date
1971-09-01

LBL-252

A PROPOSAL FOR OBSERVATION AND STUDY OF COHERENT ELECTRON/LASER INTERACTIONS IN SOLIDS

Robert W. Schmieder

September 1971

AEC Contract No. W-7405-eng-48

LBL-252

DISCLAIMER

A Proposal for Observation and Study of

COHERENT ELECTRON/LASER INTERACTIONS IN SOLIDS

Robert W. Schmieder

September 1971

Department of Physics
University of California

and

Lawrence Berkeley Laboratory
Berkeley, California 94720

ABSTRACT

Experimental work is proposed for investigating the interactions between overlapping electron and laser beams, and a crystalline solid. The work is motivated by very recent experimental and theoretical investigations that indicate that it is feasible, and that new effects are expected that may lead to a variety of new and useful experiments and measurements, some with possible technological application. The experimental technique proposed is interferometry--observation of low frequency beats in the electron beam when modulated by two laser frequencies.

The elementary theory of laser modulation of electrons is summarized. The general three-field interaction (electrons + photons + solid) is replaced by a one electron theory in which the solid and the laser photons are described semiclassically. Perturbation theory is used to solve the Hamiltonian equation of motion for the modulated electron waves. Expectation values of various observables are discussed, and the modulation of these values by the laser displayed. The modulated wavefunction is interpreted physically, and some simple results of calculations of specific effects are presented. Finally, the whole theory is criticized, and indication is given of how to improve and extend it.

The impossibility of detecting first-order modulation with a linear detector is noted, and it is shown that second-order processes lead to observable effects. The theory of such processes is developed, and simple formulae describing the expected signals are obtained. The unique features of laser-modulated electron interferometers are discussed.

Proposed techniques for observing laser modulation of electrons are described. These include measurement of electron density (called interferometry), current (modification of diffraction patterns), momentum and energy analysis, coherent excitation, and modifications of the laser beam or solid. It is concluded that at present, interferometry offers the best hope for success.

The experimental problems are investigated in detail, and possible techniques are suggested for solving them. The most serious need is for a highly monoenergetic electron beam. It is suggested that a Bragg doublet, consisting of two compensating diffracting crystals, will considerably weaken the stringent requirement on velocity resolution. Some electron sources and detectors, including a Josephson junction, are discussed and evaluated. Processes occurring in crystalline (thin film) target, such as heating and charging are examined, and criteria for selecting thickness, material, etc. are presented, as well as techniques for fabrication and coupling the laser beam into a thin film. The properties of the laser and optical system, the high vacuum system, the mechanical system and electronics of relevance to this work are discussed. For example, piezoelectric transducers and freezable metal seals are suggested for transmitting motion in the vacuum. Some concepts for the overall apparatus are presented, but the engineering design is left to further study.

A plan for a sequence of measurements and experiments is presented. This calls first for evaluating the performance of the apparatus and observing the usual two-field effects (electron diffraction, electron energy loss, etc.). Next, the interferometer fringes would be observed and their dependence on the controllable experimental parameters determined. Further study would lead to quantitative models for specific effects. A variety of high precision measurements would then be possible, including measurements of length, velocity, time delay, etc. Finally, the application of these techniques to measurements of the Aharanov-Bohm Effect and the gravitational force on elementary particles is indicated.

Finally, other research that could be performed using the same apparatus is described. These include coherent and incoherent phonon generation, energy loss spectroscopy, channelling, surface phenomena, nonequilibrium bulk effects, nonlinear optics, particle evaporation, and intense-field electrodynamics.

Table of Contents

List of Tables

List of Figures

List of Symbols

Symbol	Meaning	Page Defined
$\vec{A}(\vec{r},t)$	Vector potential of laser beam	8
$\delta\vec{A}(\vec{r},t)$	Modification of $\vec{A}(\vec{r},t)$ due to presence of $U(\vec{r})$	11
c	Speed of light	11
d	Crystal lattice spacing	9
D	Thin film thickness	9
E_0	Incident electron energy	9
$\vec{\mathcal{E}}$	Electric field of the light	24
$f_n(\vec{p},\vec{q})$ $g_n(\vec{p},K,\vec{q})$	Scattering factors	14
$\vec{G},\vec{H}$	Crystal momentum vectors	20,27
g	Gravitational acceleration	125
	Achromatism factor	66
H	Total semiclassical nonrelativistic single electron Hamiltonian	11
$\mathbf{H}$	Total system Hamiltonian	7
H_0	Kinetic energy operator for free electrons	11
i	$\sqrt{-1}$	
$\vec{j}_e$	Electron probability current density	16
$\vec{K}_0$	Incident electron propagation vector	14
$\vec{k}$	Laser propagation vector	20
$\vec{K}_n,\vec{K}_{nm}$	Modulated electron propagation vectors	14
$\vec{L}$	Vector separation of modulators in an interferometer	34
ΔL	Fringe peak-to-peak separation	42
m	Electron mass	11
$\vec{p}$	Electron momentum (operator)	11
$\langle Q \rangle$	Spacial average of Q	15
$\overline{Q}$	Temporal average of Q	15
$\vec{r}$	Observation point	11,34
$\vec{R}$	Vector from midpoint between modulators to observation point	34

Symbol	Meaning	Page Defined
$U(\vec{r})$	Electrostatic potential of solid (thin crystal)	8
$\delta U(\vec{r},t)$	Modification of $U(\vec{r})$ due to presence of $\vec{A}(\vec{r},t)$	11
$V(\vec{r},t)$	External field effect operators	11
$\vec{v}$	Electron velocity	16
$\vec{x}$	Position vector	14
β	Ratio v/c	18
$\delta,\delta_{\pm},\delta_0$	Scattering phase shift	17
ε	Ratio $\hbar\omega/E_0$	17
$\in$	Dielectric constant of the film modulator	23
θ	Diffraction angle	50
λ	Laser wavelength	9
λ_e	de Broglie wavelength of the electrons	9
Λ_1, Λ_2	Modulation wavelengths	18
ρ_e	Electron density	9
ρ_L	Laser photon density	9
ρ_S	Atom density in crystal	9
σ	Thomson coefficient	74
	Stefan-Boltzmann constant	85
	Effective collision cross section	95
ϕ_n	Phase of laser mode of frequency ω_n	13
Φ,Φ_{nm}	Interferometer phase	37
ψ	Electron wavefunction	11
Ψ	System wavefunction	7
ω,ω_n	Laser frequency	9
Ω_0	de Broglie frequency of incident electrons	14
Ω_n,Ω_{nm}	Modulated de Broglie frequencies	14

I. INTRODUCTION

Considerable interest and controversy has arisen from a 1969 experiment by Schwarz and Hora which seems to indicate that an electron beam can be coherently modulated by a laser beam using a solid material as a coupler, and that such modulation can be appreciable. The interest in this effect stems from the possibility of performing new experiments and measurements, and of constructing practical devices for information processing and communication. The controversy has developed from the apparent inadequacy of known theoretical models to account for the reported magnitude of the effect, the absence of further experimental results, and the failure of others to reproduce the original experiment. The author would like to contend that: 1) the modulation effects exist and can be appreciable; 2) a proposed new technique (interferometry) is probably the best way to observe the modulation; 3) once observed, the modulation effects may make possible a wide variety of new experiments and precision measurements. The bulk of this proposal is devoted to supporting these contentions.

The original experiment of Schwarz and Hora [I.2-8], diagrammed in Fig. 1, was conducted in three steps: 1) a beam of electrons was passed through a thin crystalline film, producing a normal Laue diffraction pattern which could be seen with the aid of a fluorescent screen; 2) the fluorescent screen was replaced with a non-fluorescent one, thus rendering the diffraction pattern invisible; 3) a high-power laser beam was focused on the edge of the film, with the reported result that light of the same color as the laser was radiated from the regions where the electrons struck the (non-fluorescent) screen. It was also reported that no radiation was observed without the laser or the film, or when the laser polarization was perpendicular to the electron velocity, that a nearby magnet

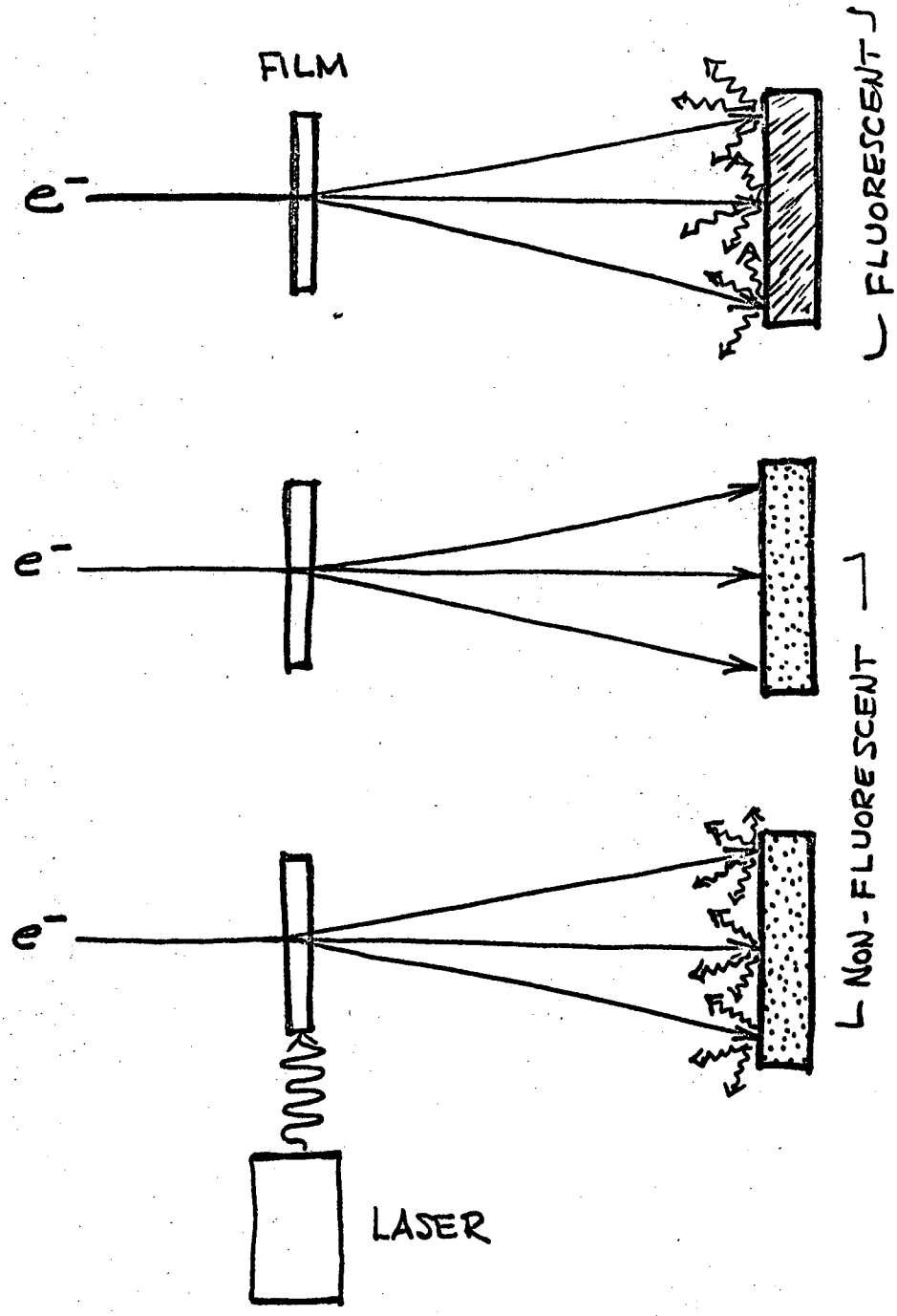

Fig. 1. Experimental observations reported by Schwarz and Hora. The first two steps are normal, but the third was new and is called the Schwarz-Hora Effect. This observation has not been repeated, and may have been spurious.

would move the radiating regions presumably as the electrons were deflected, and that the radiated intensity was dependent upon the distance from the film to the screen. Some numerical parameters of the experiment are listed in Table 1.

Table 1. Parameters of the Schwarz-Hora Experiment

Electron Beam	Energy	50 keV
	Current	$\sim$ 1 μamp
	Focus	$\sim$ 1 micron dia
Laser	Type	argon ion
	Wavelength	4880 Å ($\hbar\omega$ = 2.54 eV)
	Power	10 watts
	Power density (in film)	$\sim 10^7$ watts/cm^2
	Focus	$\sim$ 10-100 micron dia.
Crystalline Film	Material	SiO_2, Al_2O_3, SiF_2
	Thickness	600 - 2000 Å
Screens	Distance (from film)	10-35 cm
	Material	ZnS (fluor.)
		Al_2O_3 (non-fluor.)
Recording	Polaroid film	ASA 3000
	Camera	f/9 at (1/25 - 1/4) sec

The original experiment can be divided into two parts: 1) what happens at the modulating film; 2) what happens at the screen. Numerous authors [I.9-29] have studied both aspects of the experiment. Regarding the former, there is general agreement that a variety of possible mechanisms exists for producing

appreciable coherent modulation of the electrons, although the relative importance of these mechanisms cannot necessarily be determined from the theory. Regarding the latter, several mechanisms by which the electron beam can produce optical photons have been considered, but none has been able to account for more than a small fraction of the reported radiated coherent power. Furthermore, these mechanisms predict certain behavior in contradiction with the original reported observations (e.g. dependence of radiated power on electron current squared vs electron current). These considerations, and the fact that attempts to reproduce the experiment have failed [I.30], may indicate that the original observations of the non-fluorescent screen were spurious. The modulation process remains unchallenged, however, and is generally assumed to occur. This proposal concerns itself exclusively with the modulation; the re-radiation mechanism is considered merely an insensitive means of observing it.

In a broader sense, this proposal seeks to investigate the general three-field interactions between electrons, photons, and solids. The three two-field interactions, when one of the three is absent, have been extensively studied, and each is a subject of great interest: The (electron + solid) interaction leads to electron diffraction, energy loss spectroscopy, tunnelling, secondary emission, etc.; the (photon + solid) interactions produce nonlinear optics, self-induced transparency, etc.; and the (electron + photon) interaction is studied under the title of Intense Field Electrodynamics. When all three fields are present, new effects are expected; they are the main objects of this proposal.

It might be argued that the expected three-field effects would be unobservably small. However, several facts militate against this objection: 1) Both electrons and photons interact strongly with the solid, hence we might expect the solid to couple the electrons and photons to produce effects larger

than the direct electron + photon interaction; 2) Certain three-field effects are predicted to generate experimental signals that can be detected with high sensitivity in the presence of considerable background; 3) Some reasonable models have been suggested that predict certain effects to be of reasonable magnitude for performing experiments.

Our present knowledge of these effects is almost totally theoretical, probably because they lie at or just beyond the capability of existing apparatus. They do not, however, lie beyond existing technology, and with reasonable care, apparatus easily capable of observing the predicted effects can be constructed. Furthermore, there is great impetus for doing so, since many of the effects involve properties of the solid and cannot be accurately computed. There is almost universal agreement that more experimental data is needed to understand the various processes.

The author proposes to build an apparatus capable of observing the predicted effects, and then use it to study the (electron + photon + solid) interaction. The apparatus would consist of an extremely high resolution electron spectrometer, a high power laser, appropriate thin film crystalline targets, and peripheral equipment necessary to provide high vacuum, mechanical motion, single-electron detection, and pulse counting. The initial experiments would attempt to detect the modulation by observing certain predicted interference effects, and determine its dependence upon such parameters as laser power and polarization, electron energy, observation distance and angle, etc. Once the interaction is understood, a variety of new and interesting precision fundamental experiments will be possible.

This proposal is organized in an essentially chronological manner:
1) The present theory of electron modulation by laser + solid is reviewed, and

some specific effects are discussed in detail; 2) The theory of second-order interference effects is discussed; 3) Possible observation techniques are examined, and it is concluded that interferometry offers the most sensitive detection technique at present; 4) The experimental difficulties are examined, and possible techniques for overcoming them are proposed. Basic apparatus configurations are proposed, and general performance data are specified; 5) A sequence of testing, measurements, and experimentation is proposed. In addition, certain second-generation experiments that could be performed (if the effects are large enough) are described, and the large number of two-field experiments that can be performed with this apparatus (if the effects are too small) is indicated.

II. THEORY OF THE MODULATION

A. GENERAL QUANTUM MECHANICAL THEORY

The general system we wish to examine consists of three mutually interacting fields: electrons (e), laser photons (L), and a solid (S). This system presumably can be represented by a wavefunction Ψ which obeys the equation of motion

$$i\hbar \frac{\partial \Psi}{\partial t} = \mathbf{H}\Psi \quad , \tag{1}$$

where the Hamiltonian is

$$\mathbf{H} = H_e + H_L + H_S + H_{eL} + H_{eS} + H_{LS} + H_{eLS} \quad . \tag{2}$$

This hamiltonian, which is represented in Fig. 2, contains terms (H_e, H_L, H_S) which propagate the individual fields forward in time in the absence of the other fields, terms (H_{eL}, H_{eS}, H_{LS}) which represent two-field interactions, and a term (H_{eLS}) representing the true three-field contact interaction.

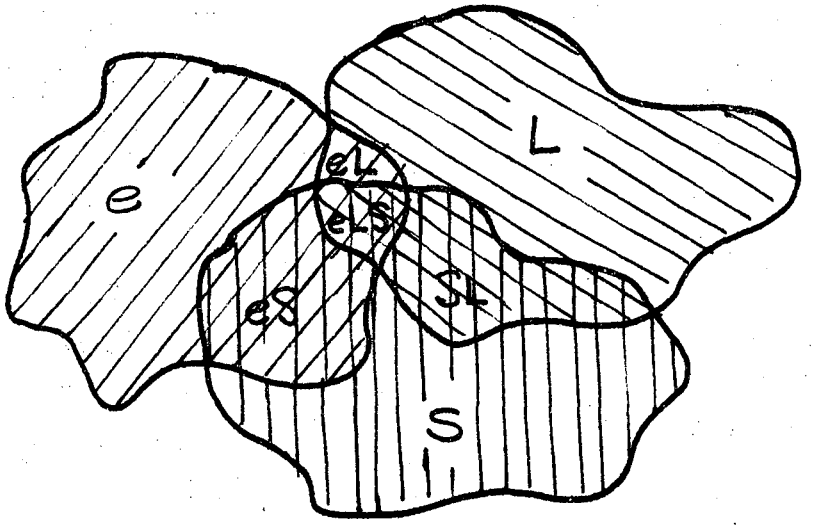

Fig. 2. Diagram of the interactions between electrons (e), laser photons (L), and a solid (S). The (eS) and (SL) interactions together produce an effective (eL) interaction that may be stronger than the direct (eL) interaction. The true triple interaction (eLS) is unknown.

Under the influence of $\mathcal{H}$, the system Ψ evolves in a complicated (but predictable) manner. In particular, energy may be exchanged between the three components (e, L, S), giving rise to observable processes such as inelastic electron scattering, photon absorption, phonon and plasmon generation, etc. Transitions $\Psi \rightarrow \Psi'$ are also possible in which no energy is exchanged; such transitions produce effects like ordinary (kinematic) electron diffraction, reflection and refraction of light, polarization of the solid, etc. In addition to the true three-field interaction H_{eLS}, psuedo-three-field terms will arise in perturbation theory, such as the second-order cross terms involving $(H_{eS})(H_{LS})$ in which the solid acts as a coupler between the electron and laser fields. This kind of interaction can be expected to lead to modifications of electron diffraction patterns and energy loss spectra due to the presence of the laser field.

No attempts have yet been made to solve Eq. (1) for Ψ. The problem is complicated by the fact that, in addition to one or a few electrons, perhaps 10^{20} atoms and 10^{10} photons are present. Hence a many-body or semiclassical theory must be invoked. The complications of dynamic electron diffraction theory, excitations of the solid state, finite beam size, channelling, and optical polarization of the solid cannot be avoided. These difficulties will have to be faced when experimental data becomes available.

B. SEMICLASSICAL SINGLE ELECTRON THEORY

Confronted with the difficulties of solving the general three-field problem, we seek some simpler theory that will allow us to make some predictions. One sensible step is to represent the solid field by a classical electrostatic potential $U(\vec{r})$, and the laser field by a classical (time-dependent) vector potential $\vec{A}(\vec{r},t)$. This will mean that the solid cannot exchange energy with either the electrons or the laser.

A more important simplification results if we treat the electrons as interacting singly with external fields. We thus assume a single electron is described by a wavefunction ψ which evolves under the control of some semiclassical external-field effective hamiltonian, to be specified in Sec. II D. Thus, we will deal with "electron modulation", ignoring transformations of the solid and laser beam.

There is considerable justification for concentrating our attention on the electrons. Table 2 lists some lengths, densities, and energies typical of these experiments. It is clear that the electrons have small size, small density, and high energy, compared with the crystalline solid and laser photons. They are therefore the "odd" component in the system.

Table 2. Typical Ranges of Experimental Parameters

	Lengths (cm)	
de Broglie wavelength	λ_e	10^{-10} - 10^{-8}
laser wavelength	λ	10^{-5} - 10^{-4}
crystal lattice	d	10^{-8} - 10^{-7}
crystal thickness	D	10^{-5} - 10^{-4}
observation distance	r	1 - 10
	Densities (cm^{-3})	
Electrons	ρ_e	1 - 10^3
Photons	ρ_L	10^{10} - 10^{16}
Atoms	ρ_S	10^{20} - 10^{22}
	Energies (eV)	
Electrons	E_0	10^3 - 10^5
Photons	$\hbar\omega$	1 - 10
Solid		
Phonons		10^{-3} - 10^{-1}
Electronic excit.		10^{-1} - 10
Plasmons, interband trans.		1 - 10

It is also of interest to consider the dimensionless numbers of the form (density) × (length)^3 which are a measure of the total number of particles present in a unit particle volume. From Table 2, we find $\rho_e \lambda_e^3 = 10^{-30} - 10^{-21}$, $\rho\lambda^3 = 10^{-5} - 10^{4}$, $\rho_s d^3 = 10^{-4} - 10$, which shows even more dramatically why the electrons can be considered the "test particles" in these experiments.

C. EXPERIMENTAL CONDITIONS

Because of the variety of experiments that could be performed, certain experimental conditions must be specified before carrying through a theoretical analysis. Some of these choices are arbitrary, others are necessary for theoretical approximations. In Table 3 are listed some of the possible conditions; those generally assumed in this proposal are underlined.

Table 3. Experimental Conditions Assumed in Theory

Electron Beam
Energy (nonrelativistic, relativistic)
Energy distribution (monoenergetic, gaussian)
Charge (e^-, e^+)
Beam Profile (plane wave, narrow pencil, focus)
Laser
Spectrum (monochromatic, polychromatic, continuous)
Polarization (linear, circular, elliptical)
Intensity distribution (plane wave, narrow pencil, focus)
Time dependence (CW, pulsed)
Wave type (travelling, standing)
Solid
Structure (crystalline, polycrystalline, amorphous)
Chemical composition (homoatomic, polyatomic)
Lattice type (cubic, other)
Dielectric constant (insulator, conductor)
Surface (perfect, graded, irregular)
Orientations
Electron motion/Laser polarization (parallel, perpendicular)
Electron motion/Laser propagation (parallel, perpendicular)
Laser propagation/Solid surface (parallel, perpendicular)

D. THE SEMICLASSICAL HAMILTONIAN

We assume that the electron is described by a wavefunction ψ satisfying the equation of motion

$$i\hbar \frac{\partial \psi}{\partial t} = H\psi \quad , \tag{3}$$

where the semiclassical nonrelativistic Hamiltonian is assumed to be

$$H = H_0 + V(\vec{r},t) \quad , \tag{4}$$

where

$$H_0 = \frac{p^2}{2m} \tag{5}$$

$$V(\vec{r},t) = U(\vec{r}) - \frac{e}{2mc}\left[\vec{A}(\vec{r},t)\cdot\vec{p} + \vec{p}\cdot\vec{A}(\vec{r},t)\right]$$

$$+ \frac{e^2}{2mc^2}\vec{A}(\vec{r},t)\cdot\vec{A}(\vec{r},t) \quad . \tag{6}$$

These terms have their usual meaning: H_0 propagates the free electron forward in time, $V(\vec{r},t)$ modifies this propagation when the external crystal field $U(\vec{r})$ and laser field $\vec{A}(\vec{r},t)$ are present. The electron momentum operator is $\vec{p} = -i\hbar\nabla$.

This formula assumes the fields $U(\vec{r})$ and $\vec{A}(\vec{r},t)$ do not interact with each other. We know, however, that the intense electric field of the laser slightly polarizes the solid, thereby modifying $U(\vec{r})$, and that the solid slightly distorts the field $\vec{A}(\vec{r},t)$ in return. Thus we should replace $U(\vec{r})$ by $U(\vec{r}) + \delta U(\vec{r},t)$ and $\vec{A}(\vec{r},t)$ by $A(\vec{r},t) + \delta\vec{A}(\vec{r},t)$. This means replacing $V(\vec{r},t)$ by

$$V(\vec{r},t) = U(\vec{r}) - \frac{e}{2mc}\,[\vec{A}(\vec{r},t)\cdot\vec{p} + \vec{p}\cdot\vec{A}(\vec{r},t)]$$

$$+ \delta U(\vec{r},t) + \frac{e^2}{2mc^2}\,\vec{A}(\vec{r},t)\cdot\vec{A}(\vec{r},t) \qquad (7)$$

$$- \frac{e}{2mc}\,[\delta\vec{A}(\vec{r},t)\cdot\vec{p} + \vec{p}\cdot\delta\vec{A}(\vec{r},t)] + \frac{e^2}{mc^2}\,\vec{A}(\vec{r},t)\cdot\delta\vec{A}(\vec{r},t) \quad ,$$

in which we have neglected the δA^2 term. In Eq. (7) the fields $U(\vec{r})$, $\vec{A}(\vec{r},t)$ represent not the total fields but only the parts present when $\vec{A}(\vec{r},t)$, $U(\vec{r})$ is absent.

The potential $U(\vec{r})$ could be further separated into $U_{Vol}(\vec{r}) + U_{Surf}(\vec{r})$, which represent the periodic inner potential and the effective surface dipole layer potential, respectively. $U_{Vol}(\vec{r})$ will be roughly a square well for electrons, while $U_{Surf}(\vec{r})$ will be a pair of plane parallel dipole sheets. The term $\delta U(\vec{r},t)$ is directly related to the optical dielectric susceptibility tensor; its time dependence is coherent with the laser field which drives it. The term $\delta\vec{A}(\vec{r},t)$ can be found by solving the boundary value problem for propagation in the dielectric. Typically, the solid will produce a notch in an otherwise uniform field $\vec{A}(\vec{r},t)$, so $\delta\vec{A}(\vec{r},t)$ will be roughly a negative square well of width equal to the crystal thickness.

E. TYPES OF EXPECTED EFFECTS

Without performing any explicit calculations, we can anticipate the general effects produced by the operator $V(\vec{r},t)$. Since we expect to use perturbation theory, we consider various terms in (V), (V)(V), (V)(V)(V), etc., leaving sums over intermediate states implied. Some explicit terms and the effects they produce are:

(U), $(U)(U)$...	Kinematic electron diffraction
$(\vec{A}\cdot\vec{p})$	Vanishes due to impossibility of conserving energy and momentum
(A^2) $(\vec{A}\cdot\vec{p})^2$	Intense field electrodynamics: Kapitza-Dirac effect, electron mass shift. Thomson scattering, etc.
(δU) $(\delta\vec{A}\cdot\vec{p})$ $(\vec{A}\cdot\delta\vec{A})$ $(U)(\vec{A}\cdot\vec{p})$ $(U)(\delta U)$	Modulated electron diffraction effects, dependent upon presence of both crystal and laser.
...etc.	

The effects of the last set of terms are mostly unknown; this proposal is directed at studying them.

F. PERTURBATION THEORY OF THE ELECTRON MODULATION

We can use the techniques of time-dependent scattering theory to calculate the electron wavefunction $\psi(\vec{r},t)$. To simplify the notation, we rewrite Eq. (7) as

$$V(\vec{r},t) = \sum_n V_n(\vec{r})\, e^{i(\omega_n t - \phi_n)} \quad . \tag{8}$$

This assumes a finite number of discrete frequencies are present, each with a given amplitude and phase. Some of the $V_n(\vec{r})$ are operators, namely those involving $\vec{p} \doteq -i\hbar\nabla$. With this form for $V(\vec{r},t)$, it is relatively simple to solve the equation of motion (Eq. (3)) for $\psi(\vec{r},t)$. We have done this by using the free particle propagator to construct the Green's function, a standard technique in scattering theory. The result is

$$\psi(\vec{r},t) = \psi_0(\vec{r},t) + \psi_1(\vec{r},t) + \psi_2(\vec{r},t) + \cdots \quad , \tag{9}$$

where

$$\psi_0(\vec{r},t) = e^{i(\vec{K}_0\cdot\vec{r} - \Omega_0 t)} \tag{9a}$$

$$\psi_1(\vec{r},t) \cong \sum_n f_n(\vec{K}_n;\vec{K}_0)\,\frac{1}{r}\,e^{i(K_n r - \Omega_n t)} \tag{9b}$$

$$\psi_2(\vec{r},t) \cong \sum_n \sum_{n'} g_{nn'}(\vec{K}_{nn'};K_n;\vec{K}_0)\,\frac{1}{r}\,e^{i(K_{nn'}r - \Omega_{nn'}t)} \tag{9c}$$

and

$$f_n(\vec{p};\vec{q}) = \left(\frac{-m}{2\pi\hbar^2}\right)\oiint d^3\vec{x}\; e^{-i\vec{p}\cdot\vec{x}}\; V_n(\vec{x})\; e^{i\vec{q}\cdot\vec{x}}\; e^{i\phi_n} \tag{9d}$$

$$g_{nn'}(\vec{p};K;\vec{q}) = \left(\frac{-m}{2\pi\hbar^2}\right)^2 \oiint d^3\vec{x} \oiint d^3\vec{x}'$$

$$\times\, e^{-i\vec{p}\cdot\vec{x}}\; V_n(\vec{x})\; \frac{e^{iK|\vec{x}-\vec{x}'|}}{|\vec{x}-\vec{x}'|}\; V_{n'}(\vec{x}')\; e^{i\vec{q}\cdot\vec{x}'}\; e^{i(\phi_n+\phi_{n'})} \quad , \tag{9e}$$

and where we have used $\vec{K}_n \equiv K_n\hat{r}$, $\vec{K}_{nn'} \equiv K_{nn'}\hat{r}$. The indices n, n' run over the same range, as specified by Eq. (8).

In these equations we have used the following notation:

$$\hbar\Omega_0 = \frac{\hbar^2K_0^2}{2m} = E_0 \qquad \text{(incident electron energy)} \tag{10a}$$

$$\hbar\Omega_n = \frac{\hbar^2K_n^2}{2m} = E_0 + \hbar\omega_n \tag{10b}$$

$$\hbar\Omega_{nn'} = \frac{\hbar^2K_{nn'}^2}{2m} = E_0 + \hbar\omega_n + \hbar\omega_{n'} \quad . \tag{10c}$$

The incident wave was assumed to be $\psi_0(\vec{r},t)$ and we have assumed the point $\vec{r}$ to be far from the modulating crystal.

Thus, we find the modulated wave to be a linear superposition of the incident plane wave $\psi_0(\vec{r},t)$, and various nearly spherical waves $\psi_1(\vec{r},t)$, $\psi_2(\vec{r},t)$, ... , with certain amplitudes and phases. The superposition is a coherent one, since all the relative phases are fixed.

G. DISCUSSION OF THE MODULATED WAVEFUNCTION

1. Physical Properties

In order to understand the nature of the modulated wavefunction ψ, it is helpful to consider the expectation values of certain operators representing physical quantities. We define

$$\langle Q \rangle \equiv \int d^3\vec{r}\ \psi^*(\vec{r},t)\ Q(\vec{r},t)\ \psi(\vec{r},t) \quad , \tag{11}$$

where we leave ψ unnormalized. Some of the quantities of interest are:

Probability density	$\doteq$	$\delta(\vec{r}-\vec{r}_0)$	(12a)
Probability current	$\doteq$	$\frac{1}{2m}\left[\vec{p}\ \delta(\vec{r}-\vec{r}_0) + \delta(\vec{r}-\vec{r}_0)\vec{p}\right]$	(12b)
Momentum	$\doteq$	$\vec{p}$	(12c)
Kinetic energy	$\doteq$	$\frac{1}{2m}p^2$.	(12d)

Using $\vec{p} = -i\hbar\nabla$, and substituting these operators and the wavefunction ψ (Eq. (9)), into formula (11) yields explicit expressions for the expectation values. For the first two quantities, the δ-function gives an immediate result:

$$\rho_e \equiv \langle \delta(\vec{r}-\vec{r}_0) \rangle = \psi^*\psi \tag{13a}$$

$$\vec{j}_e \equiv \langle \frac{1}{2m} [\vec{p}\,\delta(\vec{r}-\vec{r}_0) + \delta(\vec{r}-\vec{r}_0)\vec{p}] \rangle = \frac{\hbar}{2mi} [\psi^*\nabla\psi - \psi\nabla\psi^*] \quad . \tag{13b}$$

The general formulas are much too complicated to consider in detail here. The striking feature common to all the expectation values is the existence of additional terms that oscillate in space and time with various frequencies and wavelengths determined by the laser. Thus, we find

$$\rho_e \cong 1 + \delta\rho_e(\vec{r},t) \tag{14a}$$

$$\vec{j}_e \cong \vec{v} + \delta\vec{j}_e(\vec{r},t) \tag{14b}$$

$$\langle \vec{p} \rangle \cong m\vec{v} + \delta\vec{p}(\vec{r},t) \tag{14c}$$

$$\langle \frac{p^2}{2m} \rangle \cong \frac{1}{2} mv^2 + \delta E(\vec{r},t) \quad , \tag{14d}$$

where $\vec{v}$ is the electron velocity. Each of the quantities has small, complicated "ripples" superimposed on the free space value. In a reasonable experiment, these ripples may amount to ten percent of the DC value. They arise only when both the crystal and the laser beam are present, and they are coherent with the laser. In the next section we consider a simple case in more detail.

2. Simple Case

In order to deal with manageable formulas, we consider only the n = 0, ±1 terms of ψ_1:

$$\psi_1 = f_+ \frac{1}{r} e^{i[K_+ r - (\Omega_0+\omega)t]} + f_0 \frac{1}{r} e^{i[K_0 r - \Omega_0 t]} + f_- \frac{1}{r} e^{i[K_- r - (\Omega_0-\omega)t]} , \quad (15)$$

in which we used $(\pm) \equiv (\pm 1)$, $f_+ \equiv f_{+1}(\vec{K}_n; \vec{K}_0)$, etc. The probability density, from Eq. (13a) is

$$\rho_e = \psi_0^* \psi_0 + \psi_0^* \psi_1 + \psi_1^* \psi_0 + \cdots \quad (16a)$$

$$= 1 + \frac{2}{r} \Big\{ |f_+| \cos(K_+ r - \vec{K}_0 \cdot \vec{r} - \omega t + \delta_+)$$

$$+ |f_0| \cos(K_0 r - \vec{K}_0 \cdot \vec{r} + \delta_0)$$

$$+ |f_-| \cos(K_- r - \vec{K}_0 \cdot \vec{r} + \omega t + \delta_-) \Big\} \cdots , \quad (16b)$$

where we used $f_\pm = |f_\pm| e^{i\delta_\pm}$, etc. This result shows clearly the kind of oscillatory behavior characteristic of all observable quantities. It may be noted that in the forward direction, the f_0 term exhibits no oscillation. We can simplify Eq. (16b) further if we assume the laser photon energy is small compared to the incident energy: $\hbar\omega << E_0$. Then in the forward direction we find

$$\rho_e \cong 1 + \frac{2}{r} |f_0| \cos \delta_0 + \frac{4}{r} |f| \cos(\frac{\varepsilon}{2} K_0 r - \omega t + \delta) \cos \frac{\varepsilon^2}{8} K_0 r + \cdots , \quad (16c)$$

where we assumed $|f_+| = |f_-| \equiv |f|$ and $\delta_- = -\delta_+ = \delta$, and we used the relation

$$K_\pm = K_0 \left[1 \pm \frac{1}{2}\varepsilon - \frac{1}{8}\varepsilon^2 + \cdots\right] . \qquad \varepsilon = \hbar\omega/E_0 \quad (17)$$

It thus appears that ρ_e consists of a constant part plus a weaker traveling wave ripple of frequency ω and wavelength

$$\Lambda_1 = \frac{2\pi}{(\frac{\varepsilon}{2} K_0)} = \frac{4\pi E_0}{\omega p} = \beta\lambda \qquad \beta = v/c \quad , \tag{18a}$$

which is always less than the laser wavelength λ. In addition, the ripple has a slow spacial modulation of wavelength

$$\Lambda_2 = \frac{2\pi}{(\frac{\varepsilon^2}{8} K_0)} = \frac{16\pi E_0^2}{\hbar\omega^2 p} = \frac{mc\beta^3\lambda^2}{\pi\hbar} = \frac{mc\beta}{\pi\hbar} \Lambda_1^2 \quad , \tag{18b}$$

which can be considerably larger than λ. In Fig. 3 is plotted the probability density ρ_e with and without the modulation. It should be remembered that the pattern oscillates in time (equivalently, the Λ_1 wiggles move continuously to the right), but that the beat pattern (i.e. nodes spaced by Λ_2) are fixed in space. Thus, the modulation generates oscillations, beats, etc., quite analogous to excitations of a stretched string.

As indicated in Eqs. (14), similar oscillations are induced in all the other observable quantities ($\vec{j}_e$, $\langle \vec{p} \rangle$, $\langle p^2/2m \rangle$ etc.). In all of these, the characteristic lengths Λ_1, Λ_2 arise, and a ripple/nodal structure is superimposed on the free space value.

3. General Interpretation of the Modulated Wavefunction

Considerations like those of the preceding section suggest that the laser induces level structure in the electrons. This can be illustrated by rewriting the wavefunction, to first order, as

$$\psi \cong \psi_0' \, e^{-\frac{i}{\hbar} E_0 t} + \psi_+' \, e^{-\frac{i}{\hbar}(E_0 + \hbar\omega)t} + \psi_-' \, e^{-\frac{i}{\hbar}(E_0 - \hbar\omega)t} \quad . \tag{19}$$

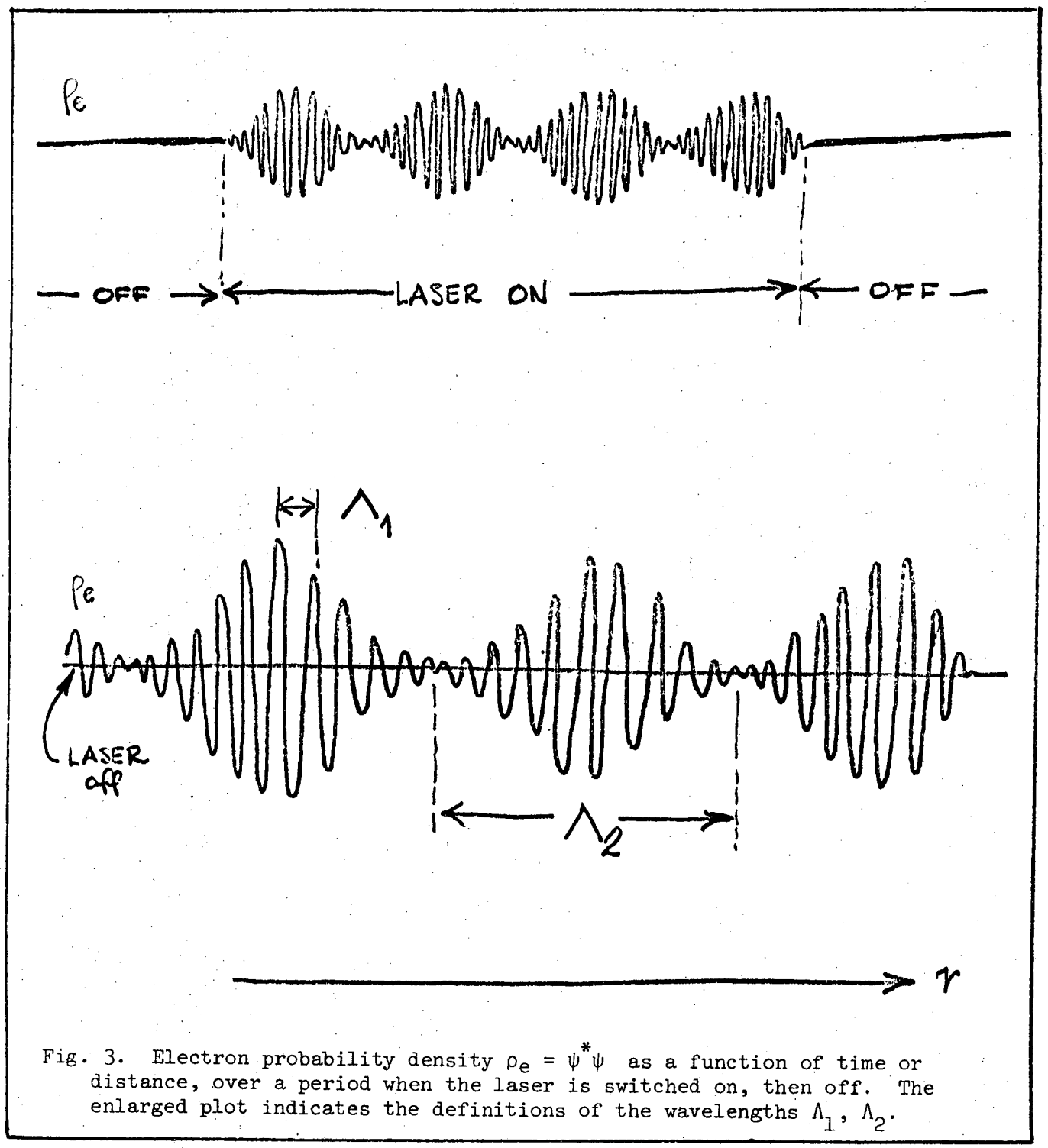

Fig. 3. Electron probability density $\rho_e = \psi^* \psi$ as a function of time or distance, over a period when the laser is switched on, then off. The enlarged plot indicates the definitions of the wavelengths Λ_1, Λ_2.

This has the appearance of a coherent superposition of three energy states: E_0, $E_0 \pm \hbar\omega$. It is quite analogous to the coherence induced in atoms or molecules by a microwave field. It is important to note that each individual electron exhibits this coherence--the process is not one in which some electrons lose or gain energy, others do not. The electrons may be thought of as rapidly oscillating among the various states, with a probability of being in the $E_0 \pm \hbar\omega$ state given by $|\psi'_{\pm}|^2$. This oscillation is such that the average energy over a period long compared to the oscillations is just E_0.

The energy sidebands lie at $\pm\hbar\omega$ from the fundamental E_0, implying that the electrons have absorbed, or emitted, single photons from the laser field. It is well-known that such a process violates energy-momentum conservation in free space, hence is kinematically forbidden. This may readily be proved by noting that the requirements $P^2/2m = p^2/2m \pm \hbar\omega$ and $\vec{P} = \vec{p} \pm \hbar\vec{k}$ (with $k = \omega/c$) together imply $1 - (v/c)\cos(\hat{p},\hat{k}) = \pm \hbar\omega/2mc^2$, which cannot be satisfied for $v/c \ll 1$ and $\hbar\omega \ll 2mc^2$. However, the electrons are not free when the solid is present, and it is possible to transfer some momentum $\pm\hbar\vec{G}$ to it while transferring negligible energy. The momentum requirement is thus $\vec{P} \pm \hbar\vec{G} = \vec{p} \pm \hbar\vec{k}$, and this is not necessarily incompatible with the energy requirement. We are thus led to the conclusion that the solid acts as an intermediary between the electron and the laser beam, absorbing or emitting the correct momentum to allow the electron to absorb or emit single laser photons. A diagram of this process is shown in Fig. 4.

It is important to note the similarity of these processes to the Mössbauer effect, in which a crystalline solid acts to couple a photon and a nucleus. In the absence of the crystal, the photon-nucleus coupling is nearly forbidden kinematically. The crystal, with its ability to absorb and deliver momentum in nearly arbitrary amounts, then provides a means of adjusting the kinematics so that the nucleus and photon can couple more strongly. The success of the

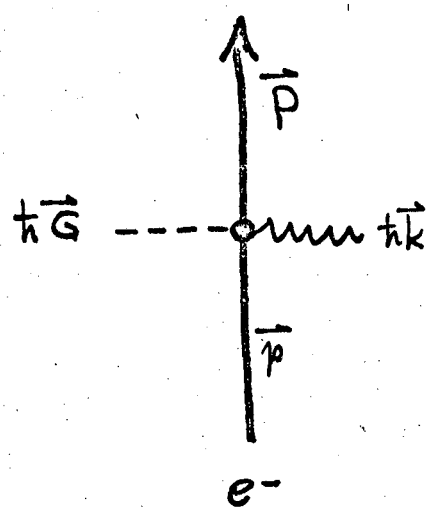

Fig. 4. Diagram for the modulation process in which a single photon is emitted or absorbed, assisted by a zero-frequency quantum which transports sufficient momentum to conserve energy and momentum.

Mössbauer mechanism depends upon the ability to transfer arbitrarily small amounts of energy to the crystal while transferring a fixed quantity of momentum. We shall shortly see that certain processes in laser modulation of electrons also involve the transfer of momentum with negligible transfer of energy.

There is another valuable way to picture the modulation process. Imagine a very long (effectively infinite) train of waves streaming past a small region containing the solid and the laser beam. As these waves pass this region, the interaction with the local fields modifies them in a predictable manner, much like the effect of a single station in an assembly line. The modifications are carried downstream, and may be observed anywhere downstream, totally intact.

If the wave train is not infinitely long, or if there is self-interaction, dispersion is introduced which will wash out the patterns at increasing distance past the modulator. It is clear that for quantum mechanical modulation of the de Broglie waves to occur, the wave train must be long enough and the modulation frequency high enough to introduce structure in the wave train before is has passed.

This model answers the question of how the interaction $V(\vec{r},t)$ can seemingly influence the electrons after they have passed the modulator: the electrons are inside the modulator long enough so that what comes out has the character of several different electrons. Since coherence exists between them, their waves can interfere to produce the spacial and temporal changes predicted, e.g. by Eq. (16c). At the other extreme, if the wave trains are very short, they pass the modulator in a short time and their internal structure is negligibly altered. They see a quasistatic potential, and what comes out depends on the phase of injection into that potential although it always has the character of a single electron. This picture shows the connection between the wave-mechanical processes of interest here, and classical particle-like effects such as occur in a klystron.

H. SOME SPECIFIC RESULTS

Several authors have performed explicit calculations of some of the effects described above. Some of these will be briefly reviewed here, in order to indicate the type of predictions and orders of magnitude involved. This is by no means a comprehensive list of predicted effects.

1. Notch Effect

One of the simplest and most studied effects results from the dielectric constant $\in$ of the solid film. The field inside the film is reduced relative to the free space field, producing a notch in the overall field. This is diagrammed in Fig. 5. The notch gives rise to a diffraction pattern similar to a (wide) slit of width D = film thickness; the pattern is concentrated in the forward direction. The external boundaries of the laser field also produce a diffraction pattern, but if the field drops off gradually, this will be extremely

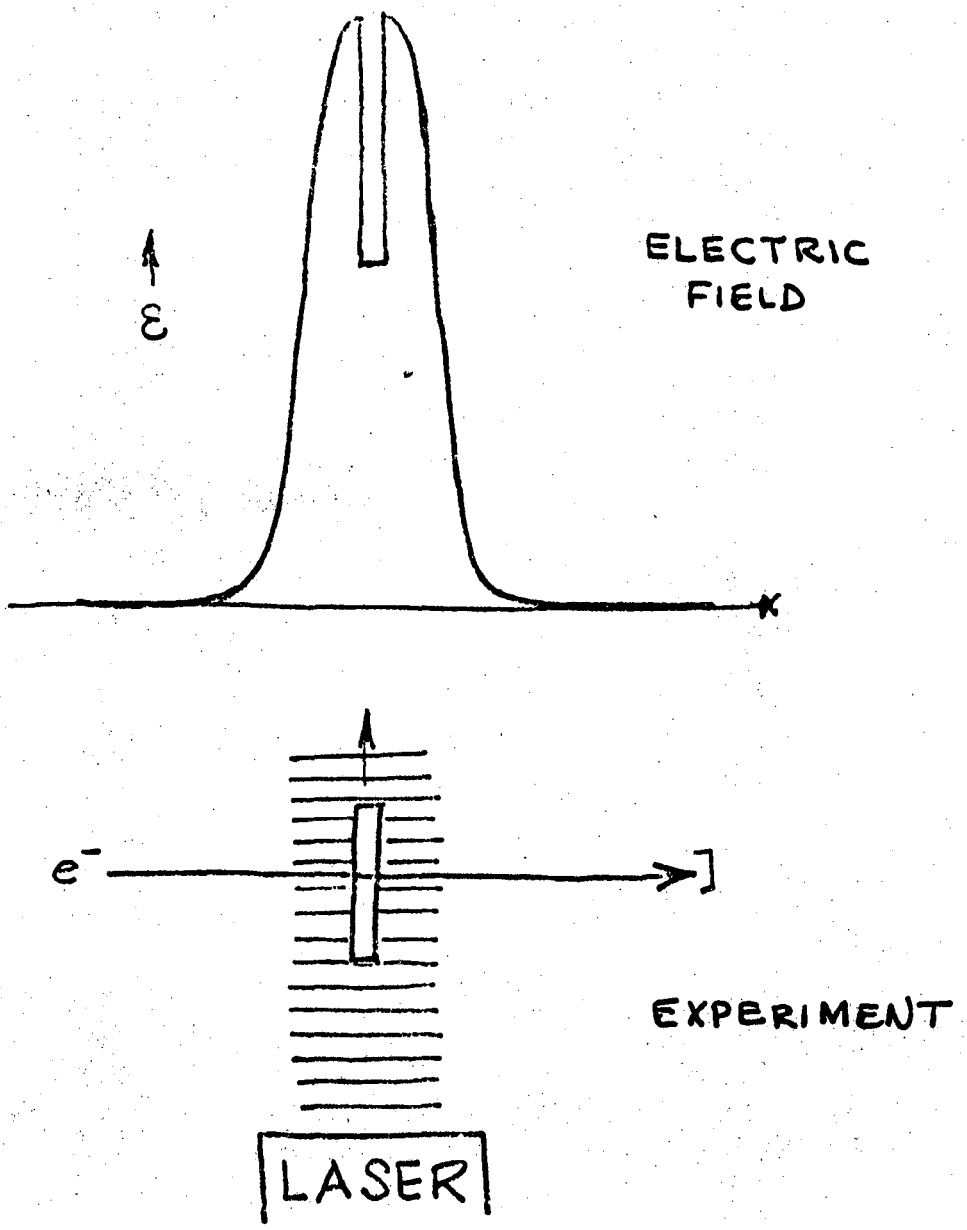

Fig. 5. The Notch Effect, one of a variety of processes leading to modulation of the electrons. The dielectric film produces a notch in the electric field of the laser. Electrons traversing the notch become modulated.

weak, and it will be assumed that the external boundaries are at $\pm \infty$. Under this circumstance the uniform-field term $\vec{A}\cdot\vec{p}$ vanishes. Thus, the entire effect can be calculated using the notch field:

$$\delta\vec{A} = -\frac{c}{\omega}\left(\frac{\in - 1}{\in}\right)\vec{\mathcal{E}}\cos(\vec{k}\cdot\vec{r} - \omega t)\,\eta(\vec{r}) \quad , \tag{20}$$

where $\in$ is the dielectric constant of the film, $\vec{\mathcal{E}}$ is the electric field of the laser beam, and $\eta(\vec{r})$ is unity inside the film, zero outside. We are here dealing with the $\delta\vec{A}\cdot\vec{p} + \vec{p}\cdot\delta\vec{A}$ term in $V(\vec{r},t)$, Eq. (7). This operator can be written

$$V_{notch} = \left(\frac{ie\hbar}{mc}\right)[\delta\vec{A}\cdot\nabla + \frac{1}{2}\nabla\cdot\delta\vec{A}] \quad , \tag{21}$$

by using the identity $\vec{F}\cdot\vec{p} - \vec{p}\cdot\vec{F} = -i\hbar\nabla\cdot\vec{F}$. Thus, there are really three effects here: 1) the $\delta\vec{A}\cdot\nabla$ effect, proportional to $\vec{\mathcal{E}}\cdot\vec{K}_0$; 2) the effect in $\nabla\cdot\delta\vec{A}$ involving $\nabla\cos(\vec{k}\cdot\vec{r} - \omega t)$; 3) the edge effect in $\nabla\cdot\delta A$ arising from $\nabla\eta(\vec{r})$. We shall discuss only the first of these.

From Eqs. (9), we find the first-order forward scattered wavefunction

$$\psi_1 = \left(\frac{-e}{2\pi\hbar\omega}\right)\left(\frac{\in - 1}{\in}\right)\vec{\mathcal{E}}\cdot\vec{K}_0\,AD\left[\frac{\sin(\frac{\omega D}{2v})}{(\frac{\omega D}{2v})}\right]$$

$$\times\frac{1}{r}\,e^{i(K_0 r - \Omega_0 t)}\,e^{-i2\pi\frac{r}{\Lambda_2}}\cos(2\pi\frac{r}{\Lambda_1} - \omega t) \quad , \tag{22}$$

where A is the transverse coherence area of the electron beam and Λ_1, Λ_2 are defined in Eqs. (18). The various observables such as probability density ρ_e can be found using $\psi \cong \psi_0 + \psi_1$. We quote some predictions obtained in this way:

a) The modulation exhibits familiar diffraction properties, via the factor $\sin(\frac{\omega D}{2v})/(\frac{\omega D}{2v})$. It varies sinusoidally with the film thickness D, and will be maximum when $\omega D/2v = (2N + 1)\pi/2$, N = 0, 1, 2 ... , and zero when $\omega D/2v = N\pi$. Such considerations can be experimentally important.

b) The modulation is maximum when the laser polarization is parallel to the direction of motion of the electron, since $\vec{K}_0 = m\vec{v}/\hbar$.

c) The modulation oscillates in time at the frequency ω, and will average to zero over long times, when detected with an integrating detector.

d) For typical experimental parameters, ($\in \sim 25$ esu, $D = 10^{-5}$ cm, $\hbar\omega = 2.5$ eV, $E_0 = 50$ keV, $\in \sim 3$) the amplitude of the modulation is of the order of several percent of the incident wave.

The presence of the crystal is felt via the factor $\eta(\vec{r})$ in Eq. (20), the Fourier transform of which gives the momentum spectrum of the crystal. Thus, the $(\delta\vec{A}\cdot\vec{p})$ term is really a term like $(U\vec{A}\cdot\vec{p})$, as distinguished from a second-order term $(U)(\vec{A}\cdot\vec{p})$ considered in the next section.

This process is particularly interesting because the electron momentum is unchanged. It appears that the photon delivers all its momentum to the crystal and all its energy to the electron.

2. Modulated Diffraction

Another effect that was indicated in Sec. II E was a second-order process involving terms like $(U)(\vec{A}\cdot\vec{p})$. This type of interaction is diagrammed in Fig. 6. Two basic processes can occur: 1) photon absorption, followed by lattice diffraction, $(U)(\vec{A}\cdot\vec{p})$; 2) lattice diffraction followed by photon absorption, $(\vec{A}\cdot\vec{p})(U)$.

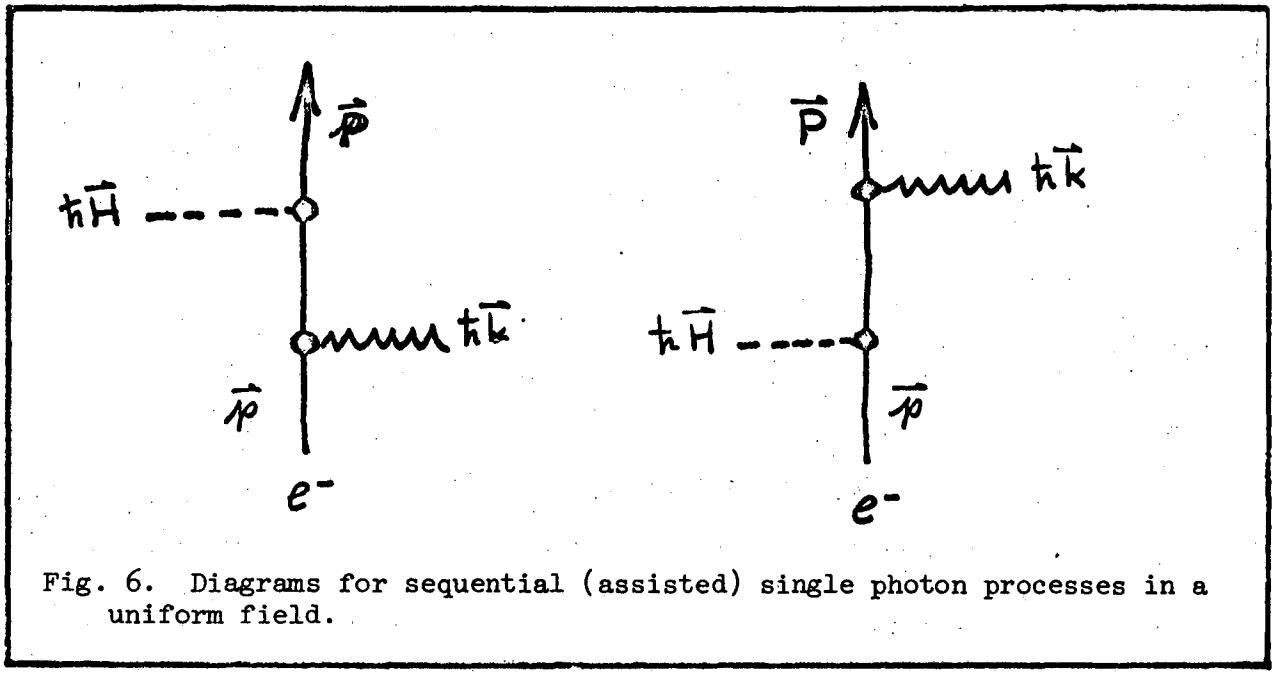

Fig. 6. Diagrams for sequential (assisted) single photon processes in a uniform field.

In this process, we can study the modulation of the beam diffracted away from the forward direction. Since the beam is not really a semi-infinite plane wave, interference between the scattered wave and the incident wave cannot occur. Thus, we must also consider the kinematically diffracted beam due to (U). Furthermore, other notch effect terms like $(U)(\delta\vec{A}\cdot\vec{p})$ may be of comparable magnitude (these are diagrammed in Fig. 7). Observables such as ρ_e will be given to lowest order by $\psi_1^*\psi_1$.

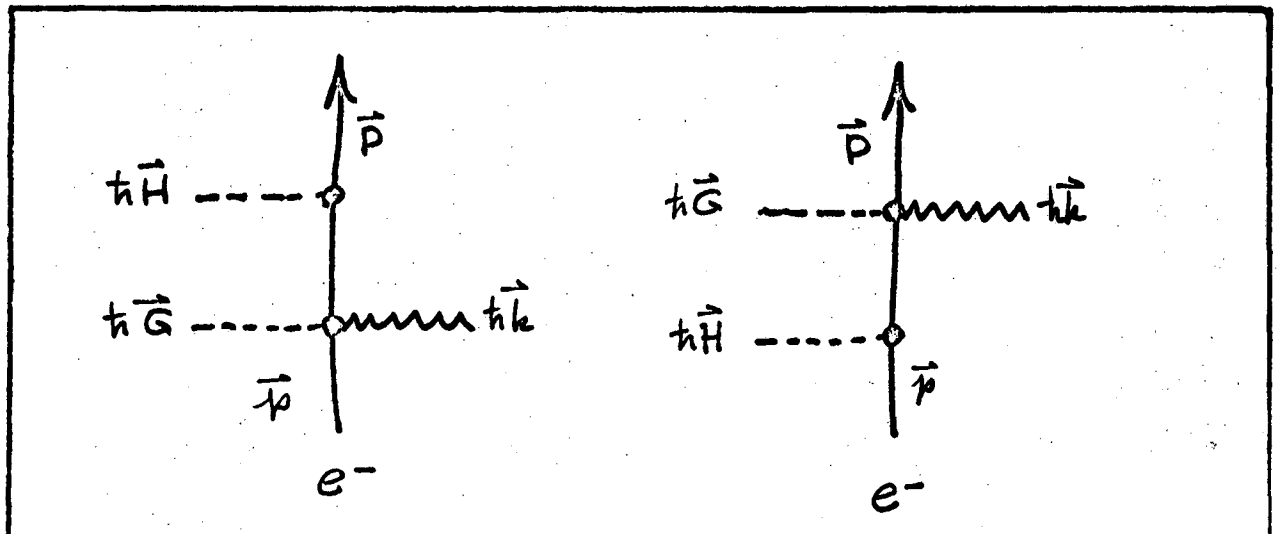

Fig. 7. Diagrams for sequential (assisted) single-photon processes in a non-uniform (e.g., notch) field.

The formulas involved are excessively complicated; we merely remark on some of the results:

a) As before, the notch field produces a slit interference pattern, but now the uniform free space field $\vec{A}$ also produces modulation. This $(U)(\vec{A}\cdot\vec{p})$ effect does not produce a slit diffraction term $\sin\xi/\xi$.

b) As before, the modulation contains a part proportional to $\hat{\mathcal{E}}\cdot\vec{K}_0$, but now contains an additional term proportional to $\hat{\mathcal{E}}\cdot\hat{r}$. That is, part of the modulation is maximum when the electric field is parallel to a diffracted beam.

c) As before, all terms involving one photon oscillate in time.

d) As before, typical experimental parameters lead to modulation amplitudes of the order of percents.

e) An entirely new effect, angular separation of the sidebands, occurs for the $(U)(\vec{A}\cdot\vec{p})$ term. In other words, diffraction of a modulated beam gives three separate beams, the normal one corresponding to E_0, and two sidebands corresponding to $E_0 \pm \hbar\omega$. This effect is the basis for a proposed measurement of the modulation, described in Sec. IV B. However, it does not appear to be a promising technique.

The phase-match (momentum) conditions for the processes in Fig. 6 are $\vec{P} - \vec{p} = \pm(\hbar\vec{k} - \hbar\vec{H})$ while for Fig. 7 they are $\vec{P} - \vec{p} = \pm(\hbar\vec{k} - \hbar\vec{G} - \hbar\vec{H})$. For these processes, the electron momentum as well as its energy are altered, but in such a way as to conserve the expectation values.

I. CRITICISM OF THE THEORY

Many of the limitations of the theory developed above are obvious from the sequence of approximations. Clearly, the most serious was the use of semiclassical fields and the reduction of the system to a single electron. This discards all the

inelastic processes associated with passage of the electrons through a solid [VIII.1-13]: excitation and ionization, phonon and plasmon generation, and so on. Since we know that the inelastic component of the transmitted beam is usually rather large, it will be important to understand them in order to understand the quantum mechanical modulation process.

In addition to this general deficiency, several specific effects should be considered in a more complete theory:

1. Coherence length of the electron. The electrons should be represented by finite wave trains, since any experiment involves some energy spread. This will tend to smear out the interference effects.

2. Coherence width of the electron. The incident beam is a narrow pencil with some angular divergence, rather than a plane wave. Certain terms representing interference with the incident wave away from forward scattering will not actually be present.

3. Boundary conditions on the laser beam. A correct analysis requires a complete solution of the effect of the dielectric solid film on the laser field. The dielectric constant, thickness of the film, frequency of the light, etc. are parameters.

4. Relativistic generalization. Typical energies (50 keV) have $v/c \sim 0.4$; relativistic corrections will modify parameters like Λ_1, Λ_2.

5. Surface effects. Crystal potential is variable, possibly irregular near a surface [IX.1-9]. The presence of an adsorbed layer may affect an experiment.

6. Crystal orientation. Energy loss, diffraction intensities, etc., depend strongly on direction electrons pass through crystal. Channelling effects will modify spacial dependences [VII.1-3].

7. Radiation. Electrons in oscillatory fields radiate (Thomson scattering). This effect is entirely classical, and can be accurately calculated [III.5,6].

8. Lorentz Force. Magnetic field of the laser beam generates a transverse force. Electrons in a traveling wave tend to be deflected into direction of wave propagation and ride crest, gaining energy from the field [III.8].

9. Spectral response of the solid. Solids can have transitions resonant with laser and be strongly pumped, thus modifying the electrostatic potential in the solid. Off-resonance, the solid is polarized by the laser field; substantial nonlinear polarization may be generated.

10. Thermal effects in the solid. Due to laser absorption and electron bombardment, the crystal is heated. In a vacuum, it may reach very high temperatures, thus modifying the diffraction patterns, energy loss spectra, etc. [VII.6,8].

11. Spin. New effects are expected when the electron spin is introduced. These small effects will be most interesting if the solid is polarized, if there is a magnetic field, etc. [VII.9].

J. EXTENSIONS OF THE THEORY

There are several experimental arrangements for which certain modifications of the theory would be needed. They are of sufficient interest to list here, although no calculations relating to any of these effects have been published. It is hoped that future work will examine these effects.

1. Reflection geometry. We have shown (Sec. II G 3) that the modulation is possibly mainly because the solid can exchange momentum without exchanging energy, thereby coupling the electrons and photons. This function can be done just as well in backscattering, at low angles if necessary. This arrangement has many advantages, but the phase matching condition $\vec{P} \pm \hbar\vec{G} = \vec{p} \pm \hbar\vec{k}$ probably means that the coupling is weaker for small v/c.

2. Positrons. The main modulation effects are the same for $e^{\pm}$, but certain differences exist since the inner crystal potential is positive. It may not be possible to obtain a positron source of sufficient luminosity and monochromaticity to perform reasonable experiments, however.

3. Modulation of the laser. In order to increase signal-to-noise it may be desirable to modulate the laser intensity, wavelength, polarization, or propagation direction. Such effects are easily incorporated in the simple theory developed above.

4. External magnetic field. In order to guide the electrons, it may be desirable to introduce a strong uniform magnetic field parallel to their motion. This field may have dramatic effects, since even without the solid, the electrons are no longer free and can absorb and emit photons [XVI.1,2]. Furthermore there are certain transverse effects in a thin film, such as Sondheimer oscillations (in which the conductivity is an oscillatory function of the applied field) [XVI.3] that will be important.

III. THEORY OF SECOND-ORDER PROCESSES; INTERFEROMETRY

A. IMPOSSIBILITY OF LINEAR DETECTION OF FIRST ORDER MODULATION

In Sec. II G.1 we showed that the general effect of the modulation on various observables (ρ_e, $\vec{j}_e$, $\langle \vec{p} \rangle$, $\langle p^2/2m \rangle$, etc.) is to add small "ripples" that oscillate in space and time. It was later shown that all single-photon processes produce effects oscillating sinusoidally in time at the laser frequency ω (e.g., Eq. (16c)). Consider now an attempt to measure these oscillations with a linear detector, for instance measuring ρ_e with a Faraday cup and electrometer. The detector cannot follow the extremely high frequency ($\omega \sim 10^{15}$ sec^{-1}) oscillations, and must take an average over some period T long compared with ω^{-1}:

$$\bar{\rho}_e = \frac{1}{T} \int_0^T dt\ \rho_e \cong 1 + \frac{1}{T} \int_0^T dt\ \delta\rho_e(\vec{r},t) \quad . \tag{23}$$

The first order terms contributing to $\delta\rho_e(\vec{r},t)$ are, from Eq. (9)

$$\psi_0^* \psi_1 + \psi_1^* \psi_0 = 2 \sum_n |f_n| \frac{1}{r} \cos[(K_n r - \vec{K}_0 \cdot \vec{r}) - \omega_n t + \delta_n] \quad , \tag{24}$$

and the integral over many cycles ($T \gg 2\pi/\omega_n$) gives exactly zero for all $n \neq 0$. (The $n = 0$ term is non-vanishing but is not due to the laser.) Thus, we conclude that no real linear detector can detect any linear laser modulation.

B. SECOND-ORDER MODULATION

The terms contributing to $\delta\rho_e(\vec{r},t)$ in second order are, from Eq. (9)

$$\psi_1^* \psi_1 \cong \frac{1}{r^2} \sum_n \sum_{n'} |f_n|\ |f_{n'}| \cos[(K_n - K_{n'})r - (\omega_n - \omega_{n'})t + (\delta_n - \delta_{n'})] \tag{25a}$$

$$\psi_0^* \psi_2 + \psi_2^* \psi_0 \cong \frac{2}{r} \sum_n \sum_{n'} |g_{nn'}| \cos[(K_{nn'} r - \vec{K}_0 \cdot \vec{r}) - (\omega_n + \omega_{n'})t + \delta_{nn'}] \quad . \quad (25b)$$

These terms introduce the important possibility of having time-independent parts, hence being observable with a real detector. Thus, if $\omega_n \pm \omega_{n'} = 0$, there generally will be a detectable modulation effect.

It is clear that all such terms represent two photon processes. Figure 8 shows diagrams of some possible processes, including those for which the solid film does not participate, such as Kapitza-Dirac diffraction.

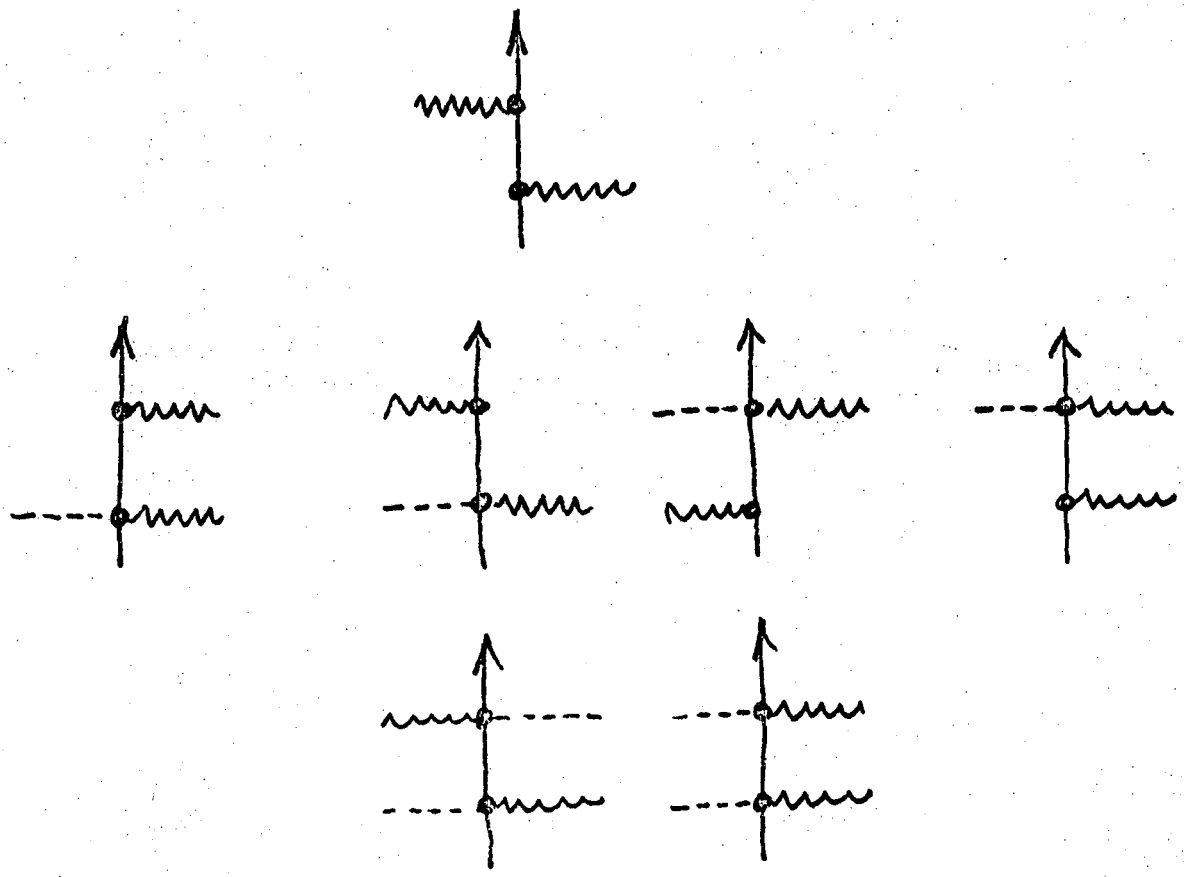

Fig. 8. Some diagrams representing two-photon processes. The top diagram does not involve the solid, and represents Compton, Kapitza-Dirac, and other processes in free space. The other diagrams represent solid-assisted processes.

The main interest in this proposal is in the terms in which the solid does participate by exchanging momentum with photons and electrons. Using Eqs. (25) in Eq. (23), we find, to second order, the important result,

$$\bar{\rho}_e = 1 + \frac{1}{r^2} \sum_{n'} \left\{ |f_n| \, |f_{n'}| \cos(\delta_n - \delta_{n'}) + |g_{nn'}| \cos \delta_{nn'} \right\} + \cdots \quad (26)$$

where we limited to the forward direction, and the sums are over all pairs n, n' for which $\omega_n \pm \omega_{n'} = 0$. This proves that second-order modulation will produce observable effects.

The other observables can be considered in the same fashion. For instance, there is a nonzero second-order shift in the kinetic energy $\langle p^2/2m \rangle$, which oscillates slowly at the laser difference frequencies and is constant exactly on resonance. This shift will probably be toward higher energy, but a negative shift could also presumably be arranged.

C. NONLINEAR (PHASE SENSITIVE) DETECTION

Suppose we have a detector whose sensitivity is a sinusoidal function of time, with frequency ω' and phase δ'. The detected signal, after integrating for time T, will be of the form

$$\bar{\rho}'_e = \int_0^T dt \, \rho_e \cos \omega' t = \int_0^T dt \, \delta\rho_e(\vec{r},t) \cos \omega' t \quad . \quad (27)$$

Using this "lock-in detector", any component of ρ_e that oscillates at the frequency ω' (within the bandwidth of the instrument) will give rise to a nonzero signal $\bar{\rho}'_e$; all other components will vanish, including the constant terms of Eq. (26).

This would be a simple technique for directly detecting the first-order modulation, by simply setting ω' equal to the laser frequencies ω_n. Unfortunately, of course, no such lock-in detector exists for such high frequencies ($\omega_n \sim 10^{15}$ Hz), so the linear modulation terms will again average to zero.

Suppose, however, that the laser contains two frequencies ω_1, ω_2 that are nearly, but not exactly equal. Then the difference $\Delta\omega_{12} = \omega_1 - \omega_2$ might be very small, hopefully within the range of conventional high frequency circuits. Typical multimode lasers have line separations of 10 to 10^3 MHz, a range regularly studied with light beating techniques [II.8], and well within the range of electro-optic and microwave device technology. In an experiment, the lock-in frequency ω' would be varied, and the detector response measured as a function of ω'. Peaks would appear at the known laser difference frequencies, and their origin as a modulation effect could be proved by varying other parameters. The spectral composition of observables such as ρ_e can be determined directly, by scanning ω' across the various $\Delta\omega_{nn'} = \omega_n - \omega_{n'} << \omega_n, \omega_{n'}$.

Consequently, we expect that lock-in techniques can be applied to the detection of the modulation, and should provide a technique of relatively high sensitivity.

D. INTERFEROMETRY (THEORY)

Introduction of multiple frequencies and lock-in detection of their differences is suggested as a new method for detecting the modulation. We can provide the multiple frequencies from a single laser or multiple mode-locked lasers overlapping the path of the electrons in the crystal film. Alternatively, we can use one or more lasers illuminating two physically separated films, as illustrated

in Fig. 9. Such a device has many interesting and unusual properties. If sufficient signal can be obtained, it could make possible many new experiments and precision measurements. Accordingly, we examine some of these properties in the next sections.

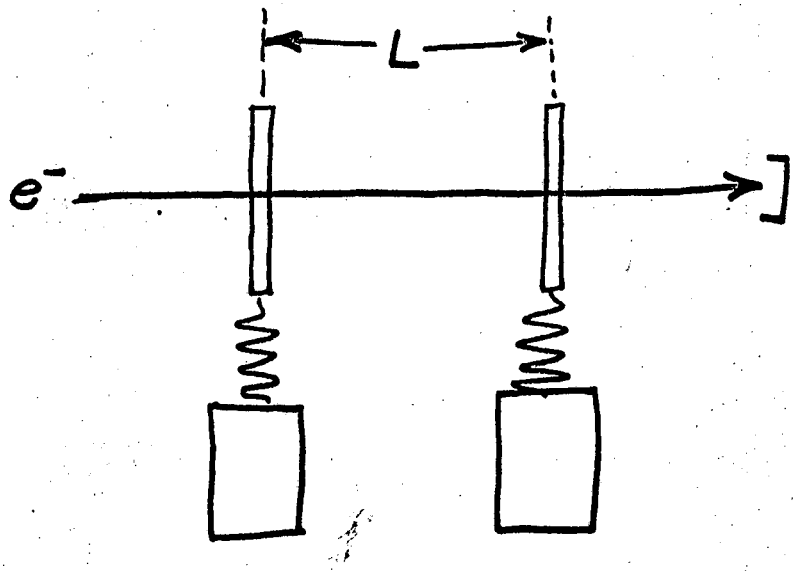

Fig. 9. A laser-modulated electron interferometer using transmission through two thin films and two lasers.

1. Theory of a Double Modulation Device

Consider the experimental arrangement diagrammed in Fig. 10, in which an electron beam interacts with two crystalline solids (a,b) illuminated by laser light of various frequencies, and is detected at some distant point $\vec{r}$ located at $\vec{R}_a$, $\vec{R}_b$ from the modulators. The vector $\vec{L}$ gives the separation of the modulators, which are located relative to the arbitrary origin by the vectors $\vec{a}$, $\vec{b}$. The vector $\vec{R} = \vec{r} - (\vec{a} + \vec{b})/2$ runs from the midpoint between the modulators to the observation point $\vec{r}$.

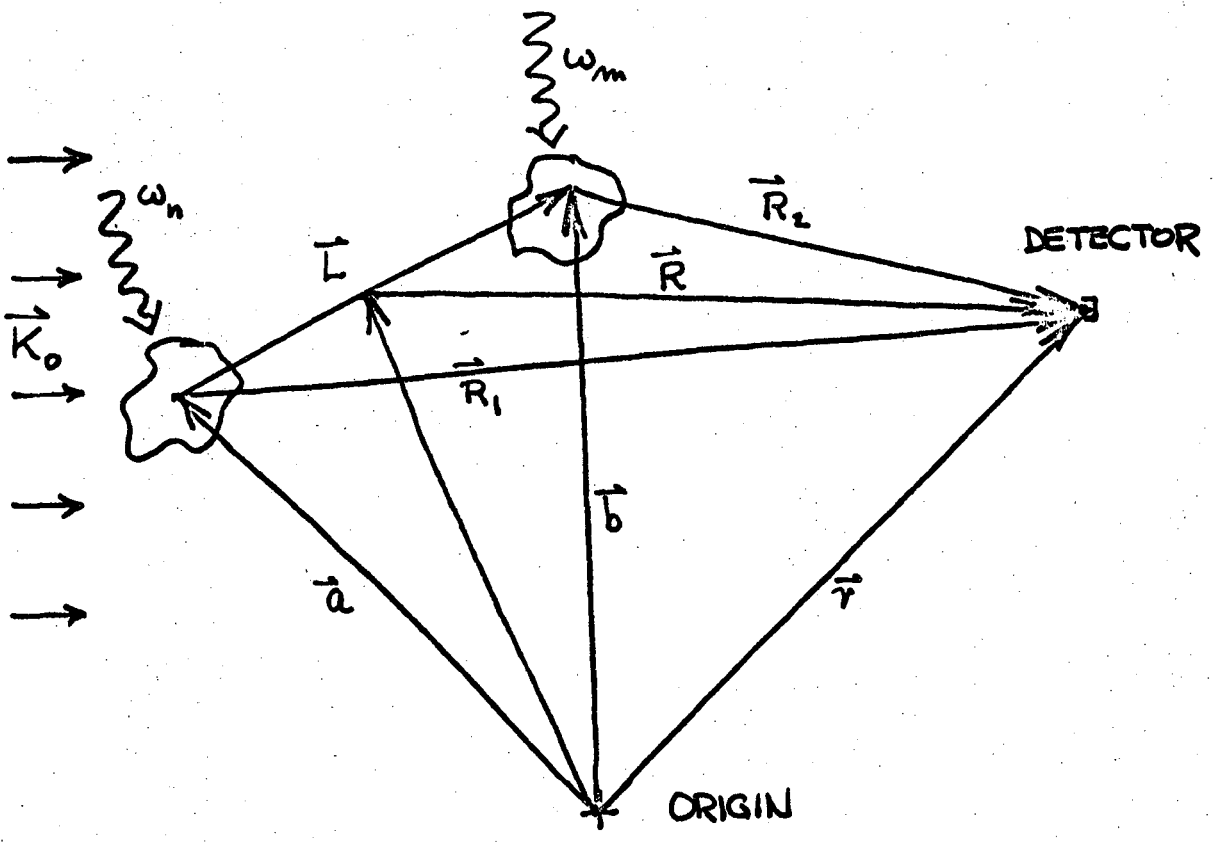

Fig. 10. Vector diagram defining the quantities used in the text to describe two-modulator interferometers. A plane wave is assumed incident from the left.

In order to compute the detected signal, it is only necessary to extend the theory developed in Secs. II F, G to include two modulators separated by $\vec{L}$. The perturbation operator $V(\vec{r},t)$ is rewritten

$$V(\vec{r},t) = \sum_n V_n(\vec{r})\, e^{-i(\omega_n t - \phi_n)} + \sum_m V_m(\vec{r})\, e^{i(\omega_m t - \phi_m)} \quad , \qquad (28)$$

where the two terms represent the two modulators. The wavefunction $\psi(\vec{r},t)$ can be found using the same techniques as before, with the result

$$\psi = \psi_0 + \psi_1^{(a)} + \psi_1^{(b)} + \psi_2^{(aa)} + \psi_2^{(bb)} + \psi_2^{(ba)} + \psi_2^{(ab)} + \cdots \quad , \qquad (29)$$

where $\psi_1^{(a)}$, $\psi_1^{(b)}$ represent the same first-order scattering as before (for each modulator independently), $\psi_2^{(aa)}$, $\psi_2^{(bb)}$ represent the same second-order scattering as before, and $\psi_2^{(ba)}$, $\psi_2^{(ab)}$ represent scattering first from a to b, then by b, and vice versa. The last two terms are new interference terms that are characteristic of double target scattering.

2. Predicted Experimental Signal

From the wavefunction ψ of Eq. (29) we can construct the various observables, such as the probability density

$$\begin{aligned}\rho_e = {} & \psi_0^*\psi_0 + [\psi_0^*\psi_1^{(a)} + \psi_1^{*(a)}\psi_0] + [\psi_0^*\psi_1^{(b)} + \psi_1^{*(b)}\psi_0] \\ & + [\psi_0^*\psi_2^{(aa)} + \psi^{*(aa)}\psi_0] + [\psi_0^*\psi_2^{(bb)} + \psi_2^{*(bb)}\psi_0] \\ & + [\psi_1^{*(a)}\psi_1^{(b)} + \psi_1^{*(b)}\psi_1^{(a)}] \\ & + [\psi_0^*\psi_2^{(ba)} + \psi_2^{*(ba)}\psi_0] + [\psi_0^*\psi_2^{(ab)} + \psi_2^{*(ab)}\psi_0] + \cdots \end{aligned} \tag{30}$$

The first term is $\psi_0^*\psi_0 = 1$. The next four pairs are the contributions from the two modulators acting independently, and have been discussed in several earlier sections. The next three pairs of terms represent new interferences due to the presence of both modulators. Consider the terms

$$\psi_1^{*(a)}\psi_1^{(b)} + \psi_1^{*(b)}\psi_1^{(a)} \cong \frac{2}{R^2}\sum_m \sum_n |f_m(\vec{K}_m;\vec{K}_0)||f_n(\vec{K}_n;\vec{K}_0)|$$

$$\times \cos\left[(\vec{K}_n-\vec{K}_m)\cdot\vec{R} - (\omega_n-\omega_m)t + \left(\frac{K_n + K_m}{2}\hat{R} - \hat{K}_0\right)\cdot\vec{L} + (\phi_n-\phi_m) + (\delta_n-\delta_m)\right]. \quad (31)$$

This result may be compared with Eq. (25a) in Sec. III B. The arguments we advanced there apply here also: For pairs of frequencies for which $\omega_n - \omega_m << \omega_n, \omega_m$, phase sensitive detection can be used to determine the magnitude of the contribution to the modulation $\delta\rho_e$; all other contributions average to zero and are unobservable. The terms in Eq. (30) involving $\psi_2^{(ba)}$, $\psi_2^{(ab)}$ are similar to Eq. (25b) and produce effects similar to Eq. (1).

The major new effect associated with having two modulators is the addition of a new term in the phase involving $\vec{L}$. This term is present in the diffracted beams even without the laser, but can be nonzero in the forward direction only if the laser is present.

In the forward direction, we can use $K_n - K_m \cong (\omega_n - \omega_m)/v$, $(K_n + K_m)/2 \cong (\omega_n + \omega_m)/2v$, to rewrite Eq. (31) as

$$\psi_1^{*(a)}\psi_1^{(b)} + \psi_1^{*(b)}\psi_1^{(a)} \cong \frac{2}{R^2}\sum_n \sum_m |f_n|\ |f_m| \cos\Phi_{nm} \quad , \qquad (31a)$$

where the total phase is

$$\Phi_{nm} = \Delta\omega_{nm}\left(\frac{R}{v} - t\right) + \frac{\omega_{nm}L}{v} + \Delta\phi_{nm} + \Delta\delta_{nm} \quad , \qquad (31b)$$

in which $\Delta\omega_{nm} = \omega_n - \omega_m$, $\omega_{nm} = (\omega_n + \omega_m)/2$, $\Delta\phi_{nm} = \phi_n - \phi_m$, $\Delta\delta_{nm} = \delta_n - \delta_m$.

Suppose now that only two laser frequencies ω_1, ω_2 are used. Then only a single difference $\Delta\omega = \omega_1 - \omega_2$ and average $\omega = (\omega_1 + \omega_2)/2$ are present, and Eq. (31b) reduces to

$$\Phi = \Delta\omega\left(\frac{R}{v} - t\right) + \frac{\omega L}{v} + \Delta\phi + \Delta\delta \quad . \tag{31c}$$

Some of the interesting properties of these results are examined in and below Section IV.1a.

E. GENERAL DISCUSSION OF INTERFEROMETERS

There are several features of the interferometers described above that are noteworthy:

a) The interferometer operates with massive charged particles, and therefore has potential for measuring external gravitational and electromagnetic fields.

b) The response of the interferometer depends upon parameters ($\Delta\omega_{nm}$, R, L, v, $\Delta\phi_{nm}$) which are experimentally convenient to measure, and should result in high sensitivity.

c) The response can be controlled by manipulating these parameters, so that many overlapping fringe systems (Φ_{nm}) can be isolated independently. This would allow determination of the spectral composition of the modulated beam, scattering phase shifts, and other fundamental properties.

d) The interfering beams (sidebands) need not be spacially separated. This would be of advantage in certain kinds of measurements, where a split beam would lead to a vanishing differential effect.

e) The phase of the electron signal is automatically locked to the laser, so the latter forms a perfect "local oscillator" with exact phase coherence.

It may be noted that the Q of these interferometers is low. In contrast to a multiple-beam optical interferometer (e.g. Fabry-Perot) which produces sharp fringes by superposing many reflected beams [II.9], the electron/laser interferometer superposes only two beams to produce broad fringes A + B cos Φ. The fringes are actually beats produced in de Broglie-wave interference, similar to light beats in laser mixing experiments [II.8]. Away from the forward direction, where only terms like $\psi_1^*\psi_1$ are present, the detection is homodyne--beating of the scattered wave with itself. In the forward direction, additional hetrodyne signals are produced by mixing the scattered wave with the unmodified incident wave ($\psi_0\psi_2$, etc.)

The interferometer may also be thought of as a nonlinear scattering medium, since the spectral distribution of the scattered wave contains new components. It is interesting to compare the nonlinear response of the interferometer to de Broglie waves with the nonlinear response of a real solid to electromagnetic waves (Table 4).

Table 4. Comparison of de Broglie and Electromagnetic Wave Propagation

Wave field / Medium	ψ e^-/laser interferometer	$\vec{\mathcal{E}}$ matter
Susceptibility	$\chi_e = \gamma_0 + \gamma_1\psi + \gamma_2\psi\psi + \cdots$	$\overleftrightarrow{\chi}_L = \overleftrightarrow{\alpha}_0 + \overleftrightarrow{\alpha}_1 \times \vec{\mathcal{E}} + \overleftrightarrow{\alpha} \cdot \vec{\mathcal{E}}\,\vec{\mathcal{E}} + \cdots$
Polarization	$P_e = \chi_e \psi$	$\vec{P}_L = \overleftrightarrow{\chi}_L \cdot \vec{\mathcal{E}}$
Frequencies generated	Optical sum and difference frequencies	Same
Particle density (cm^{-3})	$\rho_e \sim 1 - 10^3$	$\rho_L \sim 10^{10} - 10^{16}$
Energy density (erg cm^{-3})	$\rho_e E_0 \sim 10^{-9} - 10^{-5}$	$\rho_L \hbar\omega \sim 10^{-2} - 10^4$

It may be objected that since the modulation is probably small, the double modulation necessary to produce beats will be very small, and this may be true. However, we have said that the first-order modulation might very well be, say 10%, so the beats would be typically 1% (times geometrical factors). Due to the great sensitivity of the lock-in detection, it is not at all unreasonable to expect workable, perhaps sizeable, signals from an interferometer. This can only be determined by performing an experiment.

IV. PROPOSED OBSERVATION TECHNIQUES

In Chapter III we indicated the impossibility of detecting the modulation in linear processes. The essential result is that to detect the coherence in the modulated electron beam requires coherence in the detector. The only reasonable detection mechanisms presently known to the author are:

1. Interferometry, including analysis of the electron density (ρ_e), current ($\vec{J}_e$), momentum ($\vec{p}$), or energy ($p^2/2m$);

2. Coherent excitation, using an appropriate target, preferably with a resonant internal transition.

The theory of interferometry was described in some detail in Sec. III D; the following sections consider the experimental arrangements and techniques in more detail. These considerations form the basis for the proposed experimental work.

Coherent excitation of a target by the modulated beam has been considered by several authors [I.17,19-21], since the original experiment of Schwarz and Hora seemed to have operated this way. In contrast to the single-electron effects utilized in interferometry, coherent excitation is a cooperative process, and requires overlap of two or more electron wavefunctions at the target. We shall briefly discuss this method for completeness. Another possible approach would be to examine the modifications produced in the laser light, but for the reasons discussed in Sec. II B, this is not promising.

A. INTERFEROMETRIC DETECTION OF ELECTRON DENSITY (ρ_e)

The basic theory of this technique is developed in Sec. III D, and various specific experimental arrangements are suggested by consideration of Eq. (31b). We assume that the electron beam is detected by a linear device such as a current integrator. In general, the experimental techniques are

1) Lock-in detection (at the difference frequencies ω_{nm});
2) Vary the electron velocity v;
3) Vary the detector position R;
4) Vary the laser phases $\Delta\phi_{nm}$;

For a two-modulator interferometer, we can

5) Vary the modulator separation L;

Two other techniques that are not as accessible are

6) Vary the laser frequencies ω_n;
7) Vary the scattering phase shift δ_n.

Various combinations of these techniques lead to a variety of interesting effects.

1. Single-Modulator Interferometers

By illuminating a single crystalline film with two laser frequencies, we obtain the interferometer shown in Fig. 11. This geometry is by far the simplest

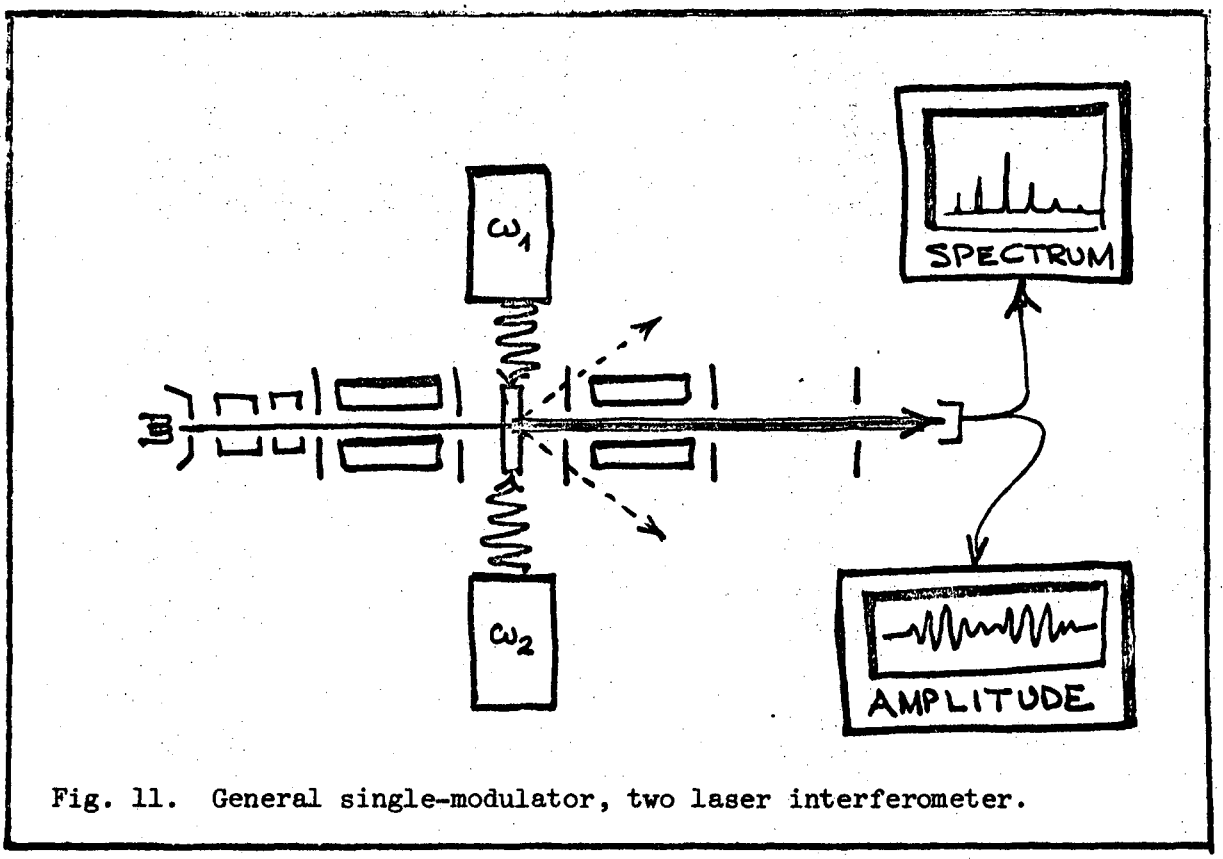

Fig. 11. General single-modulator, two laser interferometer.

and should be among the first to be tried. A single multimode laser with a series of equally spaced frequencies would be useful, since the measured spectrum would appear as a series of spikes at frequencies $\Delta\omega$, $2\Delta\omega$, $3\Delta\omega$, etc. By moving the detector along the beam direction, the sinusoidal intensity of wavelength

$$\Delta R = 2\pi v/\Delta\omega \quad , \tag{33}$$

can be observed. By varying the electron energy, the intensity will vary sinusoidally with period $\Delta E = (4\pi v/\Delta\omega R)E$. This is not a very sensitive technique, since the small $\Delta\omega$ makes the interference term relatively insensitive to the velocity.

The single-modulator device may have the greatest promise for observing the modulation, since the amplitude of the interference in a two-modulator device will be smaller by roughly D/L, the ratio of modulator size (thickness) to separation. On the other hand, the former has much less versatility than the latter, which can use mechanical coupling to increase its sensitivity.

2. DOUBLE MODULATOR INTERFEROMETERS

The double modulator interferometer produces oscillations (i.e. a fringe pattern) in ρ_e as the modulator separation L is varied. For instance, varying L while holding all other parameters constant will produce a phase change $\Delta\Phi = 2\pi$ (i.e. one full fringe) when L is changed by

$$\Delta L = \beta\lambda \quad , \tag{34}$$

where $\beta = v/c$. Thus, the peak-to-peak separation of the electron fringe is smaller than the laser wavelength λ by the factor $\beta < 1$, and in theory could be arbitrarily small. This "fringe compression effect" is similar to the reduction

in the wavelength of light moving in a medium with refractive index $n > 1$, except in this case the fringe pattern is being transferred from the light wave to the slow-moving electrons.

Experimentally, it may be difficult to hold the relative laser phase $\Delta\phi$ constant as L is varied. A more practical arrangement would use a single laser of frequency ω, and a beam splitter to direct the light to the two modulators. In this case, $\Delta\phi$ would also vary as L is changed, in the amount $\Delta\phi = 2\pi L/\lambda = \beta(\omega L/v)$. Thus, the fringe spacing is

$$\Delta L = \frac{\beta}{1 + \beta}\lambda \quad . \tag{35}$$

On the other hand, it is possible to use an optical delay line suitably mechanically coupled to the modulators to cause $\Delta\phi$ to vary arbitrarily with L. The fringes then have peak-to-peak separation

$$\Delta L = \frac{\beta}{(1 + \frac{\beta\lambda}{2\pi}\frac{\partial\Delta\phi}{\partial L})}\lambda \quad . \tag{36}$$

In particular, it is possible to negatively couple the delay line to the modulator, so that $\Delta\phi$ decreases as L increases. If we set $\Delta\phi = -\alpha(2\pi L/\lambda)$, where α is a number we can choose, we have

$$\Delta L = \frac{\beta}{1 - \alpha\beta}\lambda \quad , \tag{37}$$

and this can be larger than λ. Thus, "fringe expansion" is also possible, and could easily be made quite dramatic. In fact, it is easy to make ΔL infinite so that no fringes at all appear, or negative so that the fringes move in the reverse direction. In this operation, the interferometer acts like a Moire

fringe magnifier. Such techniques may be useful for eliminating a set of fringes associated with particular frequencies ω_n, ω_m in favor of others. This technique can be used to "zero beat" away the L dependence all the fringe patterns, or select a certain pair of frequencies to produce a single pure fringe pattern.

In addition, by zero-beating away the L dependence of Φ the strongest dependence of Φ on the velocity is also eliminated. This is seen in Eq. (31c) by setting $\frac{\omega L}{v} + \Delta\phi = 0$ (the zero-beat), leaving only the small term $\frac{\Delta\omega R}{v}$.

The fringes can also be observed by varying the observation distance R, but only if $\Delta\omega \neq 0$. In this case, moving the detector by ΔR will change Φ by $\Delta\Phi = 2\pi$ when

$$\Delta R = \frac{2\pi v/\Delta\omega}{(1 + \frac{v}{\Delta\omega}\frac{\partial\Delta\phi}{\partial R})} = -\frac{(\frac{\lambda}{\Delta\lambda})\,\beta\lambda}{1 - (\frac{\lambda}{\Delta\lambda})\frac{\beta\lambda}{2\pi}\frac{\partial\Delta\phi}{\partial R}} \quad , \tag{38}$$

where $\Delta\lambda$ is the wavelength difference corresponding to $\Delta\omega$. Since $\lambda/\Delta\lambda \sim 10^5$, the fringes are greatly magnified at the detector, and typically will be $\Delta R \sim 1$ cm. As mentioned above, it is possible to couple the optical delay line to the detector, and zero-beat the R dependence away by setting $\Delta R = \infty$.

Finally, it is theoretically possible to mechanically couple the modulators and detector so as to make $\Delta\omega\, R = \omega L + N2\pi$, N = 0, 1, 2 ... , so the dependence on R, L, ω, $\Delta\omega$, and v vanishes. This leaves only $\Delta\phi$ and $\Delta\delta$, and makes it possible to measure $\Delta\delta$, the differential scattering phase shift, by varying the laser phase $\Delta\phi$. This technique can be used to pick out a certain phase shift δ_{nm} associated with frequencies ω_n, ω_m, even in the presence of other fringe patterns merely by coupling L and R to satisfy $\Delta\omega_{nm} R = \omega_{nm} L$ and scanning $\Delta\phi_{nm}$.

Some geometries in which parts of the apparatus are coupled to give various phase relations and fringe wavelengths are shown in Fig. 12. In these

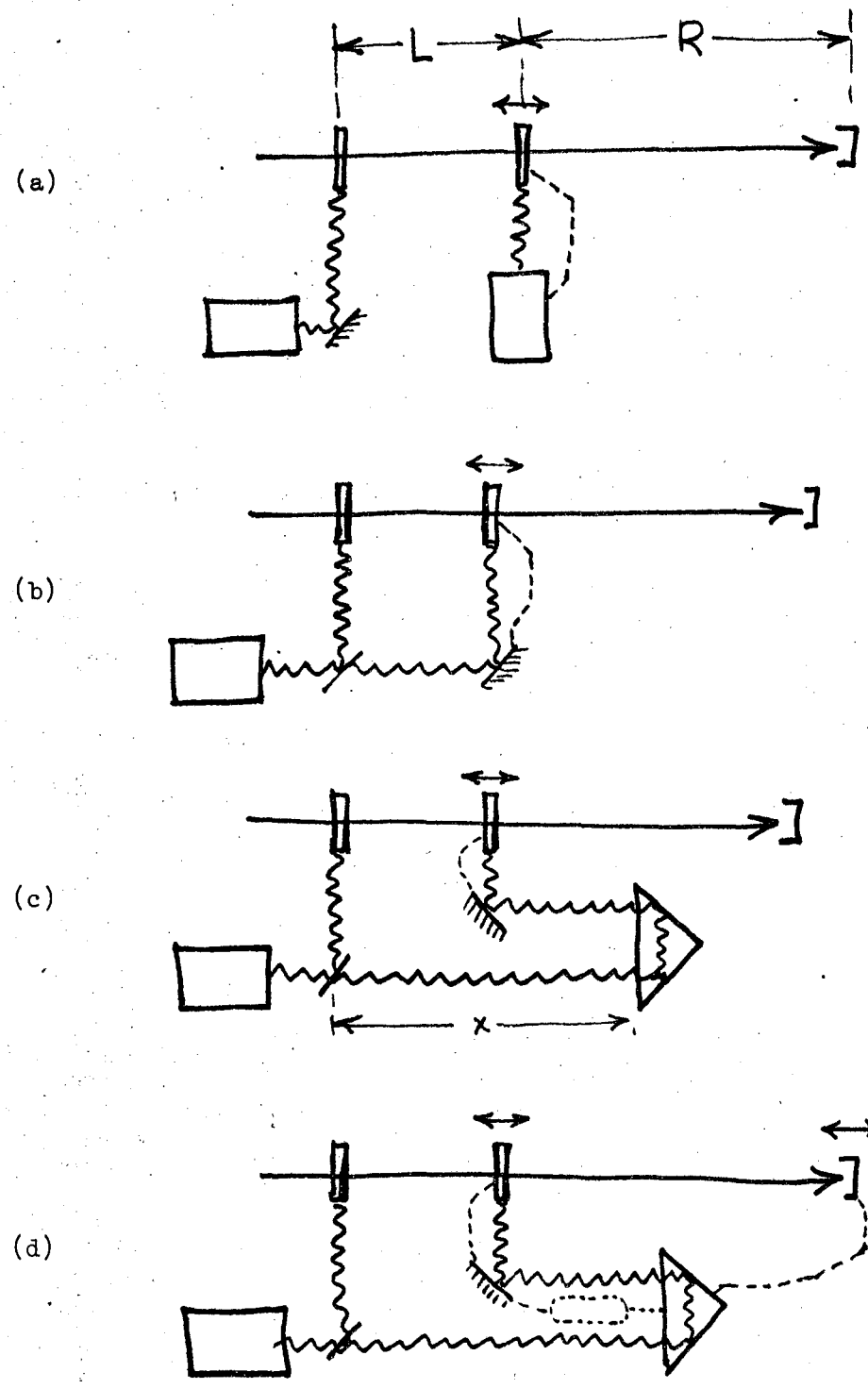

ϕ = const $\Delta L = \beta\lambda$

$\phi = 2\pi \frac{L}{\lambda}$ $\Delta L = \frac{\beta}{1+\beta} \lambda$

$\phi = 2\pi \left(\frac{2x - L}{\lambda}\right)$

$\Delta L = \frac{\beta}{1-\beta} \lambda$

$\phi = 2\pi \left(\frac{2x(R,L) - L}{\lambda}\right)$

Fig. 12. Two-modulator interferometers with various optical couplings. The dotted lines indicate mechanical coupling. (a) Constant phase coupling, producing fringe compression; (b) Positive phase coupling, producing compression with a mechanically simpler system and a single laser; (c) Negative phase coupling, producing compression or expansion; (d) A complicated system in which the second modulator, optical delay line, and detector are mechanically coupled.

diagrams, modulator a and the laser are held fixed while modulator b and the detector are varied. The total phase $\Phi = (\Delta\omega R + \omega L)/v + \Delta\phi(R,L)$ varies differently for the couplings, producing various fringe wavelengths.

So far, only forward scattering has been considered. Off-axis, there are similar effects, but some differences:

1) There is no interference with the incident wave (e.g. $\psi_0^* \psi_2$);

2) The term involving $(\vec{K}_n - \vec{K}_m)\cdot\vec{R}$ does not necessarily vanish when $K_n = K_m$ (the $\Delta\omega = 0$ case above).

Thus, we can trace out the fringes by moving the detector along the direction $\vec{R}$, even when only a single frequency laser is used. The dependence of Φ_{nm} on $\vec{R}$ and $\vec{L}$ must be determined from Eq. (31). The general conclusions reached above about mechanically coupling the modulators, detector, and optical delay lines remain valid, but the vector relations within Φ_{nm} must now be considered.

Some geometries for studying diffracted beams are shown in Fig. 13. Such devices are discussed more in the next section.

Assuming the phase matching problem is not too serious, backscattering at low energy would be of great value, since a low energy electron interacts mainly with the surface. There are certain processes that would be enhanced at the surface (e.g. those due to field gradients) and others that would be diminished (e.g. tunnelling). Diagrams of some possible devices are shown in Fig. 13 (e, f). Again, various mechanical coupling schemes can be used to control the fringe pattern, isolate individual spectral components $\Delta\omega_{nm}$, compensate for instabilities, etc.

Finally, it should be noted that coherence exists between two beams diffracted in different directions. Thus, using two detectors for two off-axis beams, and mixing the outputs will produce a fringe pattern as before, given by the

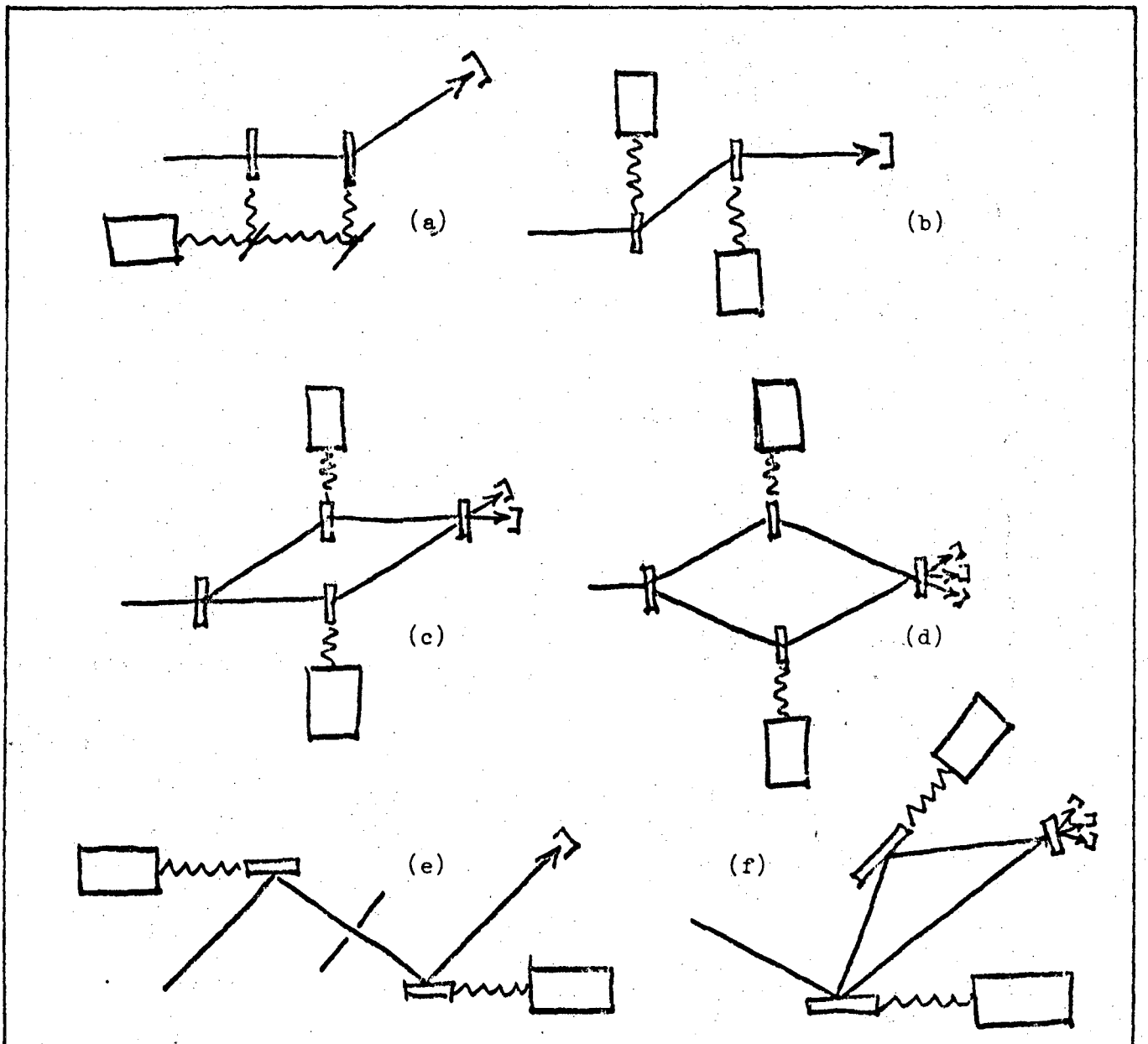

Fig. 13. Various geometries for studying laser-modulated diffracted beams.

cross-correlation function of the two diffracted beams. An experiment of this type is diagrammed in Fig. 14. However, the interference is double homodyne, and may be very small.

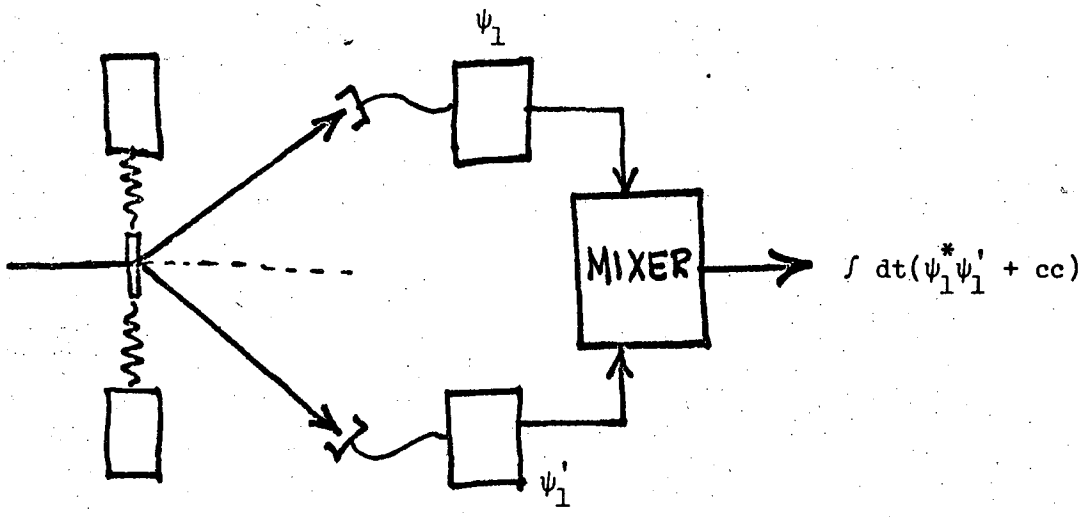

Fig. 14. A two-detector interferometer for measuring the cross-correlation function of two diffracted modulated beams.

B. DIFFRACTION PATTERN DETECTION

1. Theory

In Sec. II G.3, we showed that the first-order modulated beam can be considered a coherent superposition of three energy states, the initial energy, E_0, and two sidebands $E_0 \pm \hbar\omega$, and that these states are "real" in the sense that they conserve energy and momentum. We may then ask: What will the ordinary diffraction pattern of such a beam look like? The answer is: three separate beams, each satisfying the Bragg (or Laue) condition. This effect is understandable since the diffracting crystal Fourier analyzes the incoming beam.

The existence of spacial sidebands can be derived from the theory of Sec. II F. First, the interactions like $\delta\vec{A}\cdot\vec{p}$ and δU produce a first order modulated wave of the form of Eq. (9b). Next, this wave falls on a crystal with static periodic potential U. The diffracted wave is of the form of Eq. (9c):

$$\psi_2 = \frac{1}{R}\sum_n g_{0n}(K_{0n}\hat{R};K_n;\vec{K}_0)\, e^{i(K_{0n}R - \Omega_{0n}t)} \quad , \tag{39a}$$

where $\vec{R}$ is the vector from the diffracting crystal to the observation point, and the amplitude is

$$g_{0n}(K_{0n}\hat{R};K_n;\vec{K}_0) = f_0(K_{0n}\hat{R};K_n\hat{L})f_n(K_n\hat{L};\vec{K}_0)\,\frac{e^{iK_nL}}{L}\, e^{i\phi_n} \quad . \tag{39b}$$

We have assumed the diffracting crystal to be at a large distance L from the modulator, which is the reason g_{0n} factors into $f_0 f_n$. Thus, ψ_2 involves the factor (note $K_{0n} = K_n$)

$$f_0(K_n\hat{R};K_n\hat{L}) = \left(\frac{-m}{2\pi\hbar^2}\right)\oint d^3\vec{x}\, e^{-iK_n\hat{R}\cdot\vec{x}}\, U(\vec{x})\, e^{iK_n\hat{L}\cdot\vec{x}} \quad , \tag{39c}$$

which is the usual factor arising in kinematic diffraction. Now to obtain the diffracted beams, we expand $U(\vec{x})$ in a Fourier series

$$U(\vec{x}) = \sum_S U_S\, e^{i2\pi\vec{S}\cdot\vec{x}} \quad , \tag{39d}$$

where $\vec{S}$ is a reciprocal lattice vector. When this is substituted into Eq. (39c), the integral vanishes unless

$$K_n(\hat{R} - \hat{L}) + 2\pi\vec{S} = 0 \quad . \tag{40a}$$

This is precisely the Laue equations. By multiplying by $\hat{S}\cdot$, and using $\hat{R}\cdot\hat{S} = -\hat{L}\cdot\hat{S} \equiv S\cos\theta$, $S = N/d$, $N = 1, 2, \ldots$, (d = lattice spacing), and $K_n = p_n/\hbar$, we obtain

$$2d \sin\theta = N\frac{h}{p_n} \quad , \tag{40b}$$

which is the usual Bragg condition. Thus, the beam is diffracted into angles satisfying Eq. (40b), and there will be a different angle for each component p_n. We therefore conclude that $f_0(K_{0n}\hat{R};K_n\hat{L})$, and therefore $g_{0n}(K_{0n}\hat{R};K_n;\vec{K}_0)$, is negligibly small except at the Bragg angles $\theta = \theta_n$, which in turn means that ψ_2 has only one component at each angle. This proves that diffraction of the modulated beam will spacially separate the sidebands.

The wavefunction ψ_2 in Eq. (39), even though it is second order, is unobservable as the interference $\psi_0^*\psi_2$, since it was generated in a single photon process, and oscillates too rapidly. Observable effects can occur by considering the diffraction of a second-order modulated beam, an overall third-order event. A diagram of this process is shown in Fig. 15. In this case, the wavefunction will be

$$\psi_3 = \frac{1}{R}\sum_n\sum_m h_{0nm}(K_{0nm}\hat{R};K_{nm}\hat{L};K_m;\vec{K}_0)\, e^{i(K_{0nm}R - \Omega_{nm}t)} \quad , \tag{41a}$$

where $K_{0nm} = K_{nm}$, and

$$h_{0nm}(K_{0nm}\hat{R};K_{nm}\hat{L};K_m;\vec{K}_0) = f_0(K_{nm}\hat{R};K_{nm}\hat{L})\, g_{nm}(K_{nm}\hat{L};K_m;\vec{K}_0)\, \frac{e^{iK_{nm}L}}{L}\, e^{i(\phi_n + \phi_m)} \quad . \tag{41b}$$

Thus, the Laue equation from $f_0(K_{nm}\hat{R};K_{nm}\hat{L})$ is

$$K_{nm}(\hat{R} - \hat{L}) + 2\pi\vec{S} = 0 \quad , \tag{41c}$$

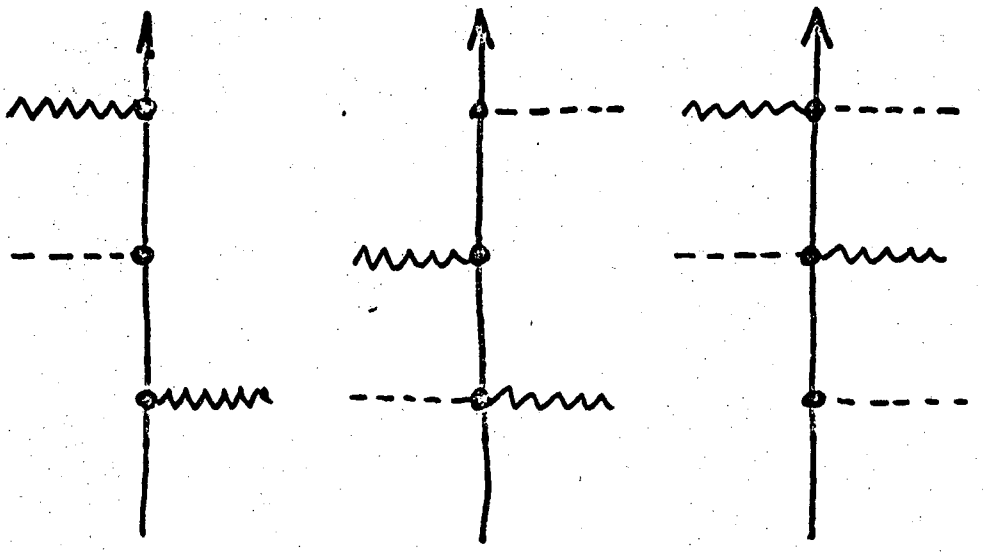

Fig. 15. Typical third-order, two photon diagrams which are involved in laser modification of electron diffraction patterns. There are many such diagrams, corresponding to all possible permutations of combinations of lines and vertices.

and the Bragg condition is

$$2d \sin \theta = N \frac{h}{p_{nm}} \quad . \tag{41d}$$

Suppose a single laser frequency difference $\Delta\omega$ is present, so that $\Omega_{nm} \Rightarrow \Delta\omega$, which is within detectable range. Then since $p_{nm}^2 = p^2(1 + \hbar\Delta\omega/E_0)$, the diffracted beams appear at the Bragg angle for E_0, and at two sideband angles separated from the E_0 beam by $\pm \Delta\theta$, where

$$\Delta\theta \cong - \frac{\hbar\Delta\omega}{2E_0} \tan \theta \quad . \tag{42}$$

We conclude that it is kinematically possible to detect modifications in the passive diffraction pattern of a laser modulated beam. The modifications will appear as weak secondary spots located symmetrically about the unshifted

spot, and lying in the plane containing the incident and diffracted beams. The angular separations will be larger for beams nearer the 180° backscatter directions, and should appear only if two or more laser frequencies are present. These predictions are illustrated in Fig. 16.

For $\theta = 45°$, $\Delta\omega \sim 10^9$ Hz, $E_0 = 50$ keV, we have $\Delta\theta \sim 5 \times 10^{-11}$ which is much too small to detect.

However, we have several parameters at our disposal: $\Delta\omega$, E_0, and θ. Clearly, we want, as nearly as possible: large $\Delta\omega$, small E_0, and an angle θ near 90°, which corresponds to 180° backscattering. From Eq. (41d), the angle θ depends on the crystal lattice spacing d, the energy $E_0 = p^2/2m$, and a set of integers $N = 1, 2, \ldots$. Combining Eqs. (41d) and (42),

$$\Delta\theta = - \frac{1}{\sqrt{\left(\frac{2d}{Nh}\right)^2 2mE_0 - 1}} \frac{\hbar\Delta\omega}{2E_0} \quad . \tag{43}$$

This result tells us that we should choose a crystal with a small spacing d, and examine the pattern at the proper angle to observe the N^{th} order diffracted beam. The intensity of the higher order beams is lower, but their dispersion is greater.

The largest $\Delta\omega$ available will be determined by the coherent mode structure of the laser: it could be as large as 10^{10} Hz.

The smallest energy E_0 available is determined by the requirement Eq. (41d) that the crystal diffract the beam, namely $E_0(\text{min}) = (h/2d)^2/2m$. This gives $\theta = 90°$, where the dispersion is theoretically infinite. However, we cannot observe the beam at this angle, but only at some angle. Suppose we assume $E_0 = 25$ eV $\doteq 5.9 \times 10^{15}$ Hz. For a cubic crystal with $2d = 8$Å, and $N = 2$ this

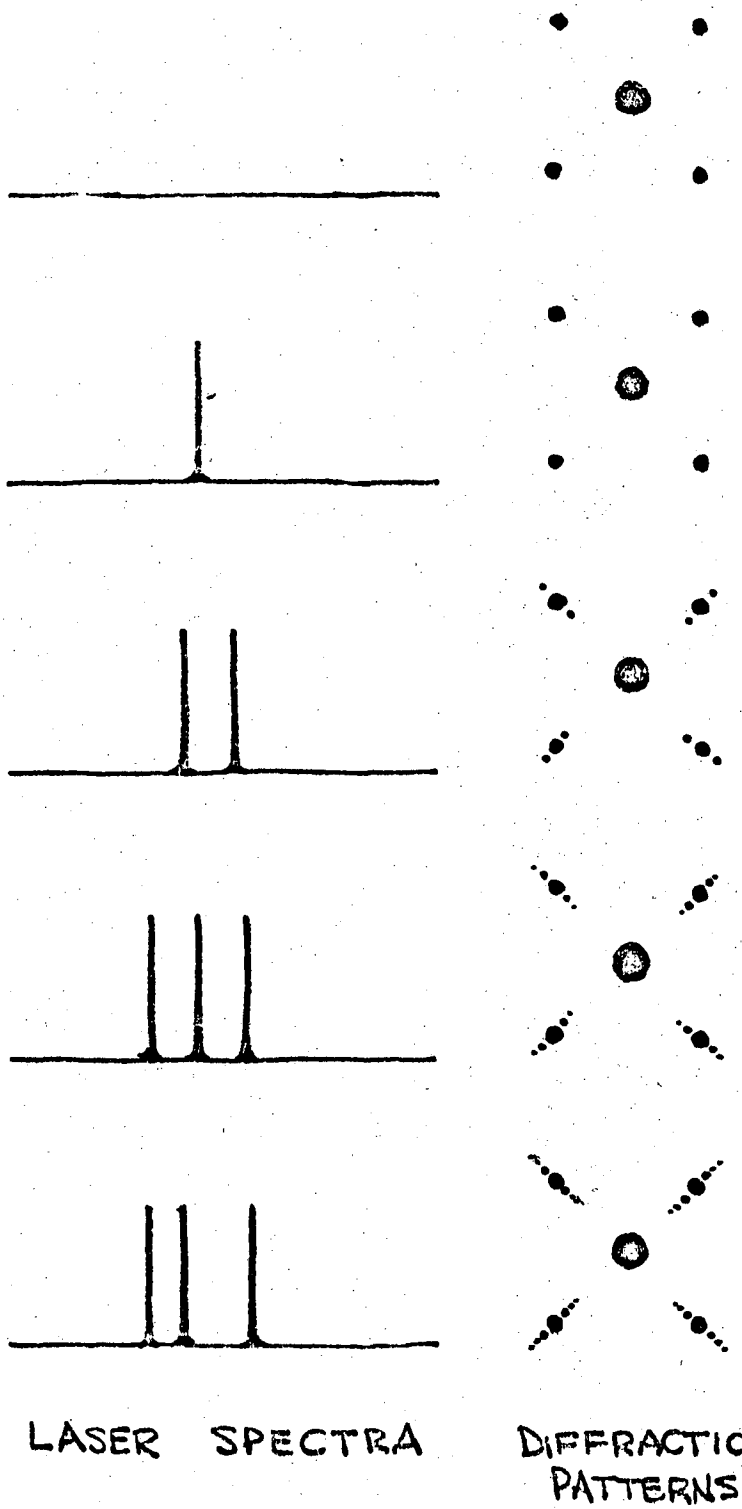

Fig. 16. Predicted modification of electron diffraction patterns, for various laser spectra. Satellite spots appear separated from the normal spots by amounts determined by the laser difference frequencies.

implies sin $\theta = 0.97$, or $\theta = 76°$. Using tan $76° = 4.0$, we find, from Eq. (42), $\Delta\theta = 0.6 \times 10^{-5}$. This is approaching the range of present experimental techniques [VIII.11], and more favorable numbers can certainly be obtained by judicious choice of the parameters. But we have not taken into account the variety of problems such as angular dispersion, finite beam width, surface irregularities, etc., which will operate to defeat precision angle measurements.

We therefore conclude that such measurements will be difficult, if not impossible, with present techniques. This conclusion may be reversed if the parameters can be more favorably adjusted, or if the other terms such as $(\delta U)(\delta\vec{A}\cdot\vec{p})$, which produce effects similar to the (U)(2 photon modul.) terms discussed above, are found to give an enhanced effect. It is possible that a high-efficiency nonlinear optical frequency multiplier (harmonic generator) might become available that would provide phase-locked laser photons at ω, 2ω, 3ω, ... , generating difference frequencies of ω, 2ω, 3ω, ... This would generate angle sidebands at $\Delta\theta = -(N\hbar\omega/2E_0)\tan\theta \sim 10^{-3}$ which is well within the range of present experimental techniques, but then we would again have the problem of finding a lock-in detector that operates at the high frequency ω.

2. Experimental Techniques

Since the prospects for detecting laser induced spacial shifts in diffraction patterns presently appear unfavorable (although by no means ridiculously so), we shall keep this discussion to a minimum. A possible experimental arrangement is shown in Fig. 17. In this experiment, a second-order modulation is induced in the beam during diffraction from a thin film guiding the laser beam. Terms like $(\delta U)(\delta A\cdot\vec{p})$ will generate angle sidebands that oscillate slowly (GHz); they are detected by a differential "slit" and lock-in detector.

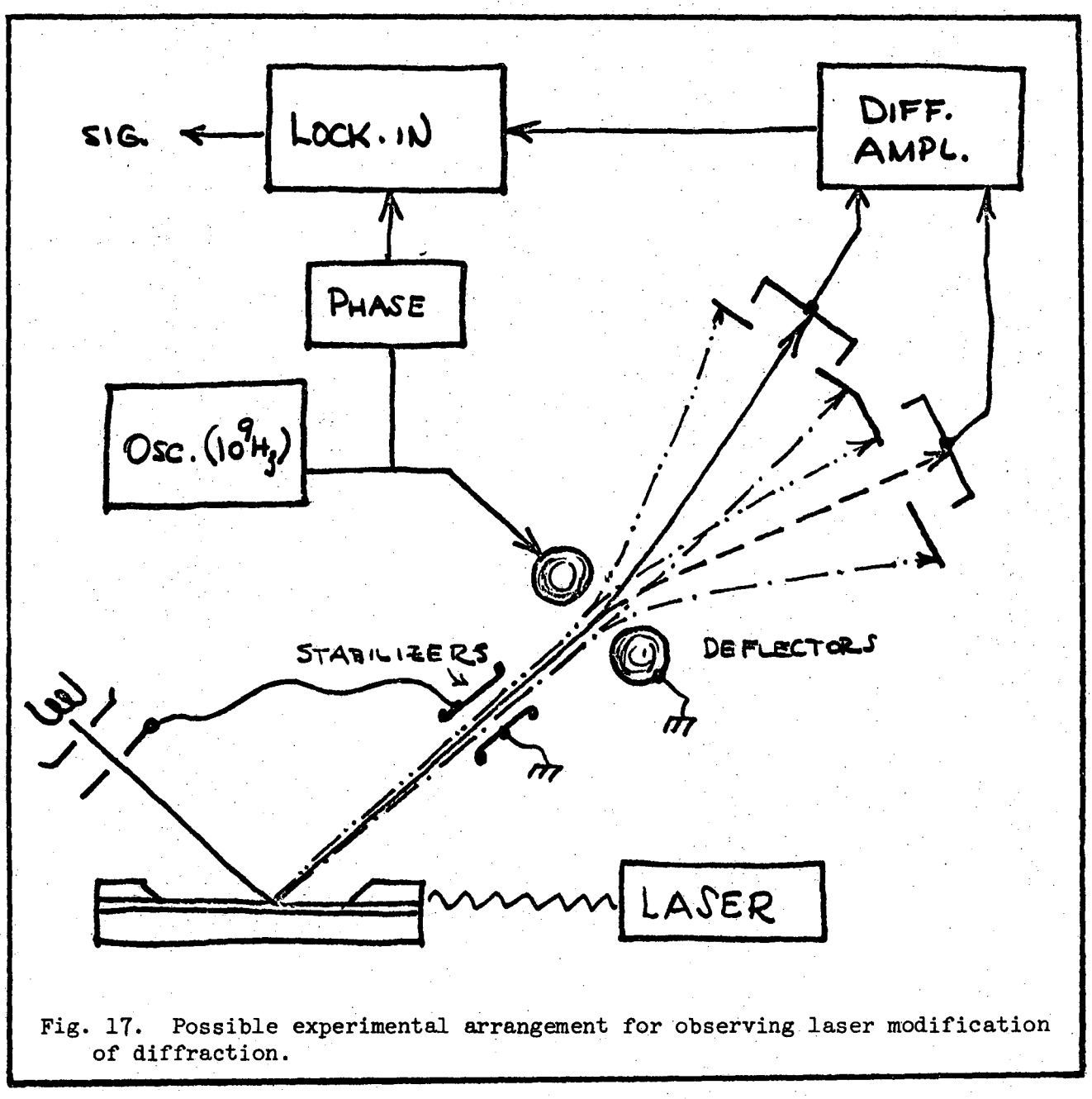

Fig. 17. Possible experimental arrangement for observing laser modification of diffraction.

Some other geometries are illustrated in Fig. 18. The hybrid system in Fig. 18a may be useful if the modulation efficiency at low energies is too small. This device would respond to terms like $(U)(\delta A\cdot\vec{p})(\delta A\cdot\vec{p})$ and $(U)(\vec{A}\cdot\vec{p})(\delta U)$. The magnetic system in Fig. 18b has the advantages that both modulations occur in 180° backscattering, thus reducing the secondary electron background, and that the same crystal is used for both modulations.

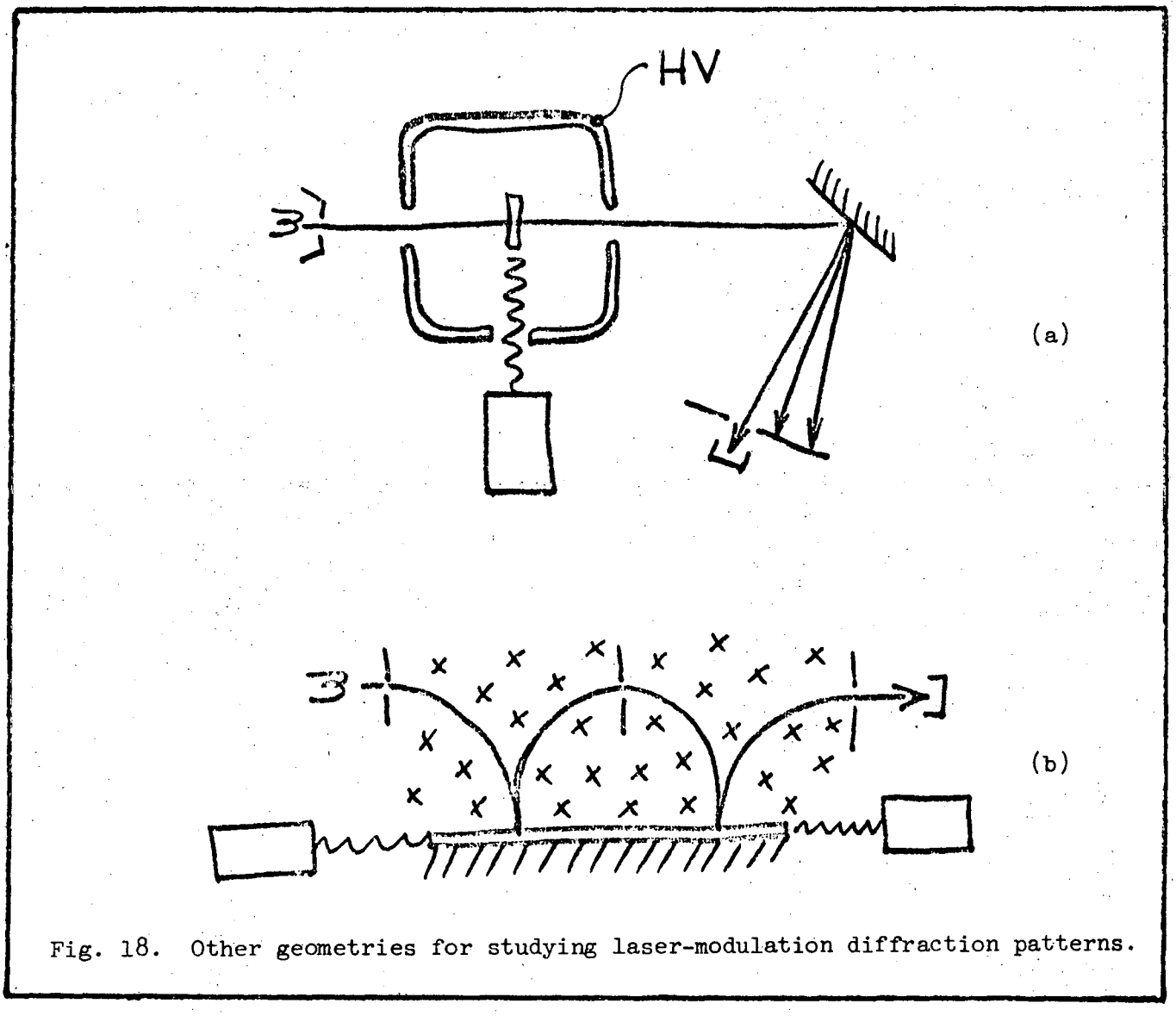

Fig. 18. Other geometries for studying laser-modulation diffraction patterns.

C. MOMENTUM ANALYSIS

In Sec. II G it was shown that the modulation produces oscillating sidebands on various observables, including the momentum $\vec{p}$. Under certain conditions, no momentum is transferred to the electrons, and no sidebands are present. The forward-scattered notch effect is one such arrangement. However, in a general case momentum sidebands are produced and presumably could be separated with a suitable analyzer. This may be a reasonable technique since an analyzer will certainly be necessary to reject the grossly inelastic beam. However, the sidebands oscillate at the laser frequencies, and thus appear as high-frequency AC currents, and as discussed before, will therefore be unobservable. It is only the second order shift appearing at low frequency, or DC, that is detectable; its magnitude will depend on the dynamics of the apparatus.

D. ENERGY ANALYSIS

Most of the remarks of the previous section apply here also. The second order shift in the expectation value of the energy should in principle be detectable with an energy analyzer, and this may prove feasible. Whether or not it does depends on the analyzer resolution, magnitude of the shift, etc.

E. COHERENT EXCITATION

The presence of coherence in the electron beam makes it intuitively reasonable that new interference effects should be manifested in inelastic scattering, as well as the elastic processes with which we have so far been concerned. The rapid oscillation among the energy states E_0, $E_0 \pm \hbar\omega$, ... means that the laser frequencies are present in a fundamental way, and in transferring energy

to an appropriate target, we would expect these frequencies to enter in a fundamental way. We may consider two types of targets: 1) linear (nonresonant) targets; 2) targets containing a transition resonant with ω.

It has been demonstrated [I.16,17] that if the target has no internal structure resonant with the laser frequency, no enhancement of energy transfer above the incoherent (no laser modulation) value occurs at that frequency. In other words, a linear target responds essentially the same to the incident beam whether it is in a superposition of eigenstates or not.

Several workers [I.17,19-21] have shown that if the modulated beam strikes a target (such as a solid) with an internal transition at the modulation frequency ω, the scattering cross section will be enhanced over the nonresonant value. It will exhibit the resonant shape of the transition and a spacial modulation at the wavelength Λ_2 as well. A large enhancement at the frequency ω is possible because it involves only energy differences, in contrast, for instance, to producing diffraction angle sidebands, which involve absolute energies. However, this mechanism is not a single-electron effect, and requires the overlap of two or more electron wavefunctions at the target, within the relaxation time of the target. Thus, it depends on the square of the beam current, which will be very small in a highly monoenergetic beam. Indeed, the failure of others to reproduce the Schwarz-Hora experiment [I.25,30] is evidence that such cooperative effects are small, at least for the conditions of the existing experiments.

This proposal does not contemplate developing this kind of experiment. It is possible that later study will reveal more favorable materials and design parameters.

D. MODIFICATIONS OF THE LASER BEAM

In principle, the laser beam is modified in its interaction with the electrons and the solid, and the three-field effects could be observed in these modifications. Certain classical effects, such as Thomson scattering in a refractive medium, diffuse diffraction from electron induced lattice vibrations, and modification of optical absorption by electron excitation and ionization processes, will modify the classical laser field in gross and observable ways. However, all these mechanisms couple the electrons to the laser incoherently, and are therefore not of interest in this proposal. The coherent coupling mechanisms all involve only a few photons, and such changes are unobservable in the laser beam.

V. EXPERIMENTAL PROBLEMS, POSSIBLE SOLUTIONS, DESIGN CRITERIA

A. GENERAL

We now consider in more detail the difficulties we expect to encounter in performing experiments like those described in Chapter IV. The components in a typical experiment are illustrated in Fig. 19, and include:

1. Electron spectrometer, including high voltage terminal, electron gun, velocity analyzer, accessory optics, and electron detectors;
2. Target system, including crystalline thin films and bulk crystals, temperature control, facilities for monitoring condition, etc.;
3. Laser system, including high power laser and accessory optics and diagnostic equipment.
4. Ultrahigh vacuum system.
5. Mechanical system for alignment, motion feed-thru, etc.
6. Electronics, including power, modulating and pulse counting equipment.

We shall consider each of these systems separately, and some special problems associated with reflection geometry, two-modulator interferometers, and operating techniques. In the following sections we shall not present a complete analysis for any particular apparatus--such analysis should be reserved for the engineering design study. What we shall do is note the essential requirements for experiments of this type, indicate whether existing materials and techniques are adequate, point out where difficulties might arise, and in some cases, suggest possible ways to overcome such difficulties.

1. Counting Rate

The most general limitation (and our ultimate concern) in these experiments will be the counting rate and signal-to-noise. It must be possible to get meaningful data over a period of hours at the most, since even if stability could be guaranteed, the necessity to make many different measurements would preclude longer runs. Since the background in the best electron detectors is somewhat

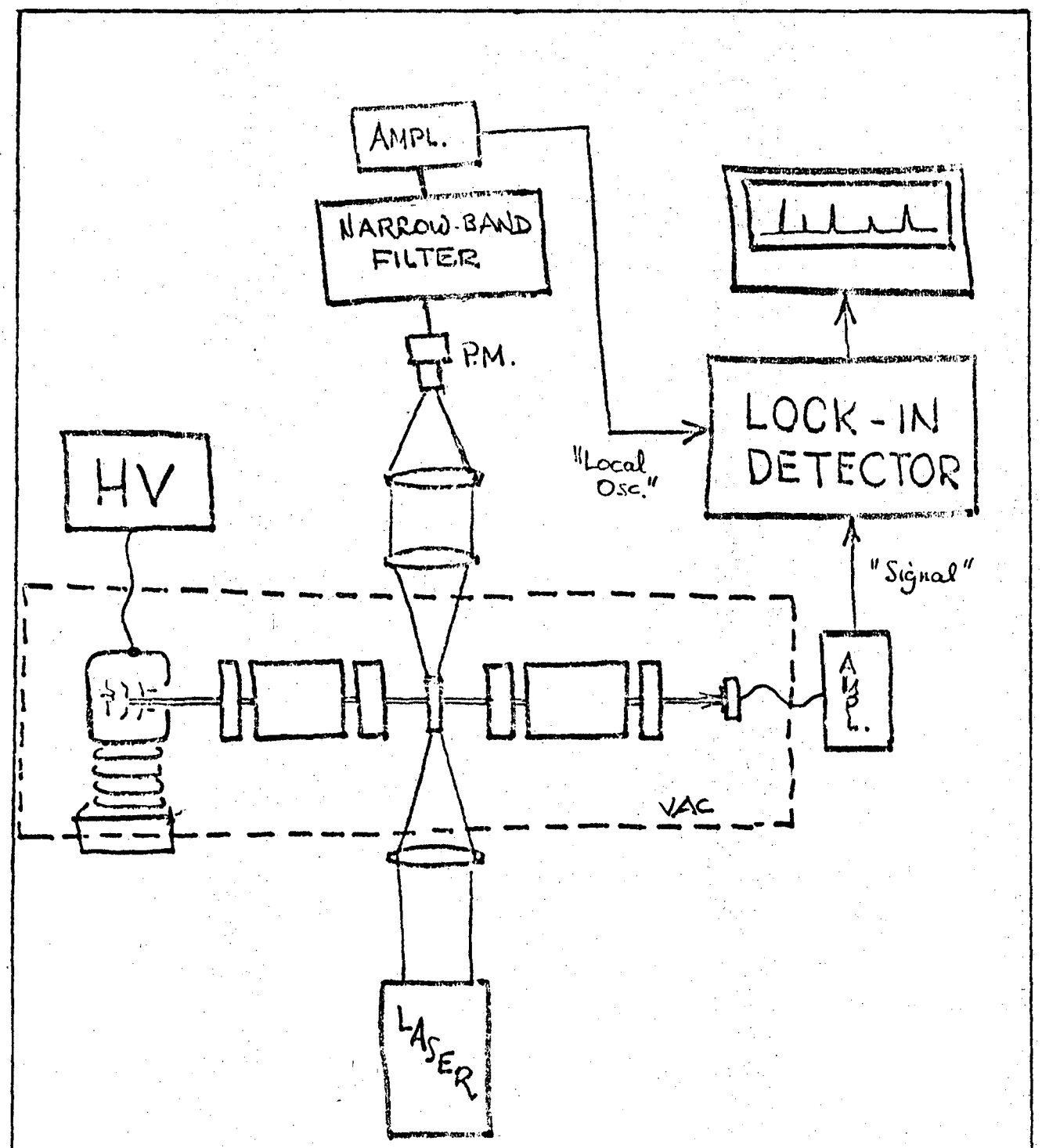

Fig. 19. General single modulator experiment, showing essential components.

below 1 count/sec, we can adopt this value as a lower design limit. This will yield 10^5 counts in 30 hours and if we are looking for a 1% effect (containing 10^3 counts), the signal-to-noise will be about 3:1 (sufficient to see the effect but not to do much with it). Alternatively, if we are able to achieve an average electron current of the order of nanoamps ($\sim 10^{10}$ electrons/sec), then in 3 hours we will have 10^{14} electrons, and a 0.001% effect containing 10^9 electrons will have a statistical error of only 1%, which should make practical devices a reality. We expect our apparatus to fall between these limits.

2. Need For Energy Spectrometer

Our need to measure the energy spectrum of the modulated beam arises from out need to isolate the coherent three-field processes from the two-field and incoherent ones. With or without the laser, the electrons lose energy in a variety of mechanisms:

1. Lattice (phonon) excitations ($\sim$ meV)
2. Optical excitations ($\sim$ eV)
3. Many body (plasmon) excitations ($\sim$ 10 eV)

In addition, the measured energy spectrum will be partly due to:

4. Auger emission
5. Secondary emission
6. Thermionic emission

There are several effects due to the presence of the laser that modify the energy spectrum:

7. Photoelectric emission
8. Heating of the solid (phonon generation)
9. Optical pumping of the solid

These are examples of three-field classical processes; they are incoherent in the sense that they involve single electrons in pure energy eigenstates.

Thus we conclude that we will require a high resolution electron monochromator/spectrometer for two basic purposes: 1) Isolate the elastically scattered beam to detect and study the coherent modulation effects; 2) Study the incoherent processes to aid in understanding the coherent ones.

These are many types of monochromators in use; the relative merits and deficiencies of some types will be discussed. The general conclusion is that a transmission spectrometer with energy 100 keV and resolution 1 meV can be built with reasonable effort and expense, and that this is sufficient to study the modulation process.

3. Need For Electron Diffraction Monitor

The same general argument given above for studying the energy spectrum applies here also, namely the need to understand the classical effects. Several effects will be important:

1) Thermal diffuse diffraction
2) Density changes
3) Stress induced defects
4) Channelling
5) Laser induced changes due to heating, such as annealing, evaporation of surface layers, etc.

We conclude that it will be necessary to observe the electron diffraction pattern in order to: 1) Isolate diffracted beams in order to study the modulation mechanisms; 2) Monitor the state of the crystalline solid.

Due to the requirement of high energy resolution, conventional PbS fluorescent screens for observing diffraction patterns will not be sufficient for high resolution work, although they should be provided for low resolution studies. It is proposed that the energy analyzer be movable so that it can scan individual diffraction spots. An angular resolution of 10^{-4} rad. and a range of 2π steradians should be achievable without undue effort.

B. ELECTRON BEAM

In the ideal case, the beam would be parallel and monoenergetic with infinitessimal cross section propagating from the source through the target to the detector. To the extent these criteria are not met, the quality of the signals will be degraded. The most critical problem is maintaining the beam coherence over paths long enough to observe the interference effects.

1. Need For High Energy

At least some of the modulation mechanisms, such as $(\delta\vec{A}\cdot\vec{p})$, $(U)(\vec{A}\cdot\vec{p})$, etc., are proportional to the momentum. Hence, the amplitude of the modulation will increase as $\vec{p}$ is increased, so a high energy (E_0 = 10 - 100 keV) beam is preferable to a low energy (E_0 = 10 - 1000 eV).

There is another reason for using very high energy: The energy loss per unit length in the target decreases at higher energy, roughly proportional to $E_0^{-1}\ \ell n\ E_0$. Thus, high energy is desirable both to maintain coherence in the modulated beam and to reduce heating of the target.

Energies up to E_0 = 100 keV are regularly used in electron spectrometers and microscopes; the power and insulation requirements are moderate and components are readily available commercially. To go to higher energies takes one into a new technological and financial domain, although the effects may be correspondingly easier to observe.

On the other hand, there are mechanisms, such as (δU), which do not increase with the momentum. Such effects may be primarily surface effects, with only the first few atomic layers contributing. At low energies ($E_0 < 10^3$ eV), electrons incident on a surface interact with roughly

$$\frac{\Delta x}{d} = 2 + \left(\frac{eV}{150}\right)^2 \qquad (44)$$

atomic layers of thickness d [VII.6]. To probe surface layers thus requires about 100 eV, the normal LEED range. At such energies, the bulk modulation effects ($\delta\vec{A}\cdot\vec{p}$), etc.) are probably negligible, and one might hope to isolate two regimes of modulation phenomena.

We thus conclude that the proposed apparatus should operate at energies up to 50 - 100 keV, but if possible, also be capable of low energy diffraction in the 100 eV range.

2. Energy Resolution

a. Coherence Requirement

The essential requirement for observing the quantum-mechanical modulation is that the electron coherence be maintained over appreciable distances. The effect of a distribution of velocities will be to reduce this coherence, hence reduce the observed effects. There are several ways in which this can be pictured. For instance, the modulator attempts to impress modifications on the electron wave train as it goes past, with wavelength $\Lambda_1 = \beta\lambda$. For this to work, the wave train must clearly be much longer than Λ_1. The length of a train of waves with energy distribution $\Delta E_0 = FW(\frac{1}{e})M$ moving in a straight line with velocity v is

$$\Delta x_L = \frac{v}{\Delta E_0/\hbar} \quad . \qquad (45)$$

The criterion $\Delta x_L >> \beta\lambda$ then implies

$$\Delta E_0 << \frac{\hbar c}{\lambda} \quad . \tag{46}$$

For λ = 5000 Å, this yields $\Delta E_0 << 0.4$ eV, say $\Delta E_0 \sim 0.004$ eV. If this resolution can be attained, roughly 100 optical cycles can be impressed on the electron wave.

The general aspects of interference between two partially coherent waves has been presented by Gabor [II.1]. The starting point is the experimental signal, given by a formula like Eq. (23), with $\rho_e = \psi^* \psi$. By a double Fourier transform, the integration over time t can be replaced by an integration over all initial energies E_0. If we assume that waves of energy E_0 are present with amplitudes multiplied by exp $- [(E_0 - E_{00})/\Delta E_0]^2$, where E_{00} is some central energy and ΔE_0 is the FW($\frac{1}{e}$)M spread, then it can be shown that the integral of the interference terms such as $\psi_1^* \psi_1$ (Eq. (31)) is multiplied by the factor

$$\zeta = e^{-2(g \frac{\Delta E_0}{\hbar} \frac{\Delta x}{v})^2} \quad , \tag{47}$$

where Δx is the path distance from the point where coherence was introduced, and g is a number dependent on the geometry (usually g = 1). Clearly this requires (for a straight path Δx = R),

$$\Delta E_0 << \frac{\hbar v}{\sqrt{2}\, gR} \quad , \tag{48}$$

which for g = 1 and v/c = 0.41 (E_0 = 50 keV), is $\Delta E_0 << (0.5 \times 10^{-5}$ eV-cm/R). This is a very stringent requirement: Even for R = 10^{-3} cm, $\Delta E_0 << 0.005$ eV, which is certainly a difficult problem for the two-modulator transmission interferometer of Fig. 9. For a single modulator of thickness $\sim 10^{-5}$ cm, the requirement ($\Delta E_0 << 0.5$ eV) is not serious.

In fact the problem of the energy spread can be almost totally eliminated, by using an achromatic interferometer. For such a device, $g = 0$, so that Eq. (47) becomes $\zeta = 1$, and there is no reduction in the interferometer fringes, even at very large distances. To see how this comes about, consider the geometrical factor [II.1]:

$$g = 1 + \frac{2E_0}{\Delta x} \frac{d}{dE_0} \Delta x \quad , \tag{49}$$

in which Δx is the path length. This equation results from considering the optical phase along various possible trajectories. In many devices, the trajectory, hence the path length, depends upon the energy E_0; i.e., the device has chromatic aberration ($g \neq 1$). In certain devices, two elements can be combined so that their individual chromatic aberrations exactly compensate, thus making the second term in Eq. (49) equal to -1, or $g = 0$. By great fortune, a diffracting crystal obeying Bragg's law is such a device.

The principle of an achromatic Bragg doublet is illustrated in Fig. 20. Two rays of slightly different momenta δp approach a crystal with a slightly diverging angle $\delta\theta$. If these rays are near a Bragg angle θ for momentum p, and $\delta\theta = \cot\theta(\delta p/p)$, then the Bragg condition $d\cos\theta = N(h/p)$ is satisfied, and the rays exit parallel, but slightly displaced. At the second crystal, the rays regain their original directions and divergence, with no relative phase shift. The only effect of the interferometer is to "cut" the rays and "displace" them by the crystal separation. The apparent source is displaced by the same amount.

A possible practical achromatic interferometer is illustrated in Fig. 21. In this configuration, the doublet is one leg of a Marton type electron interferometer [II.3-6]. It is clear that such a device will be able to reduce the

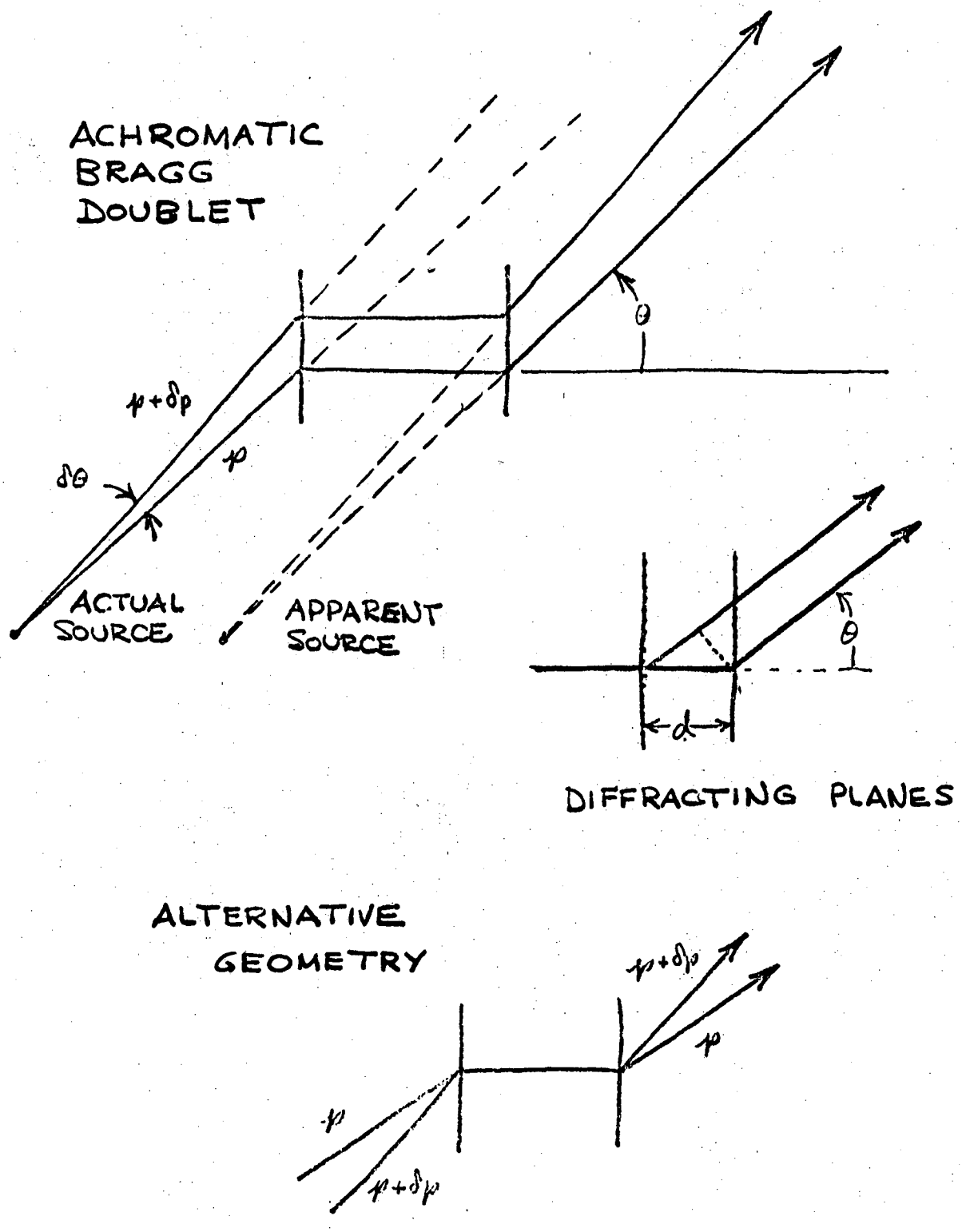

Fig. 20. Principle of the achromatic Bragg doublet. Two identical thin crystals produce zero net dispersion. The exiting beam has the same divergence as the incident beam, but the apparent source is displaced. For this to occur, the incident beam must have momentum dispersion proportional to its angular dispersion, a situation that can be realized using chromatic aberration in the monochromator. If the incident beam converges to a point on the first crystal, all beams pass to the second crystal on the same path.

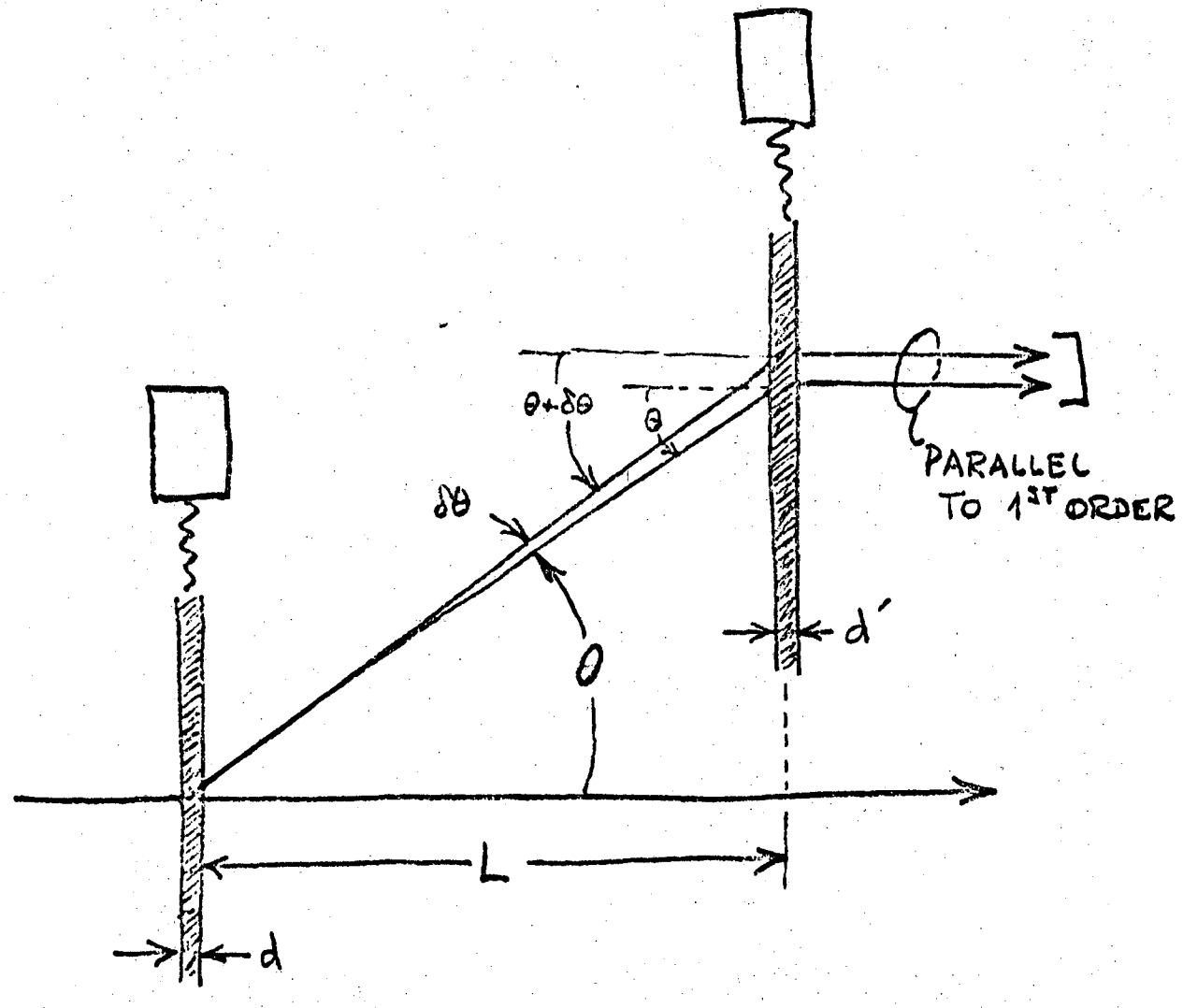

Fig. 21. Achromatic laser modulated electron interferometer. The incident beam has a distribution of momenta which produces a diffracted beam diverging from the first crystal. The path length to the second crystal is longer for larger momenta, producing a constant optical path length.

value of g to a very small value, determined mainly by the crystal perfection, the optical aberrations of the monochromator, and the apparent size of the cathode. It may be noted that if it is possible to produce slightly curved thin film crystals, a slight additional angular dispersion can be introduced which will make the Bragg doublet overall focussing.

We are also interested in the effects of energy spread on the observed interferometer fringes themselves, typically given by Eq. (31). We can ignore the

slow dependence of $|f_n|$ on the velocity v, and consider only the phase factor Φ, Eq. (31c). As one possible criterion for observing the fringes, we could require a shift δv to produce a phase shift $\delta\Phi \ll 2\pi$. Thus

$$\delta\Phi = \frac{1}{v}(\Delta\omega\, R + \omega L)\frac{\delta v}{v} \ll 2\pi \quad , \tag{50}$$

which can be rewritten

$$\frac{\Delta E_0}{E_0} \ll \frac{2\beta\lambda}{(\frac{\Delta\omega}{\omega})R + L} \quad . \tag{50a}$$

For $E_0 = 50$ keV, $\beta = 0.41$, $\lambda = 5000$ Å, $\Delta\omega/\omega = 10^{-6}$, R = 10 cm, L = 1 cm, we find $(\Delta\omega/\omega)R \ll L$, and $\Delta E_0/E_0 \ll 4 \times 10^{-5}$, or $\Delta E_0 \ll 2$ eV, say $\Delta E_0 \sim 0.020$ eV. This condition is essentially the coherence condition Eq. (48). It is interesting to note that the required energy resolution is not strongly influenced by the observation distance R, for forward scattering, and that the achromatism is achieved just for forward scattering.

We conclude that in order to observe the modulation interference in the forward direction, an energy resolution roughly $\Delta E_0 = 1$ meV at $E_0 = 50$ keV is necessary, but that by using an achromatic Bragg interferometer, the fringes can be easily seen over large distances ($\sim$ cm) with resolution in the range $\Delta E_0 \sim 10$ meV. Resolution in this range has been attained by several groups [X.8,11] using very carefully designed spectrometers of conventional design. Accordingly, this proposal will adopt $\Delta E_0 < 10$ meV as a design requirement, and $\Delta E_0 < 1$ meV as a design objective.

b. Essential Analyzer Characteristics

One fundamental problem with focusing analyzers is that various paths are different lengths, which would lead to a distribution of phases of the modulated beam and a blurring of the interference patterns. This suggests we select an analyzer with very small angular aperture, a condition consistent with the requirements of high velocity and angular resolution, but also imposing small transmitted current.

It is also important that the analyzer be as small as possible, with dimensions of the order of cm. To compensate for reduction of dispersion with size, it is usual, and in this work necessary, to pass the beam through the analyzer at a very low energy, say $E_0 \sim 10$ eV. Since we probably must perform the modulation at high energy ($E_0 \sim 50$ keV), this means we must monochromatize the beam at low energy, accelerate it to high energy to penetrate the modulating target, then decelerate it to analyze it. It will be necessary to obtain an absolute calibration of the analyzer from its geometry and applied fields, but this is not as important as stability.

c. Existing Velocity Analyzers

Electron velocity analyzers are widely used, and the literature relating to their design and performance is extensive [X.1-30]. The author has investigated various designs in relation to the proposed experiments. These include electrostatic and magnetic lenses, quadrupoles, mirrors, and various deflecting geometries including parallel plates, cylinders, spheres, and sector prisms, as well as retarded-field and pulsed time-of-flight spectrometers. Typical performance for most of the optical devices (lenses and prisms) is a resolution $\Delta E_0 \sim 10 - 50$ meV

for beam currents of 10^{-11} to 10^{-7} eV, energies $E_0 \sim 10$ - 100 eV, and angular apertures $\Delta\Omega \sim 0.1$ - 10 mrad. In some cases, somewhat better energy resolution ($\Delta E_0 \lesssim 10$ eV) was obtained by sacrificing beam current.

It thus appears that existing analyzers are very nearly sufficient to detect the modulation interference effects. On the other hand, if we hope to make precision measurements with 1 meV resolution, we will need to improve the performance somewhat.

Some analyzers are commercially available. For instance, Picker supplies a double-focusing concentric spherical electrostatic analyzer with a resolution of $\Delta E_0 = 10$ meV at $E_0 = 5$ eV, although at rather low currents. The author is not aware of a commercial system that he would recommend for these experiments.

d. Limitations of Resolution and Possible Improvements

Faced with the possible need to improve the state-of-the-art in analyzers, the author has considered some of the limits on their present performance. The following principle guided these considerations: In order to measure energies with error less than ΔE_0, the line integral of all forces over any trajectory must have an uncertainty less than ΔE_0. In other words, to measure E_0 within $\pm \Delta E_0$ over a trajectory of length Δx requires that we measure all electric and magnetic field gradients along the trajectory to within $\Delta E_0/\Delta x$, and reduce those we cannot measure below that value. Typically analyzers operate with $\Delta E_0/\Delta x \sim 10^{-3}$ - 10^{-2} eV/cm. The unique experiments of Fairbank, et al. [XV.2,3,5-7] seem to indicate that a mechanical system can be built with $\Delta E_0/\Delta x < 10^{-12}$ eV/cm, although this was obtained at currents $\sim 10^{-19}$ amp. The author feels that it should be possible to obtain $\Delta E_0/\Delta x \sim 10^{-5}$ - 10^{-3} eV/cm with nanoampere currents using generally conventional design incorporating some new features.

In the following paragraphs we discuss some of the factors limiting resolution and indicate some possible techniques of reducing them.

Asymmetry. Due to mechanical tolerances, geometry is not precisely known--circles not exactly circular, planes not exactly flat, axes not exactly coaxial, etc. Systematic errors (such as an "elliptical circle", edge effects, etc.) can be compensated using extra elements (shims and correctors), adjusted for best response. Random errors (surface roughness, waviness) cannot be compensated; may be reduced by enlarging dimensions, using simple geometry (flat surfaces are easier than cylinders). Can use optical interferometry for examining, polishing. Evaporated conductive layers on optical glass is accurate, inexpensive.

Optical Aberrations. Spherical aberration, astigmatism, chromatic aberration, distortion, etc., limit resolution for non-paraxial rays, even for perfect geometry [X.1]. Unavoidable with finite aperture. Calculations for certain systems (Einzel lens, Wien Filter) are extensive. Can be compensated with additional elements, by shaping equipotential surfaces, by ganging two or more analyzers in series, etc. Can generally reduce by reducing angular aperture, at sacrifice of current. Also possible to use microwave fields to compensate for various aberrations [X.29].

Stray Fields. External fields will have to be compensated or shielded over long path length. Very large Helmholtz coils could compensate Earth's magnetic field. High permeability (Mu metal, supermalloy) shields can reduce by factors of several hundred, but introduce irregularities that may not be tolerable. Superconducting shield may be indicated. Internal fields of electron detector, power leads, etc. can probably be partially shielded, partly compensated by correctors. Symmetrical construction insofaras possible will reduce gradients to second order. Use of low voltages and power as possible indicated.

Nonequipotential Surfaces (Patch Effect). Due to polycrystalline structure, various surface phenomena (contact potential, photoelectric work-function, thermionic work function, etc.) show small irregular variations over surface [IX.1]. Example: contact potential varies few 0.1's eV over distances of 5×10^{-3} cm in OFHC copper. Produces irregular field variations in space near surface. Total effect strongly dependent on patch structure, which is not very controllable. Periodicity in patch pattern reduces field gradients, randomness increases it [XV.3]. Adsorbed gases may modify surface dipole fields to increase ordering thereby reduce effect. Certain materials (e.g. C) show significantly less large scale variation in contact potential, indicating more favorable materials could be found. Low temperatures ($T \sim 4°K$) apparently mask patch effect, at least for OFHC copper, indicating cryogenic operation of analyzer [XV.3]. Superconducting surfaces may be better, since they are equipotential. Use of hard superconducting materials (Nb_3Sn; etc.) recommended for dimensional tolerance. Can use single crystal surfaces made from commercial bulk crystals (e.g. Cu) or grow epitaxial conducting surfaces on insulating crystals. Grids can be used to approximate equipotential while reducing space charge. Ferromagnetic and other domain materials not recommended due to irregularities.

Thermoelectric Effects. Unless the entire apparatus is isothermal, the presence of temperature gradients produces potential gradients, currents, etc. [XVIII.6]. In a single piece of material, a temperature gradient dT/dx produces a potential gradient $dV/dx = \sigma(dT/dx)$, where σ = Thomson coefficient $\sim$ microvolts per deg. A temperature gradient dT/dx = 100 deg/cm, for $\sigma = 1 \times 10^{-6}$ volts/deg, produces a potential gradient $dV/dx \sim 10^{-4}$ volt/cm, approaching the design limit. Makes it necessary to thermally stabilize. Can operate liquid He below λ-point (2.17°K) which makes it a very good heat conductor. Can thermally isolate from walls using point contact supports. For superconductors, $\sigma = 0$ (no gradients exist). Any source of heat must be examined for potential variation. Presence of contacts between dissimilar metals will produce potential double layer at junction with potential drop $\Delta V \cong \alpha T$, where α = Seebeck coefficient $\sim 10^{-5}$ volts/deg. Joule heating (I^2R) in current-carrying wires contributes to heat load. Appears important to carefully choose materials with small coefficients, use crystallographically oriented contacts, symmetrical design, local heat sinks at hot spots.

Thermomechanical Effects. Variation in temperature produces differential expansion or contraction; may alter geometric symmetry, alignment, etc. [XVIII.6]. Length change is $\Delta x/x = \alpha\Delta T$, $\alpha \sim 10^{-5}$ for metals. Cooling to liquid helium temperature produces $\Delta x/x \sim 10^{-3} - 10^{-2}$, may be significant in holding tight dimensional tolerances. Necessary to use low coefficient materials (Cermet for room temperature, etc.) May make compensatory geometry necessary, so correct dimensions obtained only at low temperature. External optical alignment *in situ* may be necessary.

Piezoelectric Effects. Mechanical stress produces electric polarization and vice versa [XVIII.6]. Quartz is mildly piezoelectric; heavily loaded member may generate substantial charge and voltage. Example: 10 lbf on crystal 1 inch square × 0.1 inch produces 0.1 μ coul, and 10 volts. Piezoelectric transducers may be useful for vernier motion in the vacuum system; the electric fields so introduced should be examined.

Surface Contamination. Adsorbed gases may be beneficial in reducing patch effect [IX.6]. Ordinary contamination leading to poor vacuum not tolerable. System must be bakeable. Surfaces of analyzer (e.g. electrostatic plates) must be free of contamination to remain equipotentials. Facility for cleaning analyzer *in situ* desirable, perhaps heavy ion (e.g. argon) bombardment. Charging of surfaces by electron bombardment critical problem. Example: charging a pair of parallel plates of area 1 cm^2 separated by 1 cm by 3 μamp-hr raises their potential to 10 meV. Means for draining charge buildup necessary. Perhaps periodic flushing with strongly electron attaching gas. At low energy, target will obtain positive charge due to secondary emission; at high energy, negative charge acquired. Auxiliary source of charge (electron gun, positive ions, radioactive source) may be necessary.

Space Charge. At high currents beam definition cannot be maintained [X.1-3]. Mutual repulsion perturbs energies. For current of $j \sim 10^3$ amp/cm^2, electron-electron interaction is $\sim 10^{-3}$ eV; will limit current. Eddy currents in conductors will damp beam energy, introduce dispersion. Image charges are present in superconducting surfaces. May need axial magnetic field to guide beam. Use of line images rather than point images may be indicated to reduce space-charge problems, increase total beam current.

e. Preferred Analyzer Design

Consideration of factors such as those of the previous section has indicated certain analyzer geometries are more likely to operate in the $\Delta E_0 \sim 1$ meV range. Some of these are shown in Fig. 22. The final choice among these and others is

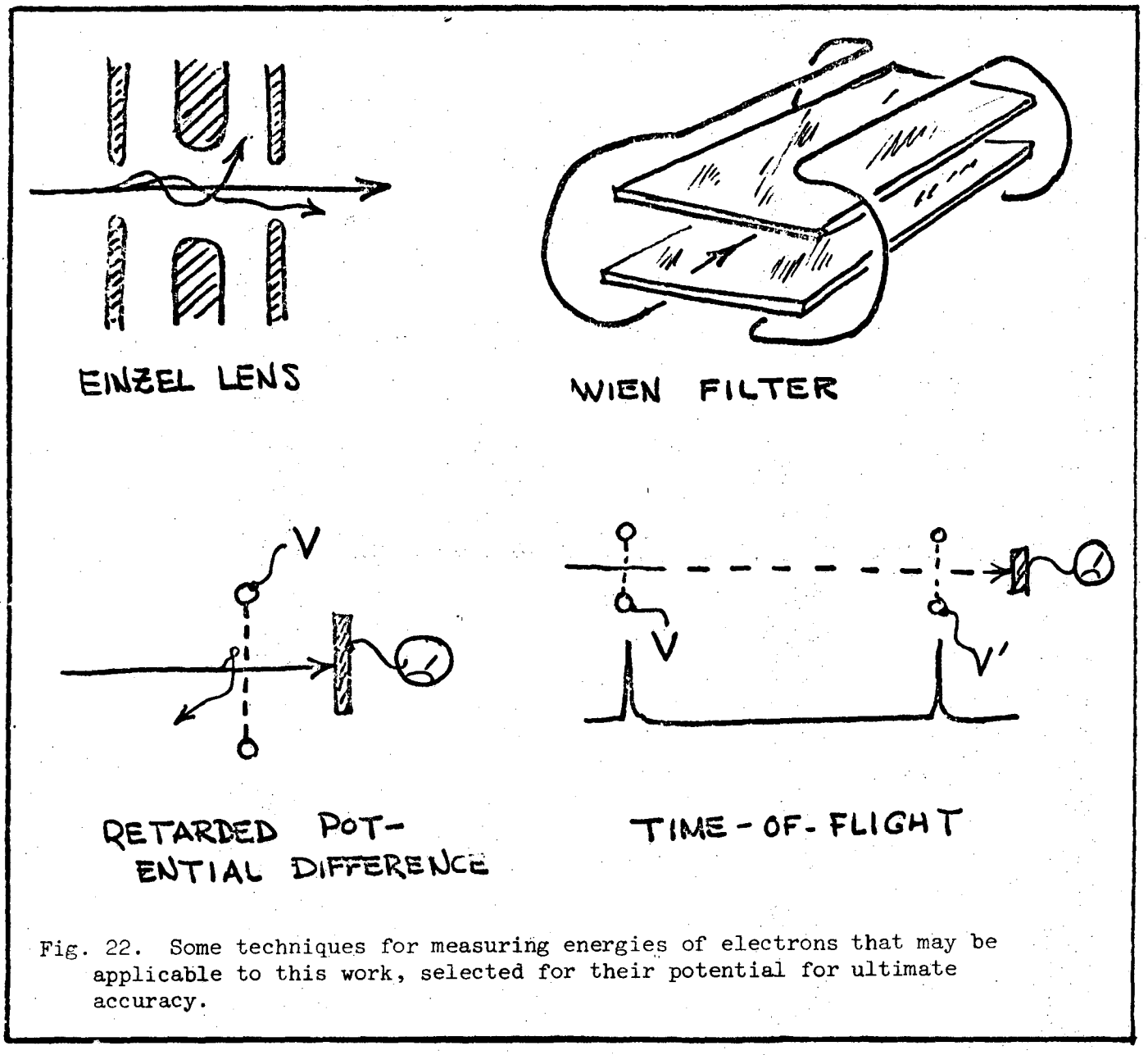

Fig. 22. Some techniques for measuring energies of electrons that may be applicable to this work, selected for their potential for ultimate accuracy.

pending further study. The Einzel lens has the potential of extremely high resolution at low current. The Wien filter seems to offer high transmission at reasonable resolution, but at the expense of complication. The retarded potential difference technique is simple in principle and develops high resolution with moderate expense, but yields an integrated signal. Time-of-flight techniques have the greatest potential at very low energies, but suffer from low duty cycle and complicated electronic support. It may be noted that a Wien filter with nonaxial injection apparently holds the record for energy resolution: $\Delta E_0 = 1.7$ meV at $E_0 = 20$ eV [X.15].

3. Electron Source

A thermionic cathode emits electrons with an energy distribution that is approximately Maxwellian, with a spread $\Delta E_0 \sim 3$ kT, which is $\Delta E_0 \sim 0.5$ eV at T = 2000°C. About 95% of the beam lies within this spread. It is obvious that as low temperature as possible is desired to make the distribution as narrow as possible. Operating at cryogenic temperatures is not very beneficial, however, since other irregularities (work function, etc.) persist.

If the source has some transverse size, rays will arrive at an observation point making slightly different angles with one another. This will place a limit on the transverse area over which the electron wavefunction is coherent (necessary for interference). The coherence of two beams overlapping at $\vec{r}$ is proportional to the factor $e^{i(\vec{K}_0 - \vec{K}_0')\cdot\vec{r}}$. If the observation point is displaced by $\Delta\vec{y}$, we can say that coherence is lost when

$$(\vec{K}_0 - \vec{K}_0')\cdot\Delta\vec{y} = 2\pi \quad . \tag{51}$$

If the source subtends an angle α at the observation point, we have $|\vec{K}_0 - \vec{K}_0'| = \sqrt{2K_0^2(1 - \cos\alpha)} = 2K_0 \sin\frac{\alpha}{2}$. To account for the velocity spread we replace K_0 by $K_0(1 + \Delta E_0/2E_0)$. The coherence width of the beam is then

$$\Delta y \cong \frac{\lambda_e}{(1 + \frac{\Delta E_0}{2E_0})2 \sin\frac{\alpha}{2}} , \tag{51a}$$

where $\lambda_e = 2\pi/K_0$ is the electron wavelength. Since we generally require coherence over a diffraction-limited laser focus, $\Delta y > \lambda$, the condition on the source size is

$$2 \sin\frac{\alpha}{2} < \frac{\lambda_e}{\lambda} \frac{1}{1 + \frac{\Delta E_0}{2E_0}} . \tag{51b}$$

For $E_0 = 50$ keV, $\Delta E_0 = 1$ meV, $\lambda = 5000$ Å, we find $\alpha \lesssim 10^{-4}$. Considering the magnification of the electron optics, and a laser focus larger than diffraction-limited, this requirement may be reduced to $\alpha \lesssim 10^{-6}$. At a distance of 10 cm, this implies a cathode radius $\sim 10^{-5}$ cm = 1000 Å.

The author has examined several possible cathode structures, including thermionic filaments, field emission points, opto-electronic cathodes [XIII.3,4], photo-cathodes, and the SRI (Stanford Research Institute) field emission sandwich tips [XIII.2]. It was concluded on the basis of small size, available current, low temperature, monochromaticity, and beam optics that the SRI device is the most promising for this work. A diagram of this cathode is shown in Fig. 23, and some of its characteristics are listed in Table 5. The main limitation of this device is its relatively low current output.

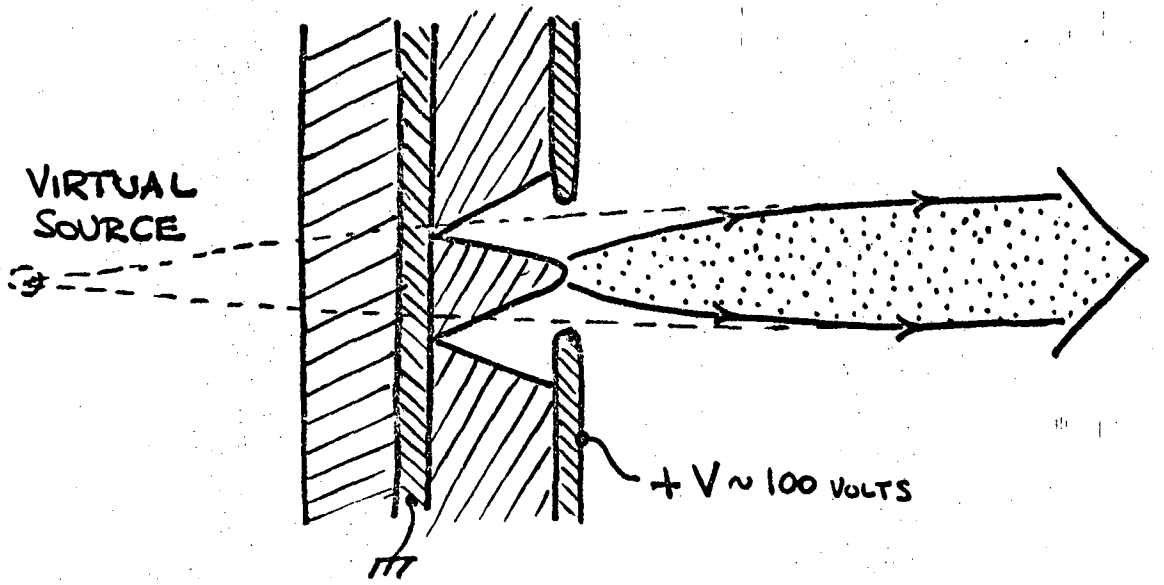

Fig. 23. Diagram of the SRI field emitting cathode, recommended for this work.

Table 5. Properties of the SRI Cathode

Size of Virtual Source	< 500 Å dia
Current	Up to 100 μamp; 10 μamp typical.
Voltage	100 - 150 volts.
Brightness	$\sim 10^{7}$ amp/cm^{2}-sr.
Energy spread	$\Delta E_0 \sim 0.2$ eV
Life expectancy	1000's hours at pressure $< 10^{-5}$ Torr and currents $\sim$ μamp.

4. Electron Gun and Optical Correctors

The SRI tip emitter has the additional advantage of producing a reasonably well collimated beam, issuing from an apparent source behind the cathode. This fact should obviate the need for an elaborate gun. However, the actual beam geometry is not known (to the author, at least), so it may be necessary to include additional elements between the emitter and the monochromator. The difficulties relating to geometrical and electrical aberrations will be the same as those encountered for the monochromator, but since the total correction needed will probably be small, this element could be made larger, thereby reducing some of the difficulties. It may also be necessary to insert a corrector between the analyzer and the detector, and on each side of the crystalline film. Details of any possible correctors would be worked out when the final electron optical design is made.

5. Electron Detector

In previous sections it has been shown that for forward scattering the various second order observables, such as $\delta\rho_e$, are not very sensitive to the distance R of the detector, even though they are strongly dependent on the interferometer spacing L. Furthermore, an achromatic Bragg doublet can be used as a forward scattering interferometer that is insensitive to the velocity spread. Hence, it appears that the detector need not have extraordinary longitudinal spacial resolution, certainly not of the order of the laser wavelength. On the other hand, it must be able to detect electrons in times $\Delta t = 2\pi/\Delta\omega \sim 10^{-9}$ sec. Hence it must have a frequency response up to $\sim 10^3$ MHz. This is within the range of the better electron multipliers currently available. In theory it is possible to use laser frequencies $\Delta\omega$ arbitrarily small or even use a single-frequency

laser so $\Delta\omega = 0$. The time response of the detector could then be very slow, or even DC. The selection of a detector depends therefore on the selection of laser frequencies.

There are certain other electrical and mechanical requirements on the detector. It must have high efficiency, weak stray fields, require small electrical power, and produce a reasonably large signal. Since the currents probably will be below 10^{-9} amp, possibly less than 10^{-12} and conceivably as low as 10^{-20} amp, it must detect single electrons and have very low background. Mechanically, the detector should be small and light-weight, able to operate at low temperatures, have a sensitive surface of simple geometry, and not be subject to microphonics.

All of these requirements apparently cannot be satisfied in any detector known to the author. Various detectors were examined for possible use, including a Faraday cup, dynode multiplers, continuous-channel multiplers, GM and proportional detectors, surface barrier detectors, and photographic plates. It has not yet been determined which of these is the best for this application, except that a Faraday cup is not very sensitive and probably not of much value here. The dynode multiplers are fast and have low background, but are large, heavy, and require high voltage. Continuous-strip multiplers, such as the strip multipliers and the Channeltron manufactured by Bendix Corporation, are small and lightweight, with low background, but they have a non-simple sensitive area, sometimes involving an additional magnetic field. GM and proportional detectors are small, simple, and inexpensive, but have a thin window holding against a high gas pressure ($\sim$ 1 atm) and may generate a large gas load to the vacuum. Surface barrier detectors are small, lightweight, with simple geometry, and operate at low temperatures, but require high quality electronics to achieve low noise. Photographic plates have advantages for measuring currents over large areas and times, but have no time resolution and must be removed from the vacuum system to be processed.

It may be advantageous to use a resonant cavity to improve the rejection of unwanted frequencies in detecting the modulation. Superconducting cavities offer the highest Q (a superconducting cavity with $Q = 2 \times 10^8$ at 2.8 GHz has been built [XI.2]) and other advantages, such as equipotential surfaces. The expected modulation difference frequencies ($\sim$ GHz) fall in a convenient experimental range. This technique would be most useful if the total current is large but the modulation is small.

Another very intriguing possibility is the use of the Josephson Effect. It is known [XI.6] that a Josephson junction is a sensitive detector of microwave and infrared radiation, so it is quite plausible that they could be used to detect electrons. This idea gains credibility when it is realized that the Josephson frequency-voltage constant is $2e/h = 483.6$ MHz/μV. That is, the natural frequency of the junction is 483.6 MHz when biassed with one microvolt. Since the capacitance of the junction is probably quite small, even a small added charge will produce a significant voltage. Thus, a Josephson junction appears to have the capability of responding to the very high modulation frequencies ($\sim$ many GHz). In practice, one would look for electron-induced current steps at microvolt bias. A possible problem is the presence of a variety of frequencies; so many steps would be produced, it may be impossible to plot the spectrum accurately.

A further development might make use of a Josephson junction in a resonant cavity. Such devices have been studied by Richards [XI.6,7], primarily for detecting the infrared. Application to electron detection seems of great potential value.

The decision as to detector will have to await other design parameters, although at the moment a surface barrier detector appears to have some advantages.

An additional feature that should be provided is a fluorescent screen. This would be of no value in observing the modulation, but will be necessary to assess the quality of the crystal films. This screen can be obtained commercially, and should be mounted in a way that it can be photographed through a window in the vacuum chamber.

C. THIN FILM CRYSTAL TARGET

1. Thickness

The films must be sufficiently thin so that the electron beam loses a small fraction of its energy in passing through it. The range of electrons in a typical material (Al) is well approximated in the range 1 keV $\leq E_0 \leq$ 300 keV, by [VIII.1]

$$R(E_0) = 0.71\ E_0^{1.72} \quad , \tag{52}$$

where E_0 is in MeV and $R(E_0)$ is in g/cm^2. For E_0 = 50 keV = 0.05 MeV, this gives $R(0.05) \cong 4$ mg/cm^2, or a thickness about 1.5×10^{-3} cm. To prevent appreciable absorption, we require the film thickness to be, say 1% of this, or $D \sim 1000$ Å.

There is another criterion on the thickness, namely the amplitude of the notch effect. From Eq. (22), the modulation is proportional to sin ($\omega D/2v$). For E_0 = 50 keV ($v/c = 0.41$), and λ = 5000 Å ($\omega = 0.6 \times 10^{15}$ sec^{-1}), this is unity for $D \cong 1000$ Å, by coincidence of the same order as the range requirement. It is interesting that the condition sin ($\omega D/2v$) = 1, implying $D = \beta\lambda/2$, indicates that the film should be a half wavelength thick.

2. Preparation

The preparation of thin single-crystal films is a fairly routine process, at least for certain materials. The important requirement is crystalline perfection, so that high quality diffraction patterns can be obtained. We have assumed that the electron beam would be focused to a spot about 1 micron in diameter, or about 20000 atomic diameters. In order to obtain maximally sharp diffraction patterns, the film must be ordered into crystallites at least this size. There appears to be no difficulty in obtaining films with this ordering.

A technique for fabricating thin single crystals films on a crystalline substrate is illustrated in Fig. 24. In this technique, the substrate is hollowed to produce a thin window area, and a crystalline film is deposited on the front. Then the back of the substrate is dissolved in a solution or vapor-etched away, leaving the free-standing film. A typical film would be a few mm in diameter and could be supported on all sides or have some free edges.

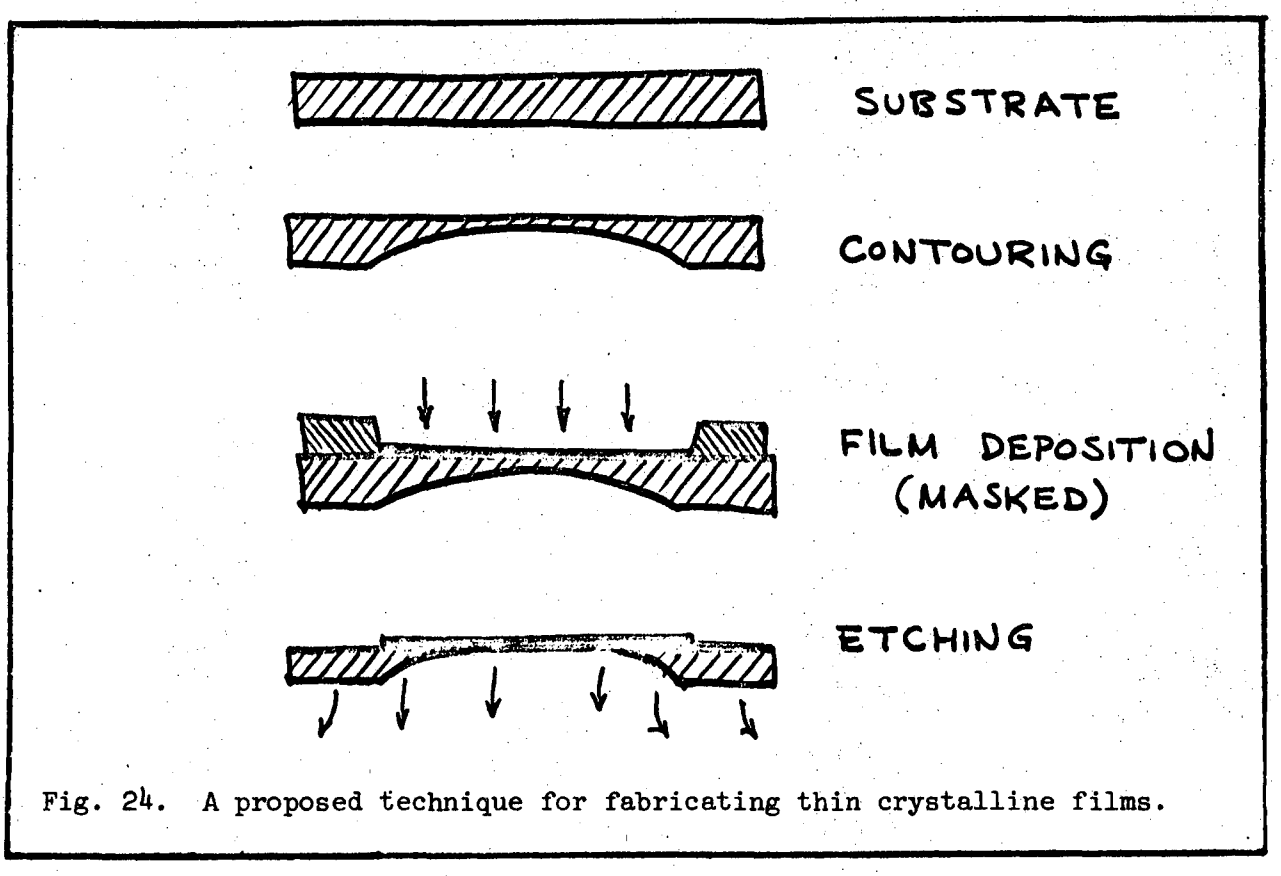

Fig. 24. A proposed technique for fabricating thin crystalline films.

3. Heating

The thin film receives power from two sources: the electron beam and the laser beam. The energy loss of the electron beam is very complicated, since there may be discrete losses due to plasmon generation, excitation, ionization, etc. We can ignore all these and estimate the loss with the Bethe formula [VIII.1]:

$$-\frac{dE}{dx} = 2\pi e^4 \frac{Z\rho_A}{E_0} \ln\left(\sqrt{\frac{e}{2}}\ \frac{E_0}{I}\right) , \qquad (53)$$

in which ρ_A = number of atoms/cm^3 in the target, e = base of the natural logarithm, and I = average ionization potential of an atom in the target (energy per electron-hole pair). Using $\rho_A \sim 1.6 \times 10^{22}$ cm^{-3} (for a crystal with 4 Å interatomic spacing), Z = 10, E_0 = 50 keV, e = 2.718, and I/Z ~ 13 eV, we find $dE/dx \sim 7.5 \times 10^{-2}$ eV/Å, or about dE = 75 eV for a 1000 Å film. If we assume a current 10^{-12} amp $\cong 6 \times 10^6$ electrons/sec are passing through the target, the total power input from the beam is $P \sim 10^{-10}$ watt.

Absorption of laser light in the film will depend on the crystal perfection, the more perfect the less absorption. Low loss glasses have been developed for fibre optic waveguides with losses of 20 db/km, although 100 db/km are more common. These noncrystalline materials probably absorb more strongly than a good crystal. If we assume a loss of 10 db/km and a power of 10 watts propagating 0.1 cm along the target, about $P \sim 3 \times 10^{-6}$ watts. Thus, the laser power load to the target probably significantly exceeds that of the electron beam.

In order to compute the local temperature rise in the film, we assume 3×10^{-6} watts is deposited in a volume 0.1 cm long, 10^{-5} cm wide, and

5×10^{-5} cm thick. Part of the heat so generated will be conducted into other parts of the film, to be radiated away, and part will be radiated directly. The conduction to a cold support will produce a temperature gradient of $dT/dy \sim 25°C/cm$ (for a silica film). Assuming the film is 0.1 cm × 0.1 cm and radiates as a black-body obeying the Stefan-Boltzmann law,

$$P = A\sigma\ (T^4 - T_0^4) \quad , \tag{54}$$

we find the film reaches a temperature of $T \sim 100°C$ when radiating to a cold ($T_0 = 0$) reservoir. This is considered acceptable, although it may produce certain thermal effects that will have to be investigated.

There is no good way to cool a freestanding film in vacuum. If the diffraction can be done in reflection, a solid film backed by a good heat sink may be of value. For a freestanding film, it may be advantageous to chop the laser at, say, 100 Hz, and bombard the film with ions at the same frequency (180° out of phase), thereby approaching isothermal operation with amplitude modulation of the laser.

4. Charging

Since the best films will be transparent crystals, they will also be thermal and electrical insulators. Due to secondary emission, the target may become electrically charged, and will modify the electron optics and effective energy of the beam. If it will be positively charged, it should be possible to discharge it either continuously or intermittantly by flooding it with electrons from a diffusive source. It may be that the diffuse edges of the beam may serve to partially neutralize the charge so no additional device is necessary. This can be readily determined in the experiment.

5. Coupling of the Laser Beam to the Film

Typical laser beams are 0.1 - 1 cm in diameter, and this beam must be compressed into about 10^4 - 10^3 Å, with negligible loss and negligible scattering. Devices for coupling lasers to thin films are currently undergoing rapid development as part of the general advances in integrated optics [XVIII.5]. Three devices known as prism, taper, and grating couplers are illustrated in Fig. 25. The grating coupler makes use of periodic variations in the refractive index (shaded in the figure) to produce a diffraction maximum at the Bragg angle, directed into the film. Coupling efficiencies of 50% have been obtained, and efficiencies of 100% are theoretically possible with graded index variations. Some couplers to backed thin films are commercially available, and it is expected that a variety of new couplers will be available in a year or two. The laser beam propagates in the film as a guided wave; the theory of such propagation is well-developed [XVIII.7].

One technique for directing the laser beam onto the thin film target is shown in Fig. 26. In this arrangement, the beam enters the chamber from below, is collimated, and is reflected from three mirrors at 45°, and from a fourth at 90° which returns the beam along its original path. A pair of quarter-wave plates, one stationary and one rotating, produce linearly polarized light at fixed orientation. In this arrangement, a standing wave is produced with polarization primarily perpendicular to the film. In rotating the entire assembly about the vertical axis, the angle between the film and the electron beam varies while maintaining constant illumination of the film.

Two techniques may be of value here: 1) Using mirrors, multiple passes through the film can increase the modulation efficiency, consistent with absorption

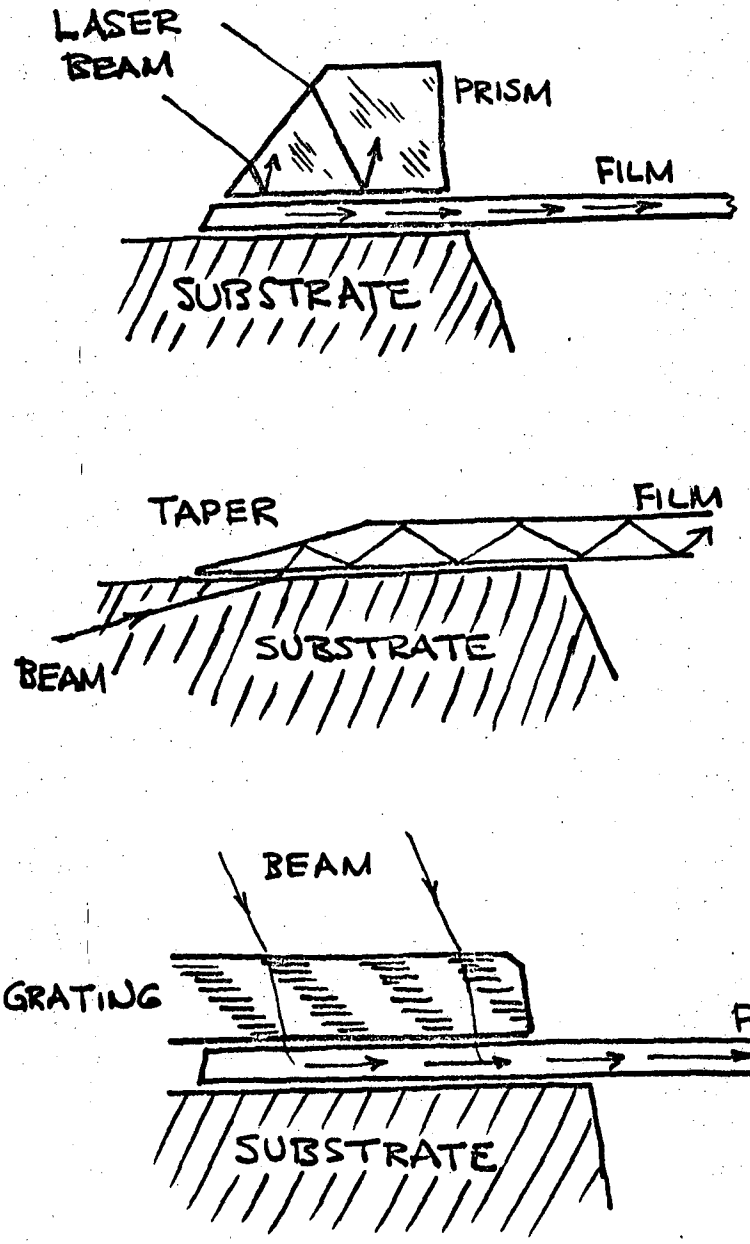

Fig. 25. Techniques for coupling laser beams into thin films. The prism method is the most studied, but may not give the best coupling. The taper coupler is somewhat more difficult to control accurately. The grating coupler, which uses a spacially periodic refractive index, has a potential of 100% efficiency, but is less studied so far.

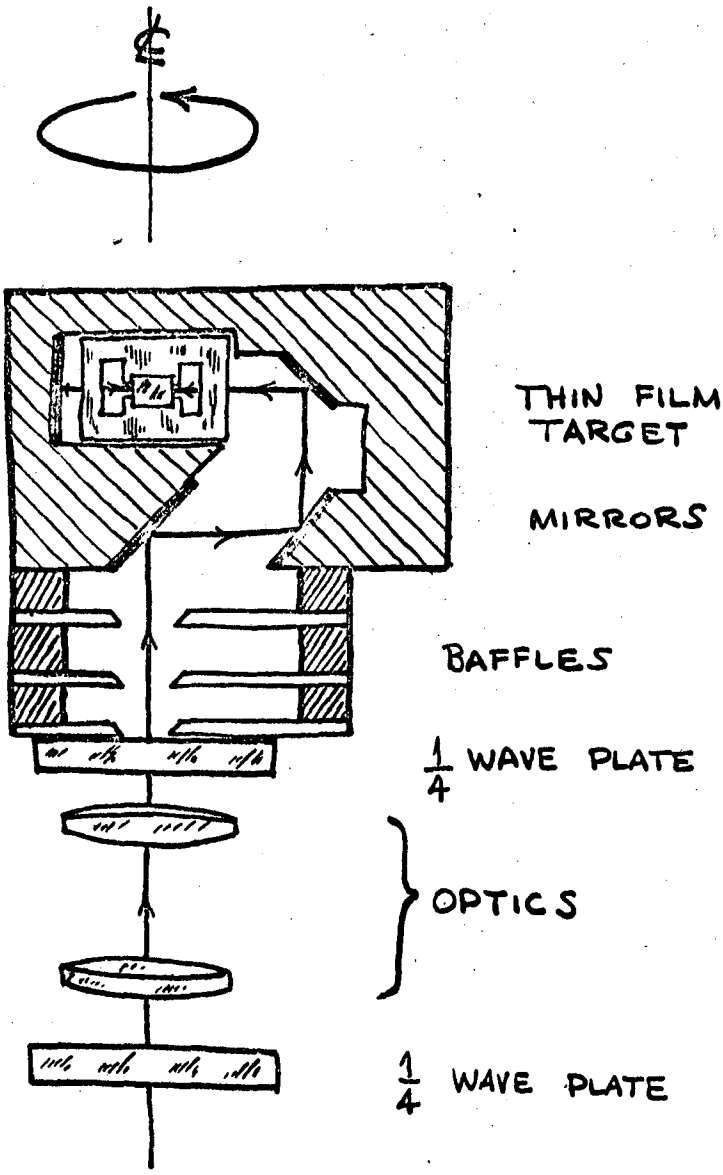

Fig. 26. Target mount design for directing laser beam at edge of thin film, with polarization always perpendicular to plane of film.

of the light in the film; 2) The modulation produced by a standing wave is different than a travelling wave, and could be used to select certain effects while discriminating against others.

6. Surface Cleanliness

Due to the unknown contribution of the surface to the modulation, cleanliness on an atomic scale is essential. This can be insured by ion bombardment and examination of the diffraction pattern on the PbS fluorescent screen. It may be necessary to provide facility for flash heating the film periodically.

7. Material

The modulation effects are predicted to depend only weakly on the chemical composition of the film--its main function is to conserve momentum. More critical are the demands of strength, transparency, lattice perfection, and thermal stability. Materials like Al_2O_3, SiO_2, LiF, SrF_2, KDP, and CdS are probably suitable. The first of these has been used most often, so would be the logical one with which to initiate work.

If the modulation is at least partially due to laser-induced polarization in the crystal, it may be advantageous to use a material with anomalous dispersion near the laser frequency. For most solids appropriate here, the dispersion is anomalous in the near ultraviolet (1000 - 3000 Å) and the near infrared (3 - 30 μ), unfortunately not in desirable laser ranges. It is interesting to speculate on the possible uses of exotic materials like ferroelectrics.

D. LASER

1. Power Requirement

No difficulties in obtaining sufficient laser power is expected. A variety of commercial lasers is available with 1 - 100 watt average output [IV.5]. It is unlikely that more than this could be used CW, due to absorption in the film. Computations indicate that modulations of percents can be expected with 5 - 10 watts.

2. Spectrum

It is probably desirable to use as short wavelength as possible, in order to separate the sidebands as much as possible from the energy E_0. Commercial lasers are available to 3371 Å (N_2); most available are 4880 Å (Ar), 5145 Å (Ar), 6471 Å (Kr), 6943 Å (Ruby), 1.06 μ (Nd), and 10.2 μ (CO_2). Most of these can be stabilized on the TEM_{00} mode, and many can operate in either CW or pulsed mode [IV.5].

A laser cavity of length ℓ will resonate at a set of frequencies equally spaced by [XVIII.10]

$$\Delta\omega = \gamma \frac{c}{\ell} \quad , \tag{55}$$

where $\gamma = \pi$ for a plane parallel cavity and 1/2 for a confocal cavity. For a 100 cm cavity, this yields $\Delta\omega \sim 10^3$ MHz and $\sim$ 150 MHz for the two types. If lock-in detection of the interferometer signals is used, the lower frequency ($\sim$ 100 MHz) would place less demand on the detector bandwidth. It may be desirable to use a longer cavity to produce a smaller frequency $\Delta\omega$.

3. Duty Cycle

CW operation would have several advantages: the thin film would reach thermal equilibrium, a laser modulator would not be required, transient electrical signals would be avoided, counting could be done continuously. However, there are several reasons why pulsed operation would be advantageous: higher instantaneous power without damage to the crystal (leading to larger modulation), provision for low frequency lock-in with detector (to reduce effective background in detector), possible gating of detector to reject counts due to scattered light, evaporated particles, etc.

Besides CW and pulsed, there is another mode that may be very powerful: intensity modulated. Suppose the incident laser intensity is modulated at some high frequency Ω_L. The results of this modulation have been investigated extensively for optical pumping experiments. The general effect is to produce resonances in the response when Ω_L is equal to one of the internal frequencies of the system. In the case of the interferometers of interest here, the frequencies $\Delta\omega_{nm}$ are present (c.f. Eq. (31)), which are in the range 100 - 1000 MHz. Thus, by mixing the two laser frequencies ω_n, ω_m in a square-law detector, the frequency $\Delta\omega_{mn} = \omega_n - \omega_m$ can be produced, amplified and used to drive the modulator exactly on resonance. The electron modulation could then be detected by varying the phase of the laser modulator. A general scheme for doing this is illustrated in Fig. 27. There are several modulators commercially available with bandwidth in the 100 MHz range, and at least one up to 500 MHz, using KDP or ADP crystals as Pockels cells [IV.5]. Typically these devices require 0.1 - 10 kV, have greater than 90% transmission, and apertures of 1 - 10 mm, although devices outside these ranges are not uncommon.

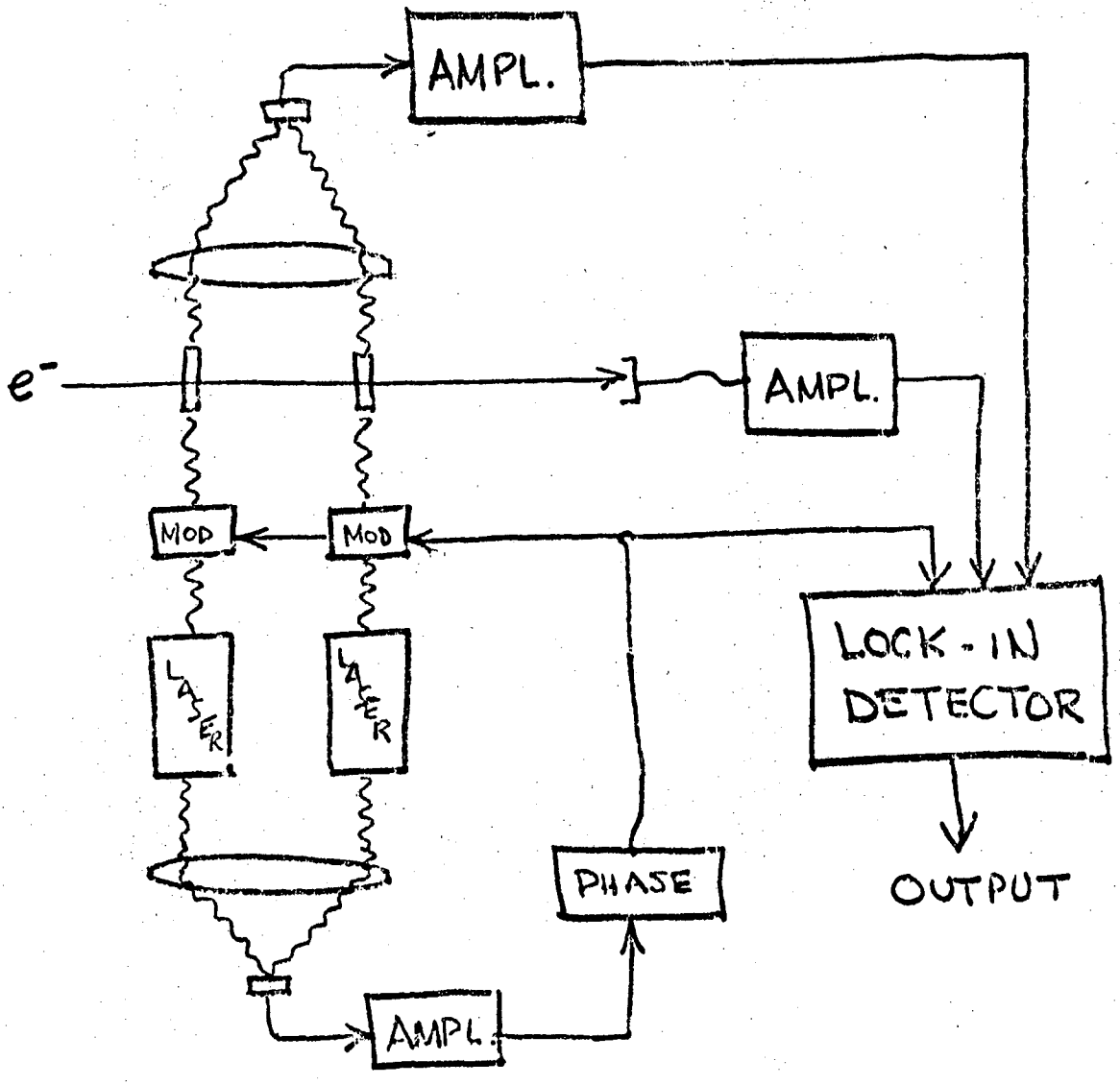

Fig. 27. A possible experimental setup using modulation of the laser intensity at the difference frequency of the lasers to produce an on-resonance signal, detected with phase-sensitive techniques.

4. Stray Light

It is likely that the electron detector will also be sensitive to the laser light. Extreme precautions will have to be taken to avoid spurious background, especially if the laser is chopped or pulsed. Non-reflecting multilayer dielectric coatings tuned to the laser wavelength could be used in areas where equipotential surfaces were not required. Baffles, stops, and traps should be used as much as possible [XVIII.8]. Since the thin film may scatter significantly, it may be better to use a deflecting analyzer than a straight-through one, or at least deflect the electrons from line-of-sight before detecting. Electron bremsstrahlung will be produced at the target, providing another incentive for deflection analysis. The choice of a detector will be partially influenced by the need to be laser-blind.

5. Other Considerations

The optical components (lenses, deflectors, mirrors, etc.) necessary to transport the high-power laser beam are all commercially available [IV.5]. All lasers operate on 110 or 220 VAC, at moderate power input. Frequency stability is not important, since the laser and the modulated electron beams are automatically exactly in phase.

These considerations lead to the conclusion that an appropriate laser and supportive apparatus is now commercially available. The final selection of a laser should be made only after certain other factors are determined, such as power handling capacity of the film. The choice between CW or pulsed operation should be deferred until more computations of required power are available. In Table 6 we list some characteristics of some lasers the author considers possibly appropriate for this work.

Table 6. Characteristics of Some Lasers

	A	B	C	D	E	F	G	H
Power	8 CW	6 CW	2 CW	30 CW	10	1.5	5 Avg*	2**
Wavelengths	4579-5145Å	4579-5145Å	4619-6764Å	10.6μ	10.6μ	1.06μ	1.06μ	1.06μ
Active Mat'l	Ar	Ar	Kr	CO_2	CO_2	Nd-YAG	Nd-YAG	Nd
Beam Diameter (mm)	1.5	1.5	1.5	1.0	6	< 4	< 4	4
Beam Divergence (mrad)	0.6	0.8	1.6	< 5	5	4	4	3
Head Dimensions (in)	8×6×60	10×13×66	10×13×70	4×5×51	7×8×38	8×6×30	8×6×30	4×4×10
Operating Voltage	208/3φ	208/3φ	208/3φ	115 AC	115	208	208	110
Price	$17990	$9950	$17200	$4200	$10500	$9990	$14940	< $3700

A. Coherent Radiation, Inc. (Model 53A).

B. Control Laser-Orlando, Inc. (Model 906).

C. Control Laser-Orlando, Inc. (Model 912 K).

D. Apollo Lasers, Inc. (Model XII).

E. Sylvania Electronic Systems (Model 948-1).

F. Coherent Radiation, Inc. (Model 60).

G. Coherent Radiation, Inc. (Model 60/460).

H. American Optical Corp. (Model AO-5).

* Q switch, Peak pwr > 1000 watts, pulse width < 0.5 μsec, Rep. rate 0.5 - 15 pps.

** Peak pwr ∿ 5000 watts, pulse width ∿ 200 μsec, Rep. rate 2 pps.

E. VACUUM SYSTEM

There are several factors that will demand the use of ultrahigh vacuum in these experiments:

1. The electron beam will spread due to scattering collisions with atoms and molecules of the background gas, leading to degradation of the beam optics and excessive charging of peripheral faces.

2. The electron energy will be perturbed by interaction with the induced electric dipole moment of polarizable atoms and molecules [XV.3].

3. Monolayers of residual gas will be deposited on cold surfaces (roughly 1 monolayer per sec per microtorr), the most critical being the thin film target, the detector, and any equipotential surfaces.

4. Positive ions formed near the cathode will bombard it, thus heating it and reducing its lifetime.

5. Laser light will be scattered from residual gas, producing a diffuse background for the detector.

6. Electron collisions will produce excited gas species which may radiate or auto-ionize, contributing to background.

We consider each of these factors in turn. For pressures below 10^{-5} Torr, the mean free path of the electrons is very long, and contributes no limitation. In the presence of an electron, a helium atom will acquire an electric dipole moment $p = \alpha\mathcal{E} = \alpha q/r^2$, where $\alpha = 0.21 \times 10^{-40}$ farad m^2 is the polarizability and $q = 2$. The potential of this dipole is $p \cos\theta/R^2$, which at the position of the electron is ($R = r$, $\theta = 0$), gives an energy $-\alpha q^3/r^4$. This is greater than 10^{-3} eV when $r \lesssim 0.7 \times 10^{-7}$ cm, giving a cross section $\sigma \sim 1.5 \times 10^{-14}$ cm^2. To keep the mean free path $1/n\sigma$ above, say 100 cm, we require $n < 0.6 \times 10^{12}$ cm^{-1}, or a pressure below about 2×10^{-7} Torr at 4°K. The formation of monolayers provides an even more stringent limitation: To permit about 24 hours of data accumulation would require, say, less than 1 monolayer per 10^4 sec, or pressures below 10^{-10} Torr. The SRI field emitter recommended for this work have an estimated life of 1000 hrs at mamp currents in 10^{-5} Torr, so will not constrain the vacuum.

At $E_0 \sim$ 10's keV, excitation and ionization cross sections are below 10^{-16} cm^2, so will make no significant contribution to the background, unless the geometry is very unfavorable.

There are a few effects in which some residual gas is beneficial:

1. Convection tends to drive the apparatus isothermal.
2. Adsorption on cold walls may tend to mask the patch effect, by concentrating atoms at patch interfaces where they counteract the dipole fields, or by increasing the periodicity of the patches at the expense of randomness [XV.3].
3. Certain atoms or molecules may assist in space charge neutralization.

We conclude that pressures in the 10^{-10} Torr range will be required. This immediately implies certain features of the apparatus--stainless steel walls, metal gaskets, no hydrocarbons, careful trapping, all bakeable (300 - 500°C) construction. The techniques for vacuum systems in this range are well-known [XII.1-10] and should constitute no serious problem. It will, however, necessitate keeping the entire system as small as possible, and will severly limit the frequency with which it can be opened for service. The necessity for baking makes the mechanical design of the spectrometer even more crucial, especially if it is to be operated at liquid helium temperatures.

F. MECHANICAL

1. Vibration

Since the spectrometer must be dimensionally stable to parts per million, microvibrations will have to be eliminated. This will probably not be difficult--a sturdy shock-mounted table should suffice. A possible source of vibration is boiling of liquid nitrogen; liquid helium below the λ-point will not boil. It may be desirable to enclose the entire apparatus in a refrigerated box, to keep the heat load low and the heat sources distant.

2. Dimensional Stability at Extreme Temperatures

It is anticipated that the apparatus will be cycled from baking temperatures ($\sim$ 300°C) to cryogenic temperatures (4°K or 77°K), maintaining dimensional integrity. There are materials (e.g. CER-VIT) with very low thermal coefficients [XII.2], but the electrical properties of the parts (contact potential, conductivity, etc.) are also important. The greatest attention will have to be paid to selection of all materials in critical places.

In order to minimize the heat load to any critical cryogenic components, such as the spectrometer, as well as maintain a clean vacuum, a cold shield may be needed. Figure 28 shows a design for a 20°K (liquid hydrogen) shield [XII.4]. In this design, the 20°K surfaces are largely shielded from the heat load by 77°K (liquid nitrogen) surfaces, while providing sufficient pumping for most gases, except helium.

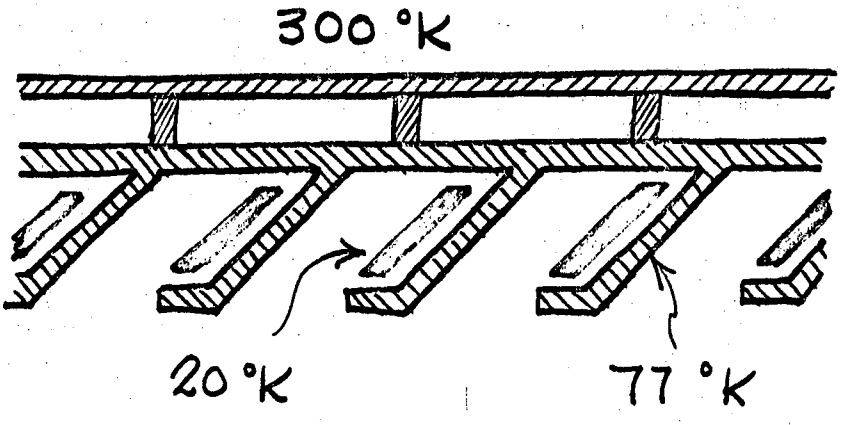

Fig. 28. Design for a 20°K (Liq. H) cold wall. The 77°K baffles carry the major heat load, while the 20°K surfaces perform most of the gas pumping.

3. Moving Parts

It is also anticipated that certain parts will have to execute motion within the chamber under vacuum, and this may present difficulties such as cold welding of the contracting parts. Any lubricants, such as molybdium disulfide or zinc stearate will have to be carefully chosen for low vapor pressure and general cleanliness, as well as sufficient lubrication. It may be necessary to operate certain parts dry.

Power transmission into the chamber can be done through an eddy current clutch across a glass window. This would avoid mechanical feed-thrus, motors inside the vacuum, and permanent fields. A more common method is to use a bellows supporting an eccentric shaft that operates a crank inside the chamber. Alternatively, the motion could be generated inside the chamber, using solenoids, motors, or transducers.

Most reasonable designs for this work involve rotating and/or sliding joints that must be vacuum tight and bakeable. The most critical need for such joints is in the mounting of the monochromator and analyzer, which must be positioned to within a few thousand angstroms, or less, and then held rigidly. This motion must be available when the device is operating, and must be positive, free of backlash, reversible, reproducible, and variable over large gross distances ($\sim$ mm) without degrading the small (10^{-5} cm) vernier motion.

Figure 29 shows a proposed new technique for mounting a monochromator or analyzer flange assembly. Instead of O-rings (which cannot be baked) or metal gaskets (which cannot be rotated or displaced), we propose using a low melting point alloy, held in place by its surface tension in a small-dimension gland. The alloy is melted by circulating a hot liquid such as oil through a tube running the length of the seal, but vacuum-isolated from it. The entire mounting is

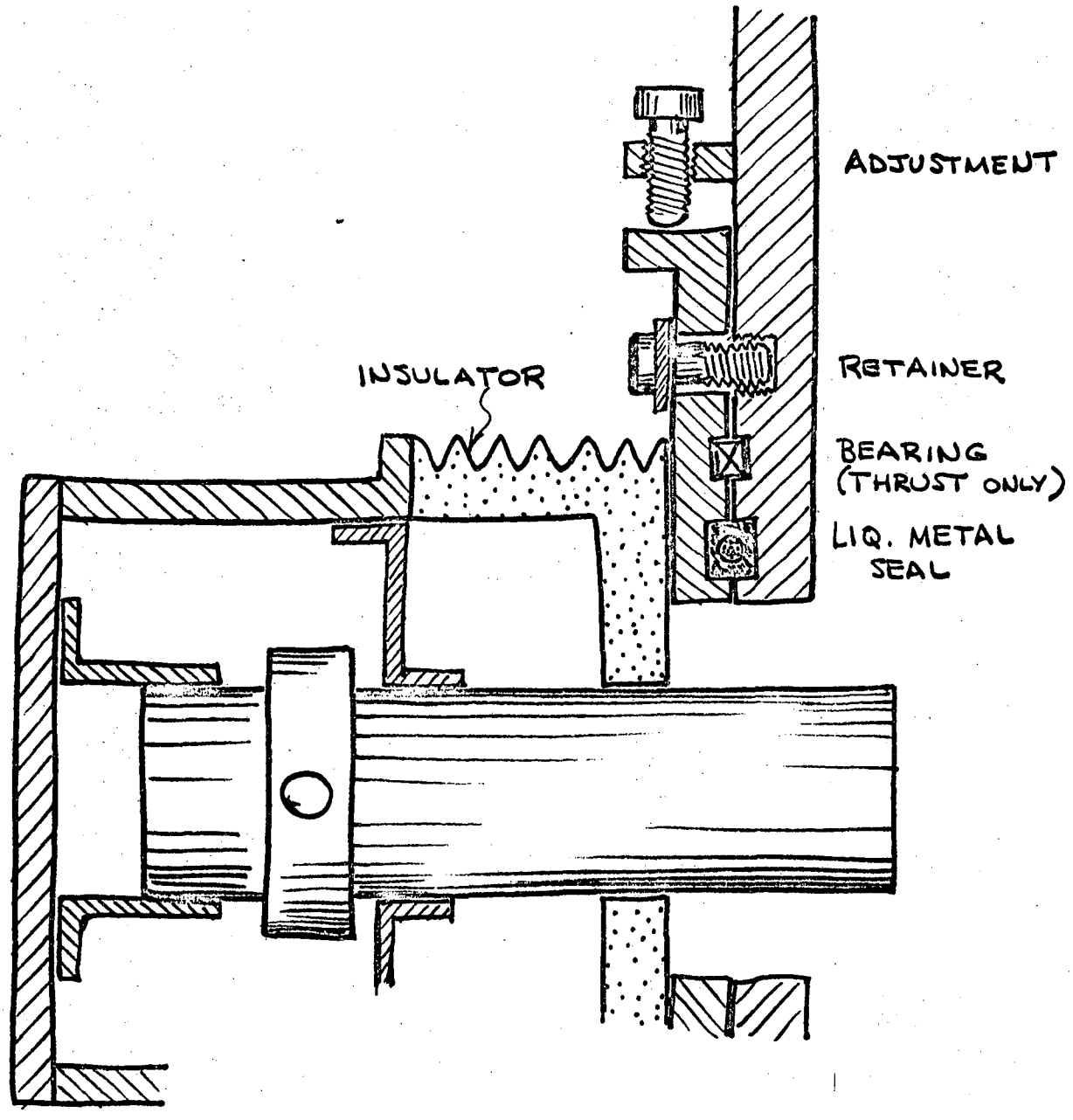

Fig. 29. Design for an adjustable flange mount for a device such as an electron monochromator. The key element is a low melting point alloy metal seal.

rigidly held in place with fine-thread screws on micrometer heads. In operation, the hot liquid is circulated until the seal melts and releases, then the flange is rotated and positioned as desired, and finally a cold liquid (e.g. tap water) is circulated to freeze the seal in place.

A variety of possible seal designs is illustrated in Fig. 30. Some experimentation will be necessary to obtain a reliable design. A variety of alloys is available with melting points between 100°C and 300°C, and with acceptable vacuum properties [XII.2]. One of these, Cerroseal-35, which is (50% Sn, 50% In) melts at 116°C, and has very low vapor pressure. It is, however, only about 1/4 as strong as ordinary lead-tin solder, and maybe a harder alloy with higher melting point would be better.

This principle can also be used for the extremely critical geometrical adjustments of the electron spectrometer. As an example, Fig. 31 shows a device for displacing a plate using a micrometer for coarse adjustments and a piezoelectric transducer for vernier motion. The positioning is permanently set when the alloy is frozen.

4. Alignment

The performance of the spectrometer will be strongly dependent on its alignment, and this may prove laborious, but not insuperable. Standard optical techniques should be sufficient, although trimming will probably be necessary for the best resolution. Piezoelectric crystals should prove valuable for very small trimming motions.

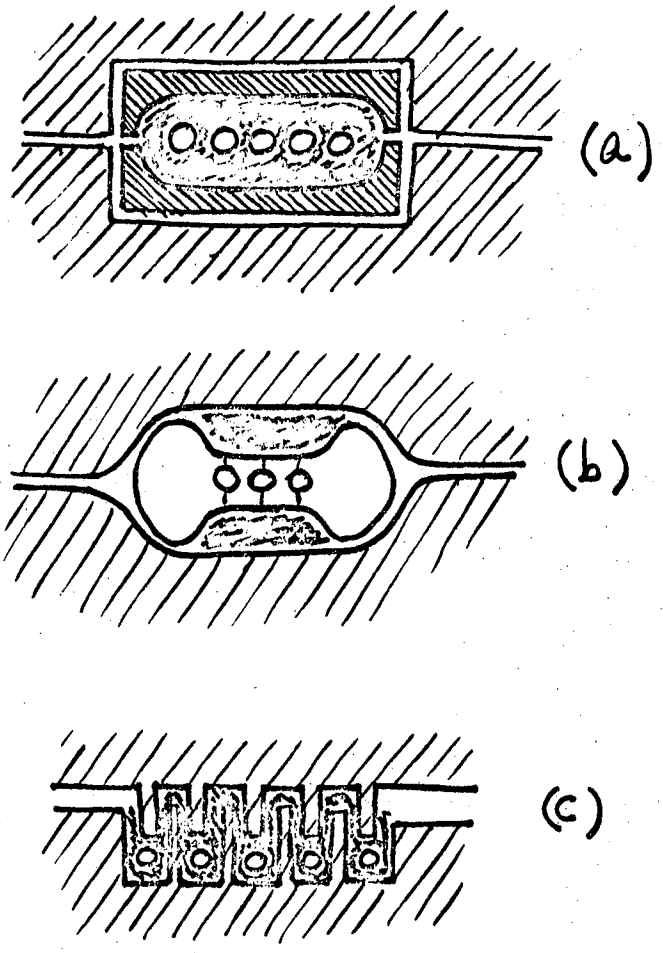

Fig. 30. Various designs for liquid metal seals. (a) Internal seal, using a pair of matched C-shaped pole pieces; (b) External seal, using a spring to retain the metal; (c) a labryinth seal. In each diagram, the heating element is represented by circles.

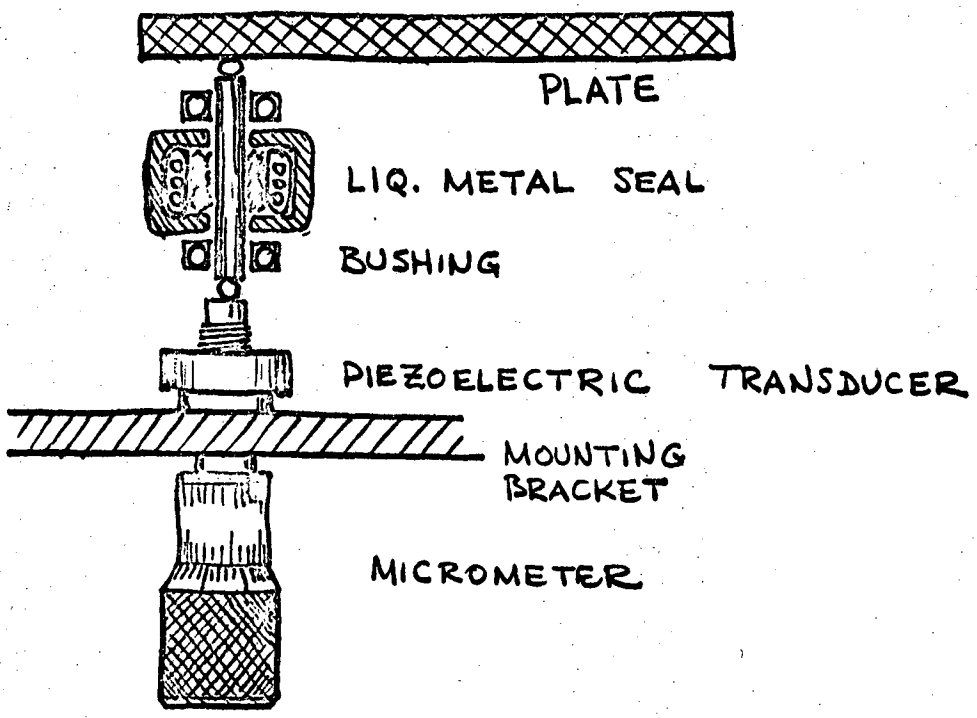

Fig. 31. A device for precise stable positioning of a plate, as an example of an application of the liquid metal seal.

G. ELECTRONICS

The most critical electrical requirement is time stability of power supplies. Use of low voltages in an electrostatic analyzer makes this requirement less critical, and if superconducting magnets are used, the stability of the persistent currents should be acceptable. This fact alone militates for a superconducting analyzer, and experience has already indicated that greater stability is indeed achieved in such systems [X.1].

No other electronic difficulties are anticipated, and no exotic equipment will be required. Power for the spectrometer, detectors, and vacuum system, fast amplifiers for the electron pulses and photomultiplier signals (for laser mixing frequency generation), 100 MHz mixer and lock-in detector, pulse-counting equipment, and monitoring equipment are all commercially available and should pose no limitation.

H. SYSTEM DESIGN

Figure 32 shows a general laboratory layout for transmission measurements. The electron source, gun, and monochromator, and the analyzer and detector are rigidly mounted in a pair of high voltage insulators which are flanged to a central chamber. The chamber supports a feed-thru for holding and manipulating the thin film target. The laser beam is directed through another side port, with appropriate optical accessories inside or outside the chamber. The system is initially pumped with a set of cryopumps, and held to base pressure by an ion pump. The entire apparatus rests on a solid, shock-mounted base. A set of Helmholtz coils and high voltage screens may be provided. Mechanical connection to the inside of the chamber is by offset bellows drives, induction drives, or air core solenoids. The electronics racks are located as far away as practicable to reduce stray fields. Liquid helium dewars are pumped to prevent boiling.

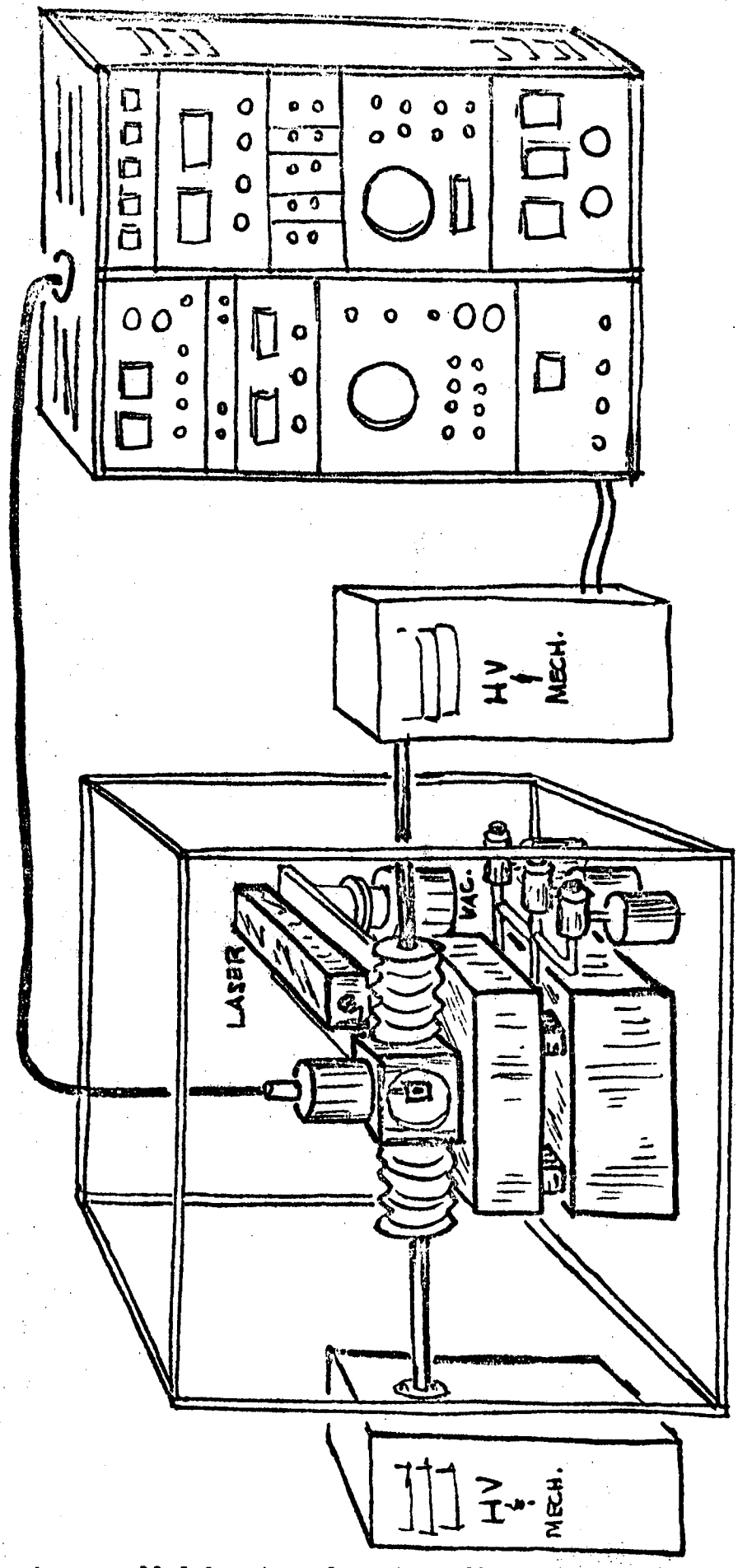

Fig. 32. An overall laboratory layout configuration.

It is not suggested that this configuration is an optimum design. One principle that may be important is maintaining bilateral symmetry. Difficulties such as optical aberrations and stray fields can be reduced to second-order by using a bilaterally symmetric design.

The entire structure in Fig. 32 must be non-magnetic. This requires putting the laser, the vacion pump, and other parts such as power supplies as far away as possible. This conflicts with the vacuum pump requirement (to be as close as possible) so a compromise must be found.

A viewing port is desirable for observing the orientation of the target, for aligning the laser and the laser and the electron beam, and for viewing a diffraction pattern on a luminescent screen. Provision for covering this port must be provided to avoid the light leak to the detector.

Another configuration, primarily for studying diffraction patterns at moderate energy resolution is shown in Fig. 33. Two options are available with this apparatus: 1) Observation of the entire pattern with the fluorescent screen; 2) Detection of the beam with the electron detector, which has high angular resolution. For the second option, two orthogonal rotating flanges are used to generate the polar and azimuthal angles, so that any diffracted beam can be directed into the detector. There are certain complications associated with attaching the target to the monochromator and rotating them together, most notably the problem of coupling the laser beam to the thin film. This problem is not at all insuperable, but does complicate the mechanical design.

In Fig. 34 a somewhat different arrangement is shown. Here the detector cryostat is mounted from below, and the target and laser beam are concentric from above. The advantage of this design is the ganging of two attachments onto one port, leaving an extra port free. Again the price paid is mechanical complexity.

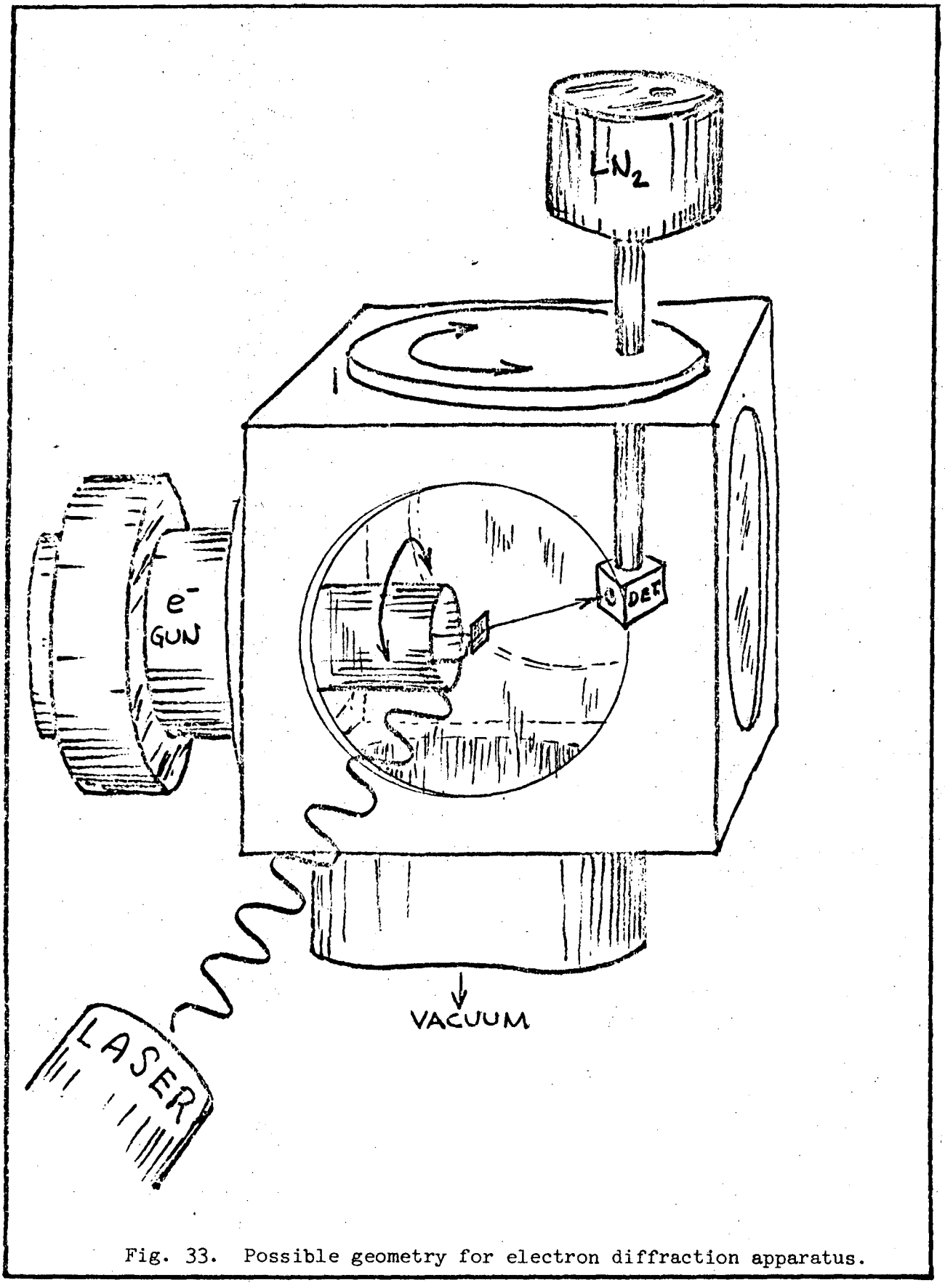

Fig. 33. Possible geometry for electron diffraction apparatus.

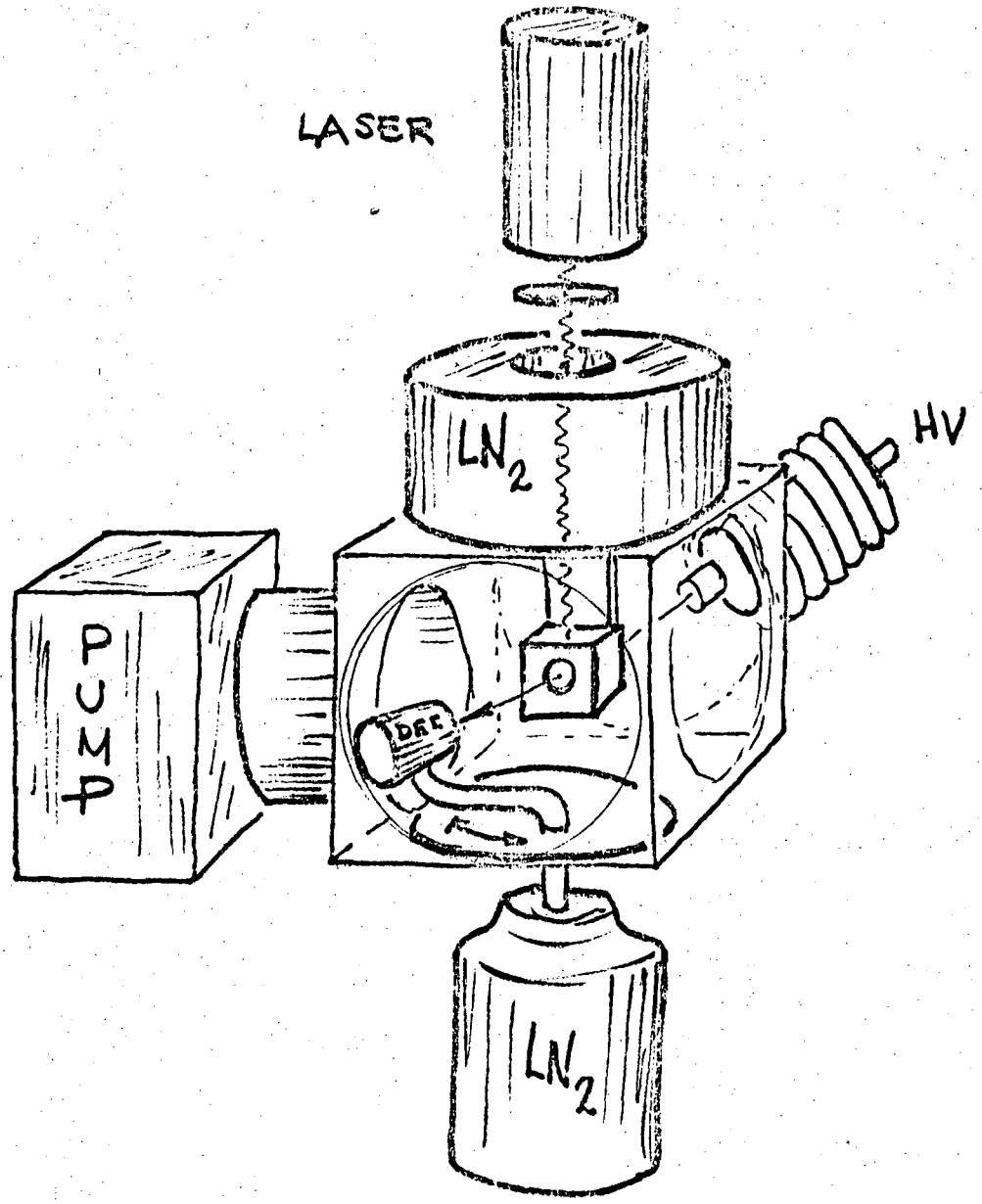

Fig. 34. Another possible geometry for electron diffraction apparatus.

VI. PROPOSED MEASUREMENTS AND EXPERIMENTS

In this chapter we describe a basically chronological program for evaluating the apparatus, observing and studying the modulation, and then performing useful experiments. It is expected that the modulation could be definitely observed and some quantitative measurements obtained within two years. Other experiments would depend on developments.

A. STUDY OF THE MODULATION PROCESSES

1. Evaluate Apparatus Performance

Upon completion of the apparatus, the first tests would be of the vacuum system. If necessary alterations would be made to reach the operating range of 10^{-10} Torr. Cycle time, pump-down time, repeatability, stability, and the effects of baking, cryofluids, and mechanical motion on the vacuum must be known. In particular, when the electron beam and laser beam are on, the pressure must change negligibly.

When the vacuum system is secure, the electron spectrometer will be tested. This probably will be done by setting the monochromator at E_0, and sweeping the analyzer across this value. Since there probably will be a variety of ways this could be done [X.25], it should be done several different ways. For instance, with an electrostatic spectrometer, the various electrodes could be swept in voltage; one technique may give better resolution than another. Another technique would be to balance the monochromator and analyzer by setting them to the same voltage, then moving them mechanically for optimum transmission. The angular resolution can be measured by moving a focal-plane collimator, deflecting the beam with a weak field, moving the detector, etc. Since the beam energy and angular distributions enter critically into the interpretation of experimental

signals, it will be essential to know the trends and numerical values of these quantities for all possible ranges.

The laser power can be measured with a commercially available detector [IV.5]. Then the focusing properties of the optical system, the stability and duty-cycle (if any) should be checked, and the effects of temperature changes and vibrations on the focus and intensity should be investigated.

Next, the temperature rise of the crystal with the electron beam, the laser beam, and both should be measured. This may be a difficult problem, unless a chopped mode is used and the relaxation time is not too short, in which case a thermocouple could be used. An optical pyrometer may be necessary.

2. Observe Laue Diffraction Pattern

The next step is to observe the classical Laue diffraction pattern, either on the PbS screen or using the goniometer supporting the energy spectrometer. The quality, cleanliness, stability, and lattice orientation of the crystal film should be determined. The amount of incoherent diffuse background should be measured, and the effects on this and the spot pattern due to heating should be observed. An attempt should be made to extrapolate any observed effects to the limit of zero temperature rise, in order to infer any non-thermal effects.

3. Measure Energy Loss Spectrum

Next, the energy spectrum of electrons passing through the film should be accurately recorded over as wide a range as possible. A phase sensitive detection technique is probably preferable to direct detection, in order to bring out any structure due to phonon and plasmon excitation, Auger and secondary emission. This should be measured as a function of temperature by heating the

crystal electrically and with the laser, and any possible difference noted. Certain films that have been extensively studied, such as Al, could serve for comparisons.

4. Observe Interferometer Fringes

Once the system appears to be operating optimally and the classical electron diffraction and loss phenomena are measured, the laser modulation effects should be sought. It is probably best to start with the simplest arrangement first, even though it may or may not produce the greatest effect. The first experiment would use a single film, illuminated with full multimode laser power. Some parameter (detector position, beam velocity, laser phase(s)), would be varied, and an attempt made to observe a periodic variation in the detected signal. These techniques are described in Sec. IV A. The first observations should be made DC, but then phase-sensitive detection locked to the laser beat frequencies should be used.

Whether or not fringes are observed with a single crystal device, a two-crystal interferometer is the next logical step. Since the achromatic Bragg doublet is least sensitive to the velocity spread, it should be the first to be tried. Again variation of detector position, velocity, laser phase, etc. should produce fringes. In addition, varying the modulator separation should produce fringes with convenient wavelengths. Once these fringes are observed, various optical delay lines can vary the fringe wavelength in a predictable way to verify the existence of the modulation.

It may be desirable to use several different two-crystal geometries, including straight through, two laterally separated crystals, etc. to determine whether the fringes are due to a peculiar instrumental effect or are really modulation effects.

The fringes should be sought using reflection geometry, if possible. The angles of the beams will be about the same as transmission, but the film can be backed with a heat sink, and the fringes may be due to different modulation effects.

5. Study Dependence of Modulation on Experimental Parameters

Once fringes are observed, the next step is to observe their dependence on various experimental parameters. The beam velocity and current, the laser power and wavelength, and the focusing of both beams should be varied. Various crystal types, thicknesses, orientations, compositions, purities and histories should be tried. If possible the film temperature should be varied, the surface intentionally contaminated, the system cycled in temperature and pressure. The results of these investigations should indicate the direction for optimizing the modulation efficiency. It is hoped (and expected) that somewhere near 20% conversion into sidebands can be achieved with optimum parameters, perhaps more.

6. Separate Qualitative Modulation Mechanisms

The next step is to attempt to analyze the fringe data into its contributions from various modulation mechanisms. The various terms in the perturbation expansion lead to different qualitative effects, such as the dependence on the laser polarization direction relative to the electron beam. It may be possible to isolate these contributions. For instance, using certain polarization, some effects are predicted to vanish, others to remain. The differences between the central and diffracted spots can be examined, the dependence on the angles of intersection of the electron and laser beams and the crystal, the possible

dependence on an applied magnetic field, and the variation with the frequency of the light may give clues to this separation. The goal would be to develop techniques for isolating the effects of each term in the perturbation expansion.

7. Study Quantitative Dynamics of the Modulation

Now we are concerned with accounting quantitatively for the magnitudes of the effects. It will be necessary to measure the absolute intensity of the laser, the inelastic scattering cross section, the spectrometer transmission, the detector efficiency, and so on. The relative intensities of the spots, their shapes and positions, the quantitative magnitude of the fringes, etc. will have to be measured. The object is to determine whether any important effects have not been included in the theory that might be influencing the observations, and to gain a more detailed understanding of the physics of the modulation process.

B. MEASUREMENTS WITH INTERFEROMETERS

As might be expected, the proposed modulation interferometers could be used to perform a variety of precision measurements. These measurements depend on quantities such as the modulation separation L, the beam velocity v, and the laser frequency ω, and can therefore be classed as measurements of length, velocity, time, frequency, etc.

1. Length Measurements

It was shown in Sec. IV A.2 that by appropriately coupling the modulator crystals and optical delay lines that a peak-to-peak fringe separation ΔL of any arbitrary value $0 \leqslant \Delta L \leqslant \infty$ can be generated. This fact can be used to compare and transfer lengths over wide ranges.

Suppose, for example, we want to determine some wavelength λ_2 in terms of laser light of known wavelength λ_1. By coupling two optical interferometers together, we can determine λ_2 by counting the number of fringes passed in each interferometer by varying the spacing the same amount for each. If N_1 fringes of λ_1 light, and N_2 fringes of λ_2 light are seen, then

$$N_1\lambda_1 = N_2\lambda_2 \quad . \tag{56}$$

The relative error in λ_2, assuming λ_1 is perfectly known, is

$$\frac{\sigma(\lambda_2)}{\lambda_2} \cong \sqrt{\frac{1}{N_1} + \frac{1}{N_2}} \quad , \tag{57}$$

where we have assumed N_1, N_2 to have normal errors $\sigma(N_1) = \sqrt{N_1}$, $\sigma(N_2) = \sqrt{N_2}$. If $\lambda_1 >> \lambda_2$, then $N_1 << N_2$, and $\sigma(\lambda_2)/\lambda_2$ will be large. However, using the laser-modulated electron interferometer, it is possible to make N_1 any number we please, presumably the largest number consistent with stability of the electron fringes. Since the relationship between λ_1 and the observed ΔL is precisely known (Eq. (36)), the unknown wavelength λ_2 can be determined with greater accuracy than with a direct comparison of fringes. In fact, in the limit $\Delta L << \lambda_2$, the error is reduced by $\sigma'(\lambda_2)/\sigma(\lambda_2) = 1/\sqrt{1 + \lambda_1/\lambda_2}$, which could give as much as orders of magnitude improvement in the accuracy.

An apparatus for making wavelength comparisons is illustrated in Fig. 35.

It may be noted that, in principle, the interferometer is sensitive to very tiny displacements, down to Å or less. It would not be practical to attempt measurements of this accuracy, however, since apparatus noise would mask the

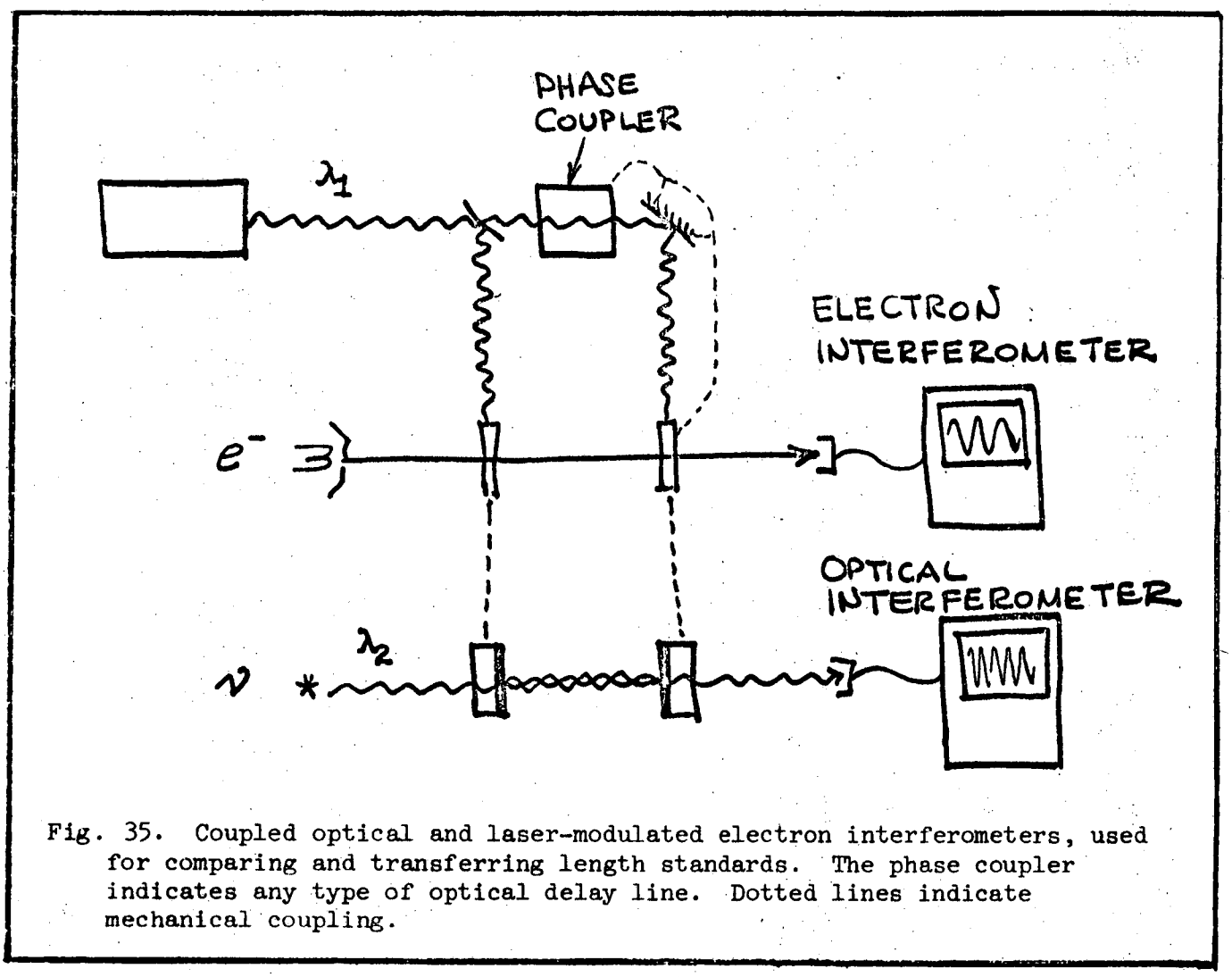

Fig. 35. Coupled optical and laser-modulated electron interferometers, used for comparing and transferring length standards. The phase coupler indicates any type of optical delay line. Dotted lines indicate mechanical coupling.

fringes. On the other hand, this very instability could be investigated by reducing ΔL until the fringes were just barely visible, and then investigating the sources of noise. Such techniques could be valuable in developing low noise mechanical devices.

2. Velocity Measurements

The interferometer fringe wavelength ΔL also involves the electron velocity $v = \beta c$, and therefore could be used to determine v directly from, say Eq. (36). The accuracy of this approach is probably not great, however, since

the error in v is proportional to the error in ΔL, which is largely due to poor statistics.

On the other hand, a non-achromatic two-crystal interferometer would be an extremely sensitive means for measuring small velocity shifts. This should be evident from the discussion of Sec. V A.2. For the conditions following Eq. (50a), shift of one full fringe represents a velocity change of 20 ppm. Such sensitivity would certainly make available many new measurements. However, the achievement of the velocity resolution necessary for successful operation of a non-achromatic interferometer is, at least presently, unlikely.

A typical velocity shift experiment is diagrammed in Fig. 36. Before passing through the interferometer, the electrons pass through some field that imparts an impulse that shifts their velocity by δv, which causes the fringe pattern to shift by $\delta\Phi$. For instance, an external time dependent (oscillating) magnetic field will produce an electric field which modifies the velocity.

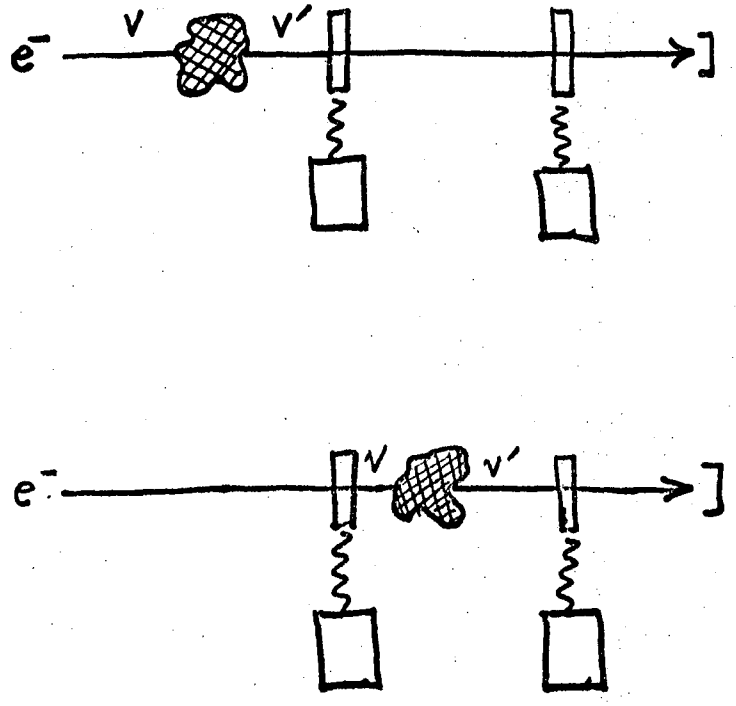

Fig. 36. Two ways of measuring a velocity shift. One method may be favored by a particular experiment or apparatus.

Since the analyzer must be readjusted to pass the electrons with modified velocity, it is not clear whether the interferometer provides any advantage in the measurement of the velocity shift, and this is probably true for ordinary measurements. There is a certain class of measurements, however, for which the interferometer may be the best or only way to measure velocity shifts. This will occur when a shift occurs as the electrons enter the interferometer, and an equal but opposite shift occurs as they leave. Under this circumstance, the analyzer setting remains the same, but the fringes are modified. The investigation of such effects may lead to new understanding of electron-solid interactions, crystalline fields, etc.

It is not difficult to imagine velocity shift mechanisms of this kind, although they may be far-fetched in the absence of either theory or experiment. For instance, it is well-known that as an electron enters a solid, the inner potential, due to incomplete shielding of the positive ions, accelerates the negative electron by several eV, so that its kinetic energy inside the solid is larger than the incident kinetic energy. Presumably when the electrons leave the process is exactly reversed, so no net shift results. However, if there is anisotropy in the crystal, there may be an associated electron polarization, so the crystal can be represented as a potential well with a sloping bottom, and sides at different potentials. The result of crossing this pseudo-double-layer will be to give the electron a kick, speeding or slowing it in its flight toward the second modulator crystal. If the second crystal is identical but reversed, the velocity is restored to its initial value, but the interferometer path has been crossed at a different velocity than that seen by the monochromator/analyzer. Actually, this shift could be measured directly using one crystal; the next example is not this way.

Consider a parallel-plate interferometer like that of Fig. 9. Due to absorption of laser light, the modulator films are heated, and radiate into both hemispheres. Thermal energy emitted leftward of the left modulator and rightward of the right modulator is absorbed far away, but energy emitted in the opposite direction is absorbed and reflected by the other modulator, which may be very near. The two films therefore act like a blackbody cavity with higher temperature inside than outside. The walls of this cavity therefore sustain a temperature gradient and two effects may happen: 1) the electrons may scatter into the cavity with slightly higher energy due to the higher internal energy density on the inside of the walls (the "radiometer effect" for electrons); 2) the temperature gradient will produce a potential drop across the film $\Delta v = \sigma \Delta T$, where σ = Thomson coefficient ($\sim$ microvolts/deg). This will also lead to a slightly higher potential inside the cavity, and the electrons will traverse the interferometer at a slightly higher velocity.

3. Time Measurements

A class of measurements for which the electron/laser interferometer is well-suited is encountered when the electrons interact with a field while inside the interferometer and suffer a time delay but no net velocity shift. Such a situation is shown in Fig. 37. Virtually any interaction would produce a delay, but large delays are associated with resonant scattering.

The effect of a time delay Δt on the fringe phase Φ can be determined from Eq. (31c) in the simple case. We can imagine the electron to travel a distance L_1 into the interferometer at velocity v, then suffer an impulse so it travels a small distance δL at velocity v', then a reverse impulse so it covers the remaining distance L_2 at v. The total phase is then

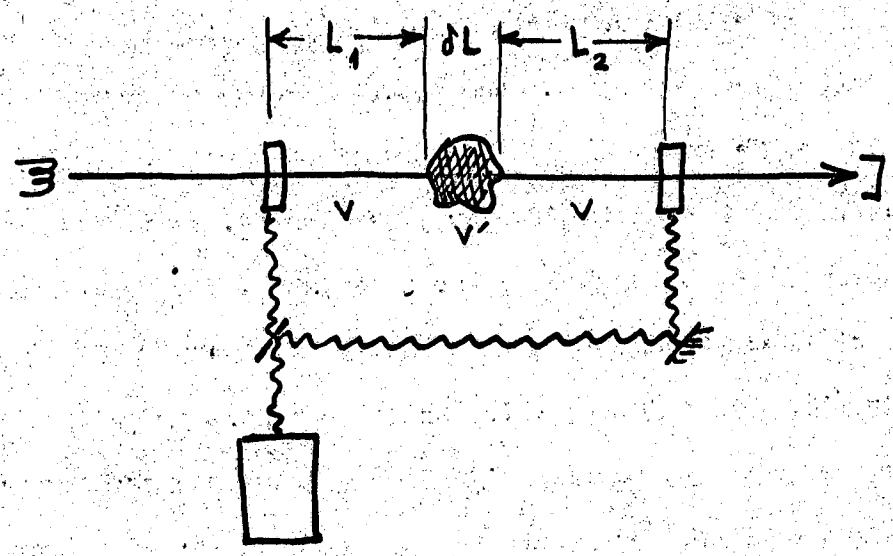

Fig. 37. Study of a time-delay interaction with a two-crystal interferometer.

$$\Phi = \Delta\omega\left(\frac{R}{v} - t\right) + \frac{\omega L_1}{v} + \frac{\omega \delta L}{v'} + \frac{\omega L_2}{v} + \Delta\phi + \Delta\delta \quad , \tag{58}$$

which may be rewritten

$$\Phi = \Phi_0 + \frac{\omega}{v}(L_1 + L_2 - L) + \frac{\omega \delta L}{v'} \quad . \tag{58a}$$

If we define the time delay $\Delta t = \delta L/v'$ and take the limit as $\delta L, v' \to 0$, then, since $L_1 + L_2 \to L$, we find

$$\Delta\Phi = \omega\, \Delta t \quad , \tag{58b}$$

where we used $\Delta\Phi \equiv \Phi - \Phi_0$. This result is easily understood by remembering that the laser is impressing modifications on the wavefunction at the frequency ω, so that the phase difference associated with a time difference Δt is simply $\omega\Delta t$.

The result of Eq. (58b) indicates an extreme sensitivity of the interferometer to time delays. Since ω is such a high frequency, a very small time delay can mean a large fringe shift. For instance, at $\lambda = 5000$ Å, a shift of one full fringe ($\Delta\Phi = 2\pi$) is produced by a delay of $\Delta t \sim 10^{-15}$ sec. This sensitivity is not vitiated when using an achromatic interferometer, since the velocity is not a parameter in Eq. (58b).

As an example of the application of this effect, consider a measurement of the level structure of core electrons in a heavy atom. For $60 \leq Z \leq 80$, the K binding energies range from about 35 keV to about 80 keV, the general range in which the electron interferometer works. Suppose a small amount of vapor is injected into the interferometer and the beam energy is scanned across the region of an atomic K-shell transition. The widths of these transitions are $\Gamma \sim 10 - 60$ eV, implying the time delay on resonance is $\Gamma^{-1} \sim (0.5 - 0.1) \times 10^{-15}$ sec, or an appreciable part of one fringe. Thus, as the energy is scanned across the resonance, the fringes will anomalously shift to one side and then return as the resonance is passed. The maximum anomalous shift is a measure of the width of the transition. In this way, both the positions and widths of core transitions can be determined, probably with comparable or better accuracy than conventional photoelectron techniques. In this case, the anomalous dispersion of the target vapor is probed with an interferometer, a technique entirely analogous to the Hook method in optical atomic spectroscopy. An additional advantage acrues from using electrons, however: the transitions that can be studied are not limited to electric dipole transitions as in the optical case.

4. Other Measurements

The fringes also depend on ω, $\Delta\omega$, and $\Delta\phi$, and in principle these could be measured. However, laser frequencies are known very accurately from ordinary spectroscopy, and the phase shift $\Delta\phi$ would usually be known *a priori* from the geometry, so the electron interferometer probably will be of no value in studying laser properties.

It was pointed out in Sec. IV A.2 that it should be possible to "zero-beat" away all parameters in Φ, leaving the fringes determined only by $\Delta\phi$ (the relative laser phase) and $\Delta\delta$ (the relative scattering phase). Thus, by scanning $\Delta\phi$ with an optical delay line, it should be possible to determine $\Delta\delta$ directly. It will, of course, be necessary to know $\Delta\phi$ absolutely, modulo 2π.

C. FUNDAMENTAL EXPERIMENTS

The laser-modulated electron interferometers proposed here combine two unique and valuable properties of ordinary electron and optical interferometers:

1. The interfering particles have charge, mass, and magnetic moment.
2. The fringes are easily controlled using ordinary optical components such as delay lines, compensators, and polarizers.

These advantages will make possible many new experiments of a fundamental nature. As two examples of experiments of this kind, we suggest measurements of the physical reality of electromagnetic potentials in Quantum Theory (the Aharanov-Bohm effect) and the gravitational force on the positron.

1. The Aharanov-Bohm Effect

The Aharanov-Bohm effect [XIV.1,2] has been taken as evidence that electromagnetic potentials have physical reality in quantum theory and cause observable effects. In the original experimental arrangement (cf. Fig. 38(a)) an electron

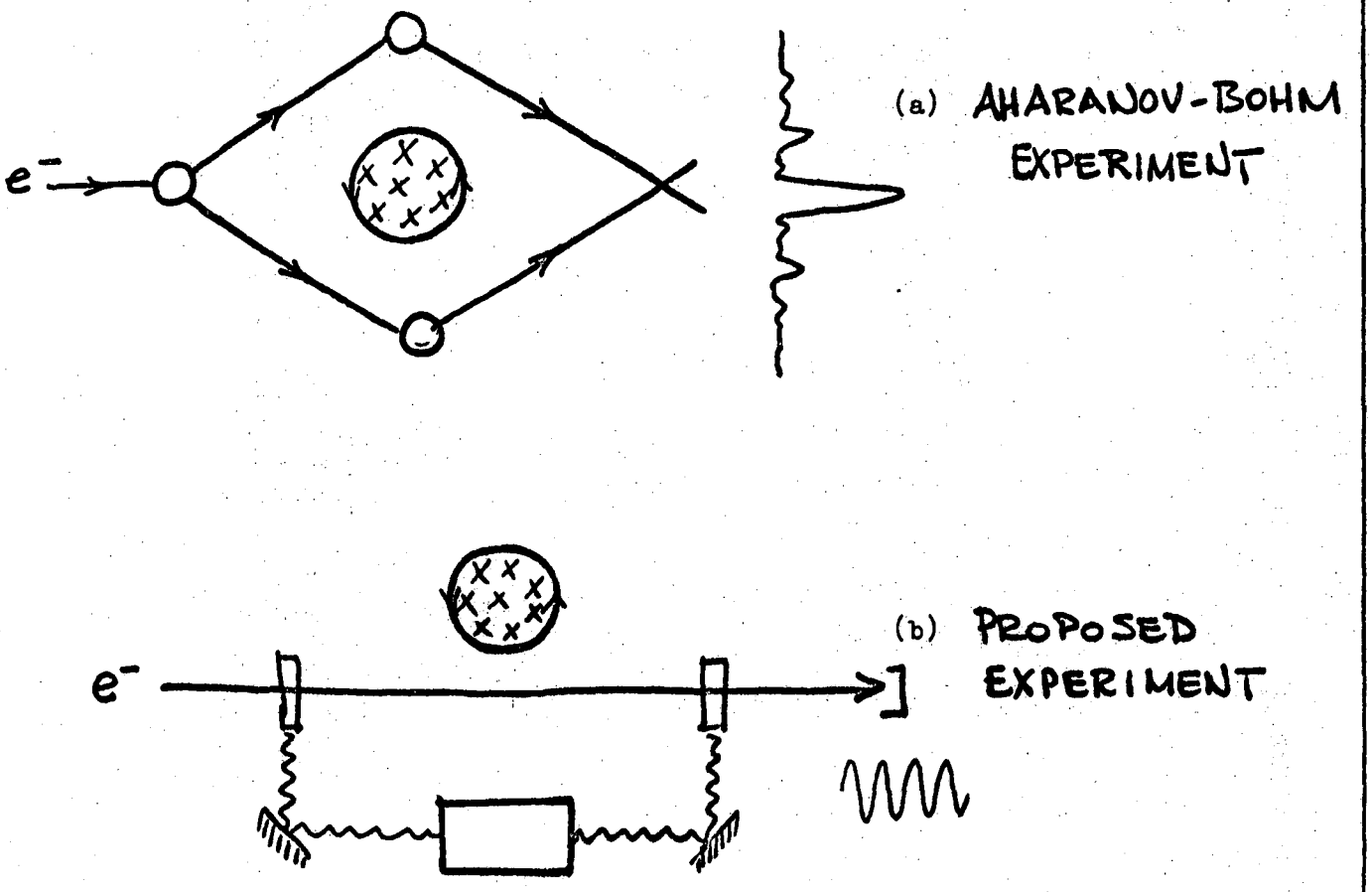

Fig. 38. Two experiments to test for electron interaction with the magnetic vector potential of a solenoid in a zero-field region. (a) The original Aharanov-Bohm experiments; (b) An experiment proposed here using a laser modulated electron interferometer.

beam is coherently separated into two beams which are passed on opposite sides of a long solenoid perpendicular to its axis and recombined on the far side where an interference pattern is observed. The pattern is found to shift as the current in the solenoid is varied. Since the electrons are (presumably) always in a field-free (but not potential-free region), this observation seems to imply the physical reality of the potentials.

The interpretation of such experiments has been criticized by Boyer [XIV.3,4] on the grounds that classical field effects could account for the observation without the need for potentials. In particular, Boyer recently has shown that second-order fields react back on the electrons in an asymmetric fashion, causing small variations in the velocities which in turn shift the interference pattern. This "time lag" effect is an entirely classical one that does not require potentials for its existence.

The author would like to suggest that such a time lag could be observed directly with a modulated electron interferometer as described above. The experiment would use a single electron beam (rather than two spacially separated beam) and a single laser frequency to generate fringes according to Eq. (31c). The solenoid would be located near the beam and its current varied. If this causes a time lag Δt, the interferometer phase will shift by $\Delta\Phi = \omega\Delta t$. At optical frequencies, a shift of one full fringe will represent $\Delta t \sim 10^{-15}$ sec. This sensitivity should be more than sufficient, since Boyer has presented an example in which a 1 cm diameter solenoid with a 1 kG field delays $\beta = 0.1$ c electrons by 2×10^{-9} sec, or roughly 10^{6} fringes. This experiment appears to be entirely feasible, and should be one of the first tried, once a working interferometer is built.

Aharanov and Bohm, and Boyer have also proposed experiments making use of electrostatic fields, such as passing the beam through hollow conductors held at some voltage. Inside the conducting shells, the field is zero but the electrostatic potential is non-zero, and fringe shifts similar to the solenoid arrangement can be predicted by invoking potential effects or time lag effects. Such experiments could also be performed using a laser/electron interferometer.

2. Gravitational Mass of Elementary Particles

The gravitational force on the positron has been a problem of great interest because of the question of its sign and magnitude [XV.1,4]. Does antimatter fall up or down? Is $|m(e^+)| - |m(e^-)| = 0$? Experimentally, little progress has been brought to bear on the problem. The author believes that the modulated electron interferometer may have some relevance to such a measurement, since it should operate as well with positrons as with electrons. Although the numbers presently appear somewhat unfavorable, we believe the proposal merits consideration as a fundamentally new approach to the problem.

Suppose we orient the interferometer path vertically (Fig. 39(a)) and permit electrons or positrons to drift upward under free fall in the earth's gravity field. If the particle velocity is v, the phase change of the modulation over a small distance dL will be

$$d\Phi = \frac{\omega}{v}\, dL \quad . \tag{59}$$

If we assume that the electron (positron) gravitational mass is m(-m), then the velocity v will be different for the particles--electrons will be slightly slowed, while positrons will speed up slightly. From conservation of energy,

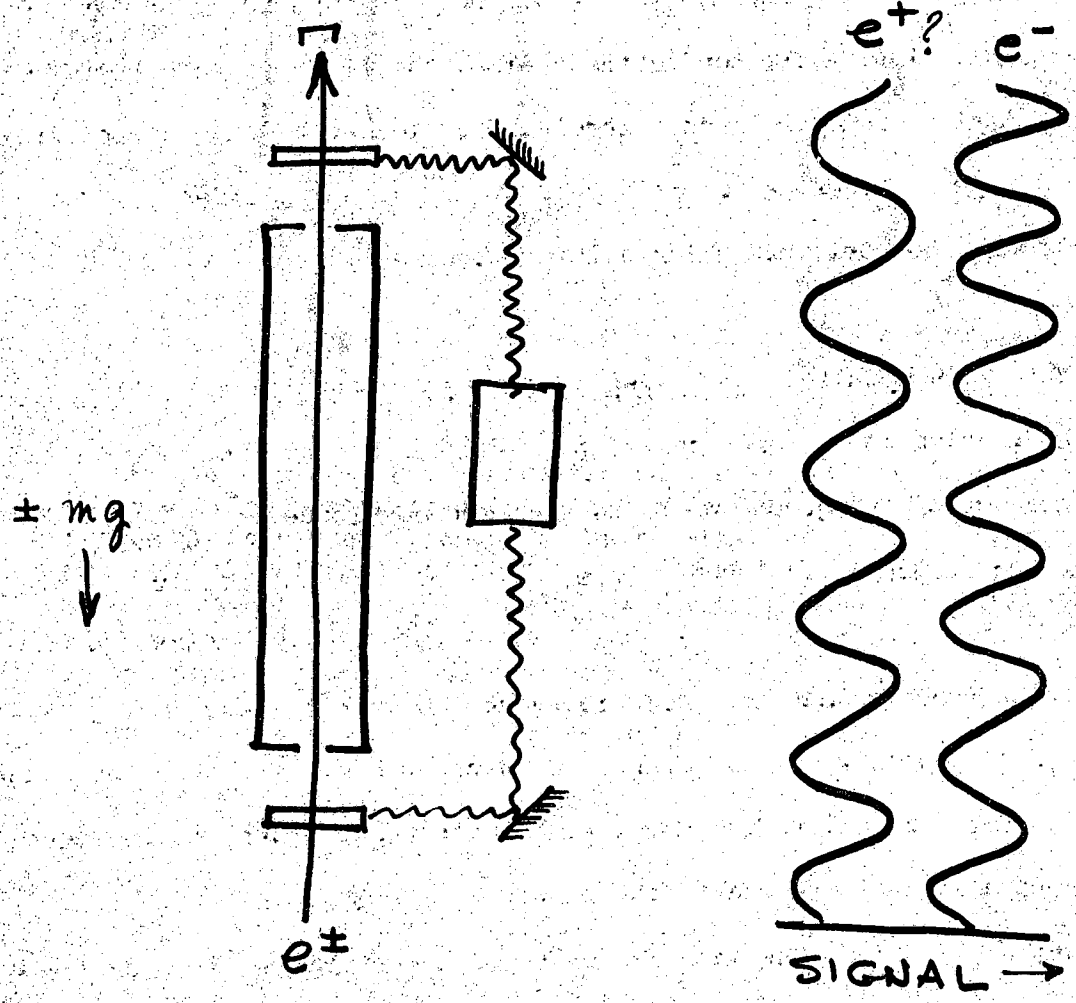

Fig. 39. Proposed experiment to measure the gravitational force on elementary particles. The particles drift along a vertical interferometer, producing a fringe pattern that depends on their velocities. Particles with positive gravitational mass will produce fringes that are slightly compressed toward the vertical, while negative mass particles will produce expanded fringes toward the vertical.

$$\frac{1}{2} mV^2 = \frac{1}{2} mv^2 \pm mgL \quad , \tag{60}$$

where v is the initial upward velocity and ± refers to $e^{\pm}$. Substituting (60) into (59) and performing the integration, we find

$$\Phi = \pm \frac{\omega v}{g} \left[\sqrt{1 \pm \frac{2gL}{v^2}} - 1 \right] \quad . \tag{61}$$

Thus, the interferometer fringes are gravitationally shifted by the amount

$$\delta\Phi \cong \mp \frac{\omega g L^2}{2v^3} \quad , \tag{62}$$

for $\delta\Phi << \Phi$. Expressed differently, the separation of adjacent fringes ΔL is altered by the amount

$$\frac{\delta(\Delta L)}{(\Delta L)} = \pm \frac{gL}{v^2} \quad . \tag{63}$$

Thus, in the free (upward) fall, the electron fringes are slightly compressed, while the positron fringes are slightly expanded. This is illustrated in Fig. 39(b). The same relations with opposite signs obviously hold for particles in free (downward) fall.

Relations (62) and (63) suggest several experimental techniques. One would be to pass electrons and positrons through the interferometer simultaneously, and look for a difference in the phase of the fringes for electrons and positrons, e.g., by varying the optical phase $\Delta\phi$ with an optical delay line. If the gravitational masses are the same, the fringe maxima would occur simultaneously. If they have opposite signs, the maximum positron signal would be obtained by shifting the phase $\Delta\phi = \omega g L^2 / v_0^3$ from the setting for maximum electron signal.

A simpler technique would be to compare the fringe spacings at the lower and upper modulators for either electrons or positrons alone. From Eq. (63), the displacement ΔL necessary to move one fringe is larger for the upper modulator, for positrons drifting upward. It is a remarkable property of the interferometer that displacing the upper modulator is not equivalent to displacing the lower one. The same asymmetry could be observed by varying the optical phase of the laser at the upper and lower modulators independently, using two optical delay lines.

At present, the numerical estimates of the shifts appear somewhat unfavorable. The particles presumably can be modulated at reasonable beam energies and then slowed for a long drift region, then reaccelerated for the second modulation, thus obtaining a larger phase shift during the slow drift. For 100 eV particles drifting over L = 100 cm and laser wavelength λ = 5000 Å, the relative phase shift is $2\delta\Phi \cong (2\pi)\ 3 \times 10^{-5}$. The change in fringe separation is very small for these conditions; $\delta(\Delta L)/(\Delta L) \sim 3 \times 10^{-13}$. However, the $1/v_0^3$ dependence of $\delta\Phi$ suggests that if we obtain 10 eV particles, the relative phase change is $\delta\Phi \cong (2\pi)\ 10^{-3}$, which is more favorable.

This interferometer technique may be compared with the time-of-flight approach of Fairbank and coworkers [XV.3,5-7]. The phase shift can be written $2\delta\Phi = \omega\Delta t$, where $\Delta t = gL^2/v_0^3$ is the gravitational time delay. For 100 eV particles drifting L = 100 cm, this is $\Delta t \cong 5 \times 10^{-20}$ sec.

The interferometer technique would not require a pulsed subthermal-velocity positron source, which is a difficult requirement. However, it would still be subject to most of the difficulties described by Fairbank and coworkers. In particular, it is still necessary to reduce all electric and magnetic field gradients to below 10^{-10} eV/cm, a very difficult experimental requirement except for a particularly simple arrangement.

VII. OTHER RESEARCH USING THE PROPOSED APPARATUS

It is possible, although in the author's opinion unlikely, that the actual magnitude of the electron modulation is much smaller than estimated, or that incoherent processes will mask the effects sought with the proposal apparatus. If this occurs, and it is not possible to increase the sensitivity and selectivity enough, it would seem important that the apparatus be useful for performing other related research. The proposed apparatus--a highly monoenergetic electron beam, a high power laser, thin crystalline targets, and an ultrahigh vacuum system--has the valuable character of enabling a particularly wide variety of such contingency experiments. A few examples will be briefly discussed; these are meant to be indicative rather than comprehensive.

A. GENERAL EXPERIMENTS

1. Thermal Diffuse Scattering

Typical of experiments that could be performed is the study of thermal diffuse electron diffraction [XI.4]. Above 0°K, oscillations and waves in the crystal modify the lattice, and permit scattering of electrons into non-Bragg directions. This produces a quasi-uniform background that depends on the temperature of the crystal. It is observed in both x-ray and electron diffraction, and is a major technique for studying the elastic constants and frequencies of the normal modes in the range 10^{11} - 10^{14} Hz. With this apparatus, well-defined pulses of laser power could be injected in small regions of the crystal, and the resulting lattice vibrations studied as a function of input energy, pulse length, time after pulse, distance from pulse, polarization of the light, etc.

2. Coherent Parametric Phonon Generation

A particularly interesting process is "phonon splitting", the coherent decay of an optical phonon into two acoustic phonons. This process has been observed recently by a "hole burning" technique [V.5]. The crystal is illuminated with laser light at two wavelengths λ_1, λ_2, thus generating an intense source of optical phonons at the frequency $\omega_p = \omega_1 - \omega_2$. The phonon spectrum is monitored by illuminating the solid with a third (shorter) laser wavelength and observing the anti-Stokes fluorescence. A dip in the fluorescent intensity is observed at $\omega = \omega_p$ due to coherently driven phonon-assisted transport of the (impurity) electronic excitation. In addition, a dip is observed at $\omega = \omega_p/2$, corresponding to the parametric splitting of ω_p phonons into two oppositely directed acoustic phonons, induced by the anharmicity of the crystal.

The proposed apparatus is well suited for studying these processes. The laser provides two lines a few hundred angstroms apart for the phonon pump, and the electron energy loss monitors the phonon spectrum. In this experiment, a peak (rather than a dip) at the energy loss $E - E_0 = \hbar(\omega_1 - \omega_2)$ would be expected, since the assisted transport would make it more likely that this energy could be transferred to the lattice.

B. EXPERIMENTS WITHOUT THE LASER

1. Energy Loss Spectroscopy (Solids)

The electron spectrometer can be used by itself to directly measure the excitation spectrum of various solids, both crystalline and amorphous. The absolute cross sections for plasmon generation, electronic excitation, secondary emission, Auger emission, and other processes can be measured. If the electron

detector is supplemented with a photon detector, optical excitation, x-ray generation, thin-target Bremsstrahlung, and other effects can also be observed, often using coincidence mode to obtain correlation functions.

The energy resolution $\Delta E_0 \sim 10$ meV (a design requirement) also makes available a reasonable portion of the phonon spectrum, virtually all of which lies below 100 meV. If $\Delta E_0 \lesssim 1$ meV, (the design objective), an entirely new domain is reached.

Energy losses below 1 meV have never been resolved, and electrons detected with such small losses are considered part of the "unmodified" spectrum: This spectrum is easily distinguished from the "modified" spectrum, which is due to energy losses greater than, say 100 meV. However, the unmodified part actually consists of a "coherent" part (scattered electrons which have transferred momentum but no energy to the crystal) and an "incoherent" part (scattered electrons which have transferred momentum and energy (say $E - E_0 \lesssim 10$ meV) to the crystal). Thus, a coherent beam of electrons passing through a solid loses coherence due to the unresolvable inelastic collisions. Gabor [II.1] has emphasized that this coherence loss is largely unmeasured; the only current experimental technique is electron interferometry, which indicates the degree of coherence in the beam, but gives no information about the origin of the loss of coherence. It is reasonable to expect that mapping the phonon spectrum below 1 meV will lead to significant improvements in our understanding of electron interferometry, electron microscopy, and crystal structure.

2. Energy Loss Spectroscopy (Atomic and Molecular Vapors and Gases)

The technique of electron energy-loss spectroscopy now is widely used to measure the energy levels of atoms and molecules. The advantage lies in the

ability to pump states not reachable by photon absorption, although this is offset somewhat by the relatively large electron energy spread. Reduction of the spread to 1 meV would resolve many multiplets, the Na $3^2P_{3/2} - 3^2P_{1/2}$ doublet (18 cm^{-1}) for example. It may be noted that the natural width of atomic core transitions for $Z \gtrsim 10$ exceeds 1 meV; hence the apparatus could be used for resonant excitation and absorption with effectively monochromatic projectiles. In this way both energies and lifetimes could be measured by scanning the primary beam across an absorption line.

3. Channelling

It is assumed that the angular resolution of the spectrometer will be $\Delta\theta < 10^{-4}$ rad. Since the FWHM of a channelled beam is $\sim 10^{-4} - 10^{-3}$ rad, it should be easy to make quantitative measurements of various channelling phenomena [VII.1-3]. Such information will be particularly valuable, since the laser modulation phenomena may depend strongly on channelling effects. This is because well-channelled particles interact less strongly with the lattice (as seen by increased range, decreased x-ray production, etc.), while certain modulation mechanisms directly involve the lattice structure (e.g. polarization of the crystal by the laser). Such information is of interest in its own right.

4. Patch Effect

The individual crystallites in a solid have typical dimensions 5×10^{-3} cm, and contact potentials varying by several tenths eV [IX.1]. Since it should be possible to focus the electron beam to dimensions $\sim 10^{-4}$ cm, it is possible to spacially resolve the patches. To measure the variations in contact potential, we can measure the variations in apparent Bragg angle. This is so because the

electrons are accelerated by the patch potential as they enter the solid, and Bragg scatter at angles determined by the modified momentum, not the incident momentum [VII.6]. If W is the work function for a certain crystallite, then the Bragg angle is shifted by $\delta\theta \sim \sqrt{W/E_0}$, which can be large enough to measure easily. The measurements of W over the surface would be done by measuring $\delta\theta$ over the surface. Such measurements should provide direct information on patch structure, and perhaps lead to techniques for reducing or compensating it.

6. Gunn Effect

It was discovered by Gunn [XIII.10] that certain semiconductors, notably GaAs, develops a single domain of negative electrical resistance when subjected to an electric field larger than some threshold, and that this domain appears at the negative terminal and moves to the positive terminal, where it vanishes, permitting the formation of a new domain at the negative terminal, thus producing oscillations from an applied DC voltage. Typically these oscillations occur at some MHz. The structure of the inverted domain could be probed with the electron spectrometer, and should prove quite interesting since it is a non-equilibrium system. The oscillation provides an automatic frequency reference for phase sensitive detection. Of particular interest would be the return to equilibrium after the domain passes.

C. EXPERIMENTS WITHOUT THE ELECTRON BEAM

1. Nonlinear Optics

No review of the maturing field of nonlinear optics [V.1] is needed here. It is obvious that with the high power laser and thin crystalline films of controlled quality, that only an additional optical photon detection system is needed to enter

this large field. There is better motivation for this than mere curiosity, however. Since the electron/laser interferometer operates with second-order effects, the effects of nonlinear-polarization of the solid may be significantly present. Interpreting the interferometer signals may depend at least partly on understanding the nonlinear optical response of the solid.

2. Electron Evaporation

In pulsed mode, the laser can generate local temperatures of many thousands of degrees, producing thermionic emission. Such effects have received considerable study [IV.4]. The energy resolution of the proposed spectrometer would probably have to be degraded for spectral analysis of the emittants. Of interest would be the dependence on crystal orientation and material.

D. EXPERIMENTS WITH NO CRYSTAL TARGET

1. Intense-Field Electrodynamics

A large number of second order effects are expected in the interaction of free electrons with intense electromagnetic fields. Eberly [III.1], has reviewed this interesting field and has described a variety of experiments that have been suggested. Some of the predicted effects are:

a) Mass Shift: In the laser field $\vec{A}$, the electron mass-energy relation is $E^2 = p^2c^2 + m^2c^4 + e^2A^2$, indicating the rest-mass-squared suffers a shift Δm^2 proportional to the intensity of the electromagnetic field;

b) Reflection: Electrons of total energy less than $(\Delta m^2/2m)c^2$ cannot penetrate the electromagnetic field; they are reflected;

c) Refraction: An electron entering an intense field through a sharp boundary suffers a velocity change $\Delta v_x/v_x = -(1/2) \times (\Delta m^2/m^2)(c/v_x)^2$. The electron is deflected away from the propagation direction of the electromagnetic wave. Electrons traversing a laser beam at a distance b from a focus of half-angle α and radius a is deflected through an angle $\delta\theta \cong (\alpha/\tan^2\alpha)(a/b)^2(c/v)^2(\Delta m^2/m^2)$ (the Kibble Experiment);

d) Diffraction: Electrons incident on a standing electromagnetic wave are preferentially scattered into Bragg directions. (The Kapitza-Dirac Effect);

e) Thomson Scattering: A free electron elastically scatters photons with total (nonrelativistic cross section $\sigma_T = 8\pi r_0^2/3$). Mass shift gives an intensity dependent modification of σ_T;

f) Compton Scattering: A free electron inelastically scatters photons. The cross section is modified slightly by the mass shift. Wavelength shift is modified by $\Delta\lambda = \lambda_c(1 + \Delta m^2/m\omega)$, where λ_c = Compton wavelength, ω = photon frequency;

g) Harmonic Generation: Multiple photon absorption in Compton scattering generates photons of frequencies $\omega_N \approx N\omega$, N = 1,2...;

h) Parametric Decay: An electron may induce the decay of one photon into two;

To this list could be added a variety of polarization phenomena; the analogs of Faraday rotation, birefringence, and Brewster-angle polarization.

Eberly discusses the experimental difficulties with observing these small effects. In some cases, it appears impossible, but it should be noted that at least one group appears to have observed Kapitza-Dirac Diffraction [III.9,10]. It is unlikely, but certainly not out of the question, that the proposed apparatus could be used for these observations.

2. Optical Klystron

In the oscillating electric field of the laser, the electrons suffer classical velocity shifts dependent upon the total optical phases traversed, thus producing a bunching like that of a klystron. This bunching would be unobservable with an incoherent detector, but might be observable using two lasers to form an interferometer. The magnitude of the bunching is probably small.

APPENDIX I

PRELIMINARY EXPERIMENT

As an initial attempt to study the laser effects on electron diffraction, the author has measured the energy spectrum of 75 to 90 eV electrons backscattered from a platinum crystal illuminated with an argon laser. A Varian LEED system with a CdS viewing screen on which could be observed the normal diffraction pattern from the (100) and (111) faces was used. The energy spectrum was measured by applying a bias voltage to a grid between the crystal and screen, and recording collected current versus bias voltage. The bias was swept linearly over convenient ranges at 1.5 eV/min, and the signal (electron current) was stored in a 1024 channel Nuclear Data ND-800 "Enhancetron" signal averager, synchronized with the bias sweep. Repeated sweeps were accumulated to improve the signal-to-noise ratio.

With the laser off, the normal diffraction pattern could be observed on the screen, and the quality of the surface assessed. The energy-loss spectrum showed the normal features (c.f. Fig. 40): a large no-loss (elastic) peak at E_0, a very large peak near zero energy due to secondaries, and a characteristic loss spectrum which is ascribed to the generation of surface plasmons. The latter identification is based on an observed energy $E - E_0 = -17.5$ eV of the smaller peak compared to the predicted surface plasmon energy $\hbar\omega_s = \hbar\omega_p/\sqrt{2} = 15.9$ eV, where $\hbar\omega_p$ is the volume plasmon energy, measured to be $\hbar\omega_p = 22.5$ eV [VIII.1].

The laser was a Coherent Radiation Model 52 having a total power output on 8 lines (4579 Å to 5145 Å) of 3.5 watts. The laser beam entered the LEED chamber through a glass port and impinged on the Pt crystal at a near-glancing angle, with the electric vector oriented nearly perpendicular to the crystal face. Some measurements were also made with the laser striking the crystal near 45°,

with the electric vector again in the plane of incidence. The laser was not focused and had a diameter of about 1 mm, which was about the diameter of the electron beam at the crystal.

In operation the laser was mechanically chopped at 900 Hz, and an AC signal obtained photoelectrically from a window reflection was used as a reference in a Princeton Applied Research HR-8 lock-in detector with a time constant of 10 seconds. The screen current, representing the diffracted electrons, was fed in as the signal. In this way, the output of the lock-in detector, averaged in the Enhancetron, should show no structure except at energies at which electrons are being "lost" (from the incident energy) or "gained" (into sidebands). The only structure that would appear would be coherent with, and presumably due to, the laser.

No positive evidence of energy sidebands or shifts was obtained. From the data and the experimental conditions, one can say that any modifications were less than 1% of the no-loss peak for an incident laser flux of 100 W/cm^2. This result is not a very stringent upper limit on the effect, but definitely rules out an anomalously high conversion which might be implied by the Schwarz-Hora experiment.

Several differences between this experiment and that of Schwarz and Hora should be noted: Our power flux was much lower (100 W/cm^2 compared to 10^7 W/cm^2), our crystal is a conductor (Pt) while theirs was an insulator (Al_2O_3), and our laser wave was not guided in a thin film as was theirs.

The author found that the crystal heated to several hundred °C with the laser on. Since the elastic diffraction pattern and the energy loss spectrum are temperature dependent, this will be a source of difficulty in such experiments. High frequency laser modulation or pulsed laser operation is therefore desirable.

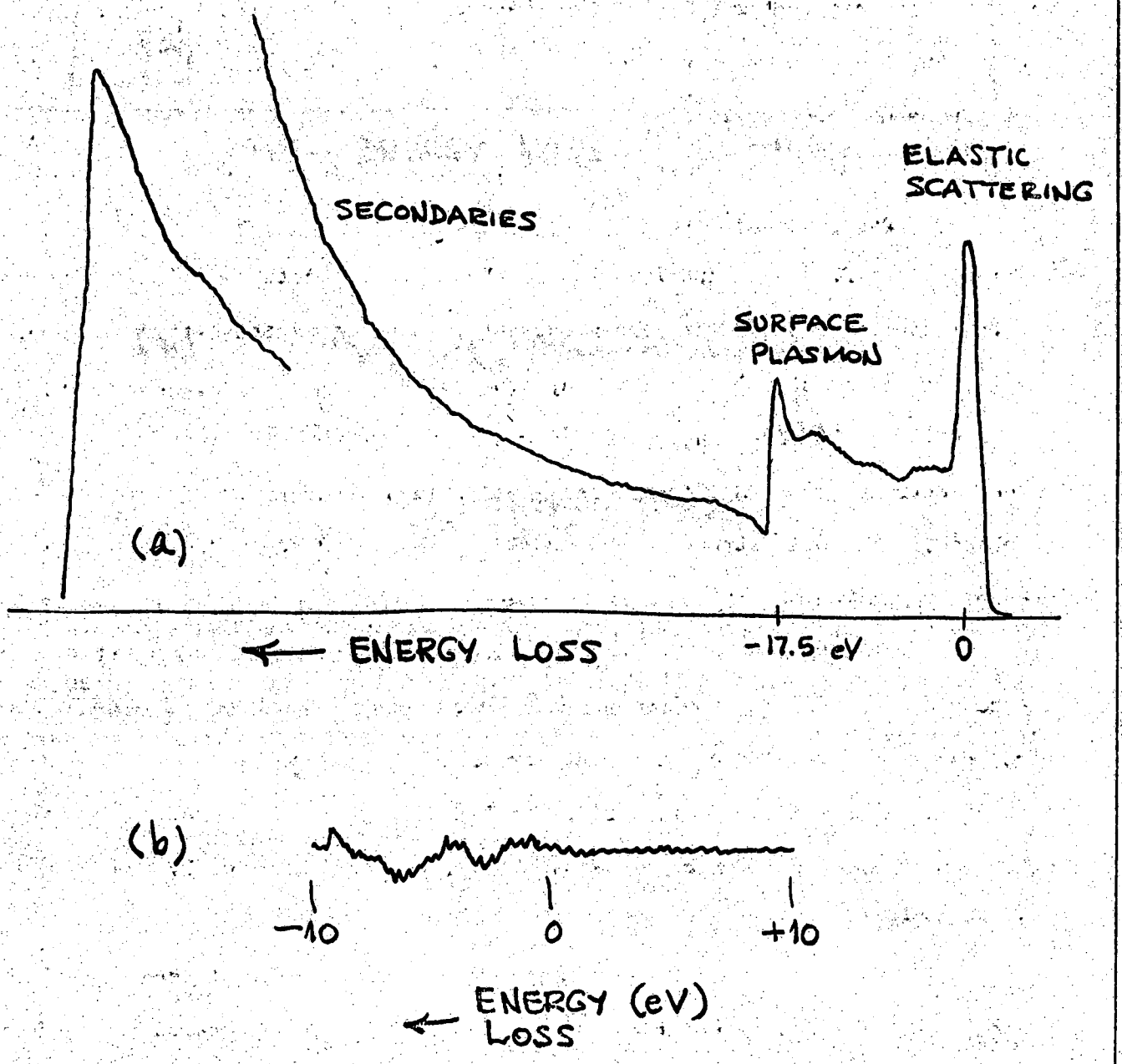

Fig. 40. Results of preliminary experiment on laser-modification of low energy electron diffraction energy spectra. (a) The direct energy loss spectrum without the laser shows the normal features. (b) With the laser on and using lock-in detection, the only structure that would appear would be coherent with (and presumably due to) the laser.

BIBLIOGRAPHY

I. Electron Modulation by Laser Beams

(Entire literature through September 1971)

1. Comment on the Solution of the Schrodinger Equation for a Nonrelativistic Electron in the Presence of Both a Periodic Crystal Potential and Monochromatic Laser Radiation
   H. H. Nickle, Phys. Rev. 160, 538 (1967).
   [A potentially important paper in which invariance properties of the hamiltonian are used to write the exact wavefunction in terms of the solutions to an ordinary differential equation. The wavefunctions are Bloch waves modulated by the long wavelength of the laser.]

2. Amplitude Modulation of an Electron Wave by a Light Wave
   H. Schwarz, Bull. Am. Phys. Soc. 13, 897 (1968).

3. Modulation of an Electron by a Light Wave
   H. Schwarz and H. Hora, Appl. Phys. Letters 15, 349 (1969).

4. Electrons for Carrying Light
   Anon., Nature 225, 15 (1970); 225, 502 (1970); 225, 1173 (1970).

5. Laser-Induced Electron Transmission Diffraction Patterns of Crystalline Films
   H. Schwarz, Proc. Electron Microscopy Conference, Grenoble (France) 1970, Vol. II, p. 151.

6. Modulation of Electron Beams by Laser Light
   H. Schwarz, Trans. N. Y. Acad. Sci. 33, 150 (1971).

7. Quantum Mechanical Bunching of Electron Beams Scattered by a Laser Light Within a Solid Dielectric
   H. Schwarz, Second Int'l. Conf. on Light Scatt. in Solids, Paris, France, July 19-23 (1971).

8. Required Monochromaticity of an Electron Beam Modulated at Optical Frequencies
   H. Schwarz, submitted to Appl. Phys. Letters (1971).

9. Modulation of an Electron Beam by a Light Wave
   P. L. Rubin, JETP Letters 11, 239 (1970).

10. Concerning the Effect of Schwarz and Hora
    A. D. Varshalovich, M. I. D'yakanov, JETP Letters 11, 411 (1970).

11. Quantum Theory of Optical Frequency Modulation of an Electron Beam
    D. A. Varshalovitch, M. I. D'yakanov, 60, 90 (1971).

12. Intensity Relationships in the Schwarz-Hora Effect
    L. L. Van Zandt, Appl. Phys. Letters 17, 345 (1970).

13. Theory of the Schwarz-Hora Effect
L. L. Van Zandt and J. W. Meyer, J. Appl. Phys. 41, 4470 (1970).

14. Optical Modulation of Electrons
A. R. Hutson, Appl. Phys. Letters 17, 343 (1970).

15. Hypothesis for the Schwarz-Hora Effect
B. M. Oliver and L. S. Cutler, Phys. Rev. Letters 25, 273 (1970).

16. The Schwarz-Hora Effect and Modulated Electron Waves
L. S. Cutler and B. M. Oliver, Preprint (November 1970).

17. Monochromatic Radiation from a Coherent Modulated Beam of Charged Particles
L. D. Favro, D. M. Fradkin, and P. K. Kuo, Phys. Rev. Letters 25, 202 (1970).

18. Spacial Dependence of Intensities in the Schwarz-Hora Experiment
L. D. Fradkin, P. K. Kuo, and W. B. Rolnick, Appl. Phys. Letters 18, 352 (1971).

19. Coherent Excitation by a Modulated Particle Beam
L. D. Favro, D. M. Fradkin, and P. K. Kuo, Nuovo Cimento 4, 1147 (1970).

20. Energy Transfer via Scattering of a Coherent Modulated Electron Beam
L. D. Favro, D. M. Fradkin, and P. K. Kuo, Phys. Rev. D 3, 2934 (1971).

21. Cross-Section Enhancement by Scattering with Correlated Nonstationary States
L. D. Favro and P. K. Kuo, Phys. Rev. D 3, 2931 (1971).

22. The Use of Relativistic Energies to Overcome Energy Resolution Difficulties in the Schwarz-Hora Experiment
L. D. Favro, D. M. Fradkin, P. K. Kuo, and W. B. Rolnick, Appl. Phys. Letters (to be published).

23. Electron Diffraction Patterns from Laser Illuminated Crystals
A. Salat, J. Phys. C 3, 2509 (1970).

24. Radiation from a Beam of Modulated Electrons (The Schwarz-Hora Effect)
C. Becchi and G. Morpurgo, Phys. Rev. D 4, 288 (1971).

25. An Attempt to Reproduce the Schwarz-Hora Effect
R. Hadley, D. W. Lynch, E. Stanek, and E. A. Rosauer, Appl. Phys. Letters 19, 145 (1971).

26. Discussion of the Schwarz-Hora Effect
G. R. Hadley, E. J. Stanek, and R. H. Good, Jr., Preprint (1971).

27. The Schwarz-Hora Effect: Bunching of Dirac Particles by Monochromatic and Envelope-Modulated Laser Beams
R. M. Bevensee, Lawrence Radiation Laboratory Report UCRL-51050 (1971).

28. Proposed Laser Modulated Electron Interferometer
R. W. Schmieder, Lawrence Berkeley Laboratory Report LBL-220 (1971).

29. Private communications to the author
D. Wohlleben (1971).

30. Optical Modulation of Electron Beam
G. B. Lubkin, Physics Today 24, No. 6, 17 (1971).
[Review of Progress through June 1971.]

II. Electron Coherence, Interferometry

1. Theory of Electron Interference Experiments
D. Gabor, Rev. Mod. Phys. 28, 260 (1956).
[A vitally important presentation of the basic concepts of coherence and interference in electron waves. Of crucial value in this work.]

2. Collective Oscillations and Characteristic Electron Energy Losses
D. Gabor, Phil. Mag. (8) 1, 1 (1958).
[Discussion of coherence in electron energy loss measurements.]

3. Electron Interferometer
L. Marton, Phys. Rev. 85, 1057 (1952).
[Proposal of the three-crystal interferometer.]

4. Electron Beam Interferometer
L. Marton, J. A. Simpson, and J. A. Suddeth, Phys. Rev. 90, 490 (1953).
[Observation of electron interference fringes.]

5. An Electron Interferometer
L. Marton, J. A. Simpson, and J. A. Suddeth, Rev. Sci. Inst. 25, 1099 (1954).
[Description of a successful instrument.]

6. The Theory of the Three-Crystal Electron Interferometer
J. A. Simpson, Rev. Sci. Inst. 25, 1105 (1954).
[Optical analog.]

7. Photon Electron Interaction - Crystals Without Fields
H. Y. Fan, Handbuch der Physik 25 (2a), 156 (1967).
[A detailed review of the interactions of solids with photons and with electrons.]

8. Light Beating Spectroscopy
   H. Z. Cummins and H. L. Swinney, Prog. in Optics 8, 135 (1970).
   [A review of the phenomena associated with the mixing of two light waves of different frequencies, much of which applies to electron waves as well.]

9. Two-Beam Interferometry
   W. H. Steel, Prog. in Optics 5, 145 (1966).
   [A comprehensive review of optical interferometers, of value in comparing with electron interferometers.]

10. Fourier Transform Spectroscopy
    P. L. Richards, in Spectroscopic Techniques for Far Infrared, Submillimetre, and Millimetre Waves, D. H. Martin, Ed., North Holland Pub. Co., Amsterdam (1967), p. 31.
    [A review of the techniques of transforming intensity vs distance information into intensity vs frequency.]

III. Interaction of Free Electrons and High Intensity Optical Photons

1. Interaction of Very Intense Light with Free Electrons
   J. H. Eberly, Prog. in Optics 7, 359 (1969).
   [A comprehensive and valuable review of nonlinear effects such as mass shift, reflection, refraction, diffraction, and intensity dependent shifts in Thomson and Compton scattering.]

2. Nonrelativistic Quantum Theory of an Electron in an Arbitrary Intense Electromagnetic Laser Field
   H. H. Nickle, J. Math. Phys. 7, 1497 (1966).
   [Solution of Schrodinger equation.]

3. Nonlinear Scattering of Electrons by Laser Beam
   P. T. Chang, Phys. Letters A24, 130 (1967).
   [Consistency of experimental results with energy conservation.]

4. New Nonlinear Parameter in Electron Laser-Light Interaction
   Z. Fried and J. F. Dawson, Phys. Letters 31a, 99 (1970).
   [Characterization of the interaction between two laser beams and an electron beam, all mutually perpendicular.]

5. Classical Theory of High-Intensity Laser Radiation Scattered Off Free Electrons
E. S. Sarachik and G. T. Schappert, Nuovo Cimento Letters 2, 7 (1969).
[Discusses harmonic production in high-intensity Thomson scattering.]

6. Classical Theory of the Scattering of Intense Laser Radiation by Free Electrons,
E. Sarachik and G. T. Schappert, Phys. Rev. D 1, 2738 (1970).
[Complete discussion of high-intensity Thomson scattering, including electron trajectories, harmonic spectrum, etc.]

7. Bremsstrahlung from Electrons Traversing a Focused Laser Beam
G. T. Schappert and K. W. Billman, Phys. Rev. A 2, 547 (1970).
[Predicts experimentally observable bremsstrahlung in the near infrared.]

8. Single-Cycle Electron Acceleration in Focused Laser Fields
M. J. Feldman and R. Y. Chiao, Phys. Rev. A4, 352 (1971).
[Computes energy gain of a free electron in a high-intensity laser pulse during a single half optical cycle.]

9. Observations of Stimulated Compton Scattering of Electrons by Laser Beam
L. S. Bartell, H. B. Thompson, and R. R. Roskos, Phys. Rev. Letters 14, 851 (1965).
[Experimental data on Kapitza-Dirac Effect.]

10. Stimulated Compton Scattering of Electrons by Laser Beam
L. S. Bartell and H. B. Thompson, in Phys. of Quantum Electr., San Juan Conf. (1967), p. 129.
[General discussion of the effect.]

11. The Reflection of Electrons from Standing Light Waves
H. Schwarz, Z. Phys. 204, 276 (1967).
[Description of Experiments.]

12. Experimentelle Prüfung der Streuwahrscheinlichtkeit für Elektronen beim Kapitza-Dirac-Effect
H.-Chr. Pfeiffer, Phys. Letters 26A, 362 (1968).
[An attempt to observe Kapitza-Dirac diffraction.]

13. Multiple Scattering in the Kapitza-Dirac Experiment
G. T. Schappert, Phys. Letters 29A, 6 (1969).
[Obtains scattering probability $P < 1$ by considering multiple scattering.]

14. Electron Scattering from a Standing Light Wave
R. Gush and H. P. Gush, Phys. Rev. D3, 1712 (1971).
[Calculations of transition probability for various conditions.]

15. Trapping of Electrons in a Spatially Inhomogeneous Laser Beam
N. J. Phillips and J. J. Sanderson, Second Rochester Conf. on Coherence and Quantum Optics, Rochester (1966), p. 151.
[Abstract only: Trapping increases interaction time.]

16. Motion of a Charged Particle in a Constant $\vec{B}$ and a Transverse em Wave Propagating Along $\vec{B}$
    C. S. Roberts and S. J. Buchsbaum, Phys. Rev. A135, 381 (1964).
    [A classic calculation of relativistic trajectories in low frequency fields.]

IV. High Power Lasers

1. Effects of High-Power Laser Radiation
    J. F. Ready, Academic Press, New York, (1971).
    [The first comprehensive presentation of heating, damage, particle emission, breakdown, and applications of high-power lasers.]

2. Laser Interaction and Related Plasma Phenomena
    H. Schwarz and H. Hora, Eds., Plenum (1971).
    [Conference papers.]

3. High Power Pulsed Lasers
    D. J. Bradley, Sci. Prog. (GB) 57, 227 (1969).
    [Review.]

4. Charged-Particle Emission Upon Ruby. Laser Irradiation of Transparent Dielectric Materials
    D. L. Rousseau, G. E. Leroi, and W. E. Falconer, J. Appl. Phys. 39, 3328 (1968).
    [Observations of laser pulse generated thermal evaporation of electrons and ions, and the reduction of the emission by thorough cleaning.]

5. Interaction of Intense Photon and Electron Beams with Plasmas
    R. A. Kidder, in Proc. Int'l. Sch. Phys. "Enrico Fermi", Academic Press, New York (1971), p. 306.
    [Discussion of some linear and nonlinear effects.]

6. Introduction to Laser Physics
    B. A. Lengyel, J. Wiley and Sons, Inc., New York (1966).
    [An elementary survey of various properties and types of lasers.]

V. Nonlinear Optics

1. Nonlinear Optics
   N. Bloembergen, W. A. Benjamin, Inc., New York (1965).
   [A standard introductory text and reprint volume.]

2. Nonlinear Optical Materials
   J. G. Bergman, Jr., and S. K. Kurtz, Matl. Sci. Engng. (Neth.) 5, 235 (1970).
   [Collection of data and references.]

3. Dielectrics
   W. F. Brown, Jr., Handbuch der Physik 17, 1 (1955).
   [An extensive review of all significant properties of dielectrics.]

4. Transport Phenomena in Insulator Films
   in Thin Film Phenomena, Chopra, Ed., McGraw-Hill (1969).

5. Generation and Detection of Large-k-Vector Phonons
   M. J. Colles and J. A. Giordmaine, Phys. Rev. Letters 27, 670 (1971).
   [Used two lasers to pump phonon spectrum and burn holes in fluorescence.]

VI. Optical Modulation of Xray Diffraction; Xrays

1. Mixing of X-ray and Optical Photons
   P. M. Eisenberger and S. L. McCall, Phys. Rev. A3, 1145 (1971).
   [A detailed discussion of nonlinear effects involving Xrays and Optical photons, including sum and frequency generation. Much of the discussion is also applicable to electrons and optical photons.]

2. Optically Modulated X-ray Diffraction
   I. Freund and B. F. Levind, Phys. Rev. Letters 25, 1241 (1970).
   [Effect of optically modulating a target on Xray diffraction.]

3. Xray Parametric Conversion
   P. Eisenberger and S. L. McCall, Phys. Rev. Letters 26, 684 (1971).
   [Nonlinear Xray + optical photon phenomena, including the parametric conversion of a photon into two photons. Observation of the effect is reported.]

4. Diffuse X-ray Reflection from Crystals
W. A. Wooster, Clarendon Press, Oxford (1962).
[A complete treatise on non-Bragg diffraction, most of which is equally valid for Xrays and electrons. Describes acoustic sinusoidal modulation of the diffraction to produce sidebands.]

5. The Continuous Xray Spectrum
S. Town Stephenson, Handbuch der Physik 30, 337 (1957).
[A brief but adequate review of observations of electron Bremsstrahlung at X-ray energies.]

VII. Electron Diffraction; Channelling

1. Motion of Energetic Particles in Crystals
S. Datz, et al., Ann. Rev. Nucl. Sci. 17, 129 (1967).
[Review of channelling, etc.]

2. Influence of the Crystal Lattice on Motion of Energetic Charged Particles
J. Lindhard, Mat. Fys. Medd. Dan. Vid. Selsk. 34, (1965).
[A classic discussion of the physics involved.]

3. Quantal Treatment of Directional Effects for Energetic Charged Particles in Crystal Lattices
P. Lervig, J. Lindhard, and V. Nielsen, Nucl. Phys. A96, 481 (1967).
[A valuable discussion of particles moving in crystals.]

4. Electron Diffraction Methods
H. J. Yearian, in Methods of Experimental Physics, Vol. 6, K. L.-Horovitz, V. A. Johnson, Eds., Academic Press, New York, (1959), p. 246.
[A survey of electron diffraction techniques and observations.]

5. Dynamical Theory of Electron Diffraction
K. Kambe and K. Molière, Adv. Structure Res. by Diff. Meth. 3, 53 (1970).
[An outline of dynamical electron diffraction theory and some recent results.]

6. Low Energy Electron Diffraction
G. A. Somorjai and H. H. Farrell, Adv. in Chem. Phys. (to be published).
[Review of methods and results of investigation of surface chemistry by LEED techniques.]

7. Back Reflected Intensity for the Laue Case
R. M. Stern, H. Taub, and H. Wagenfeld, J. Phys. Soc. Japan 28, 723 (1970).
[Calculation of diffracted intensities using dynamical theory, showing that, due to interference of various scattered waves, the current leaving the crystal is periodic in the crystal thickness.]

8. Temperature Dependence of Electron Elastic Diffraction by Aluminum Films
J. F. Graczyk, J. Appl. Phys. 40, 3510 (1969).
[Finds intensities at 77°K are 1-2 times those at 296°K, the factor depending linearly on the film thickness.]

9. Spin Polarization of Elastically Scattered Electrons
H. Boersch, R. Schliepe, and E. Schriefe, Grenoble Electron Microscopy Conf., Vol. II, p. 141 (1970).
[High energy electrons scattered by a solid through large angles are strongly polarized.]

VIII. Energy Loss of Electrons Passing Through Matter

1. The Passage of Fast Electrons Through Matter
R. D. Birkhoff, Handbuch der Physik 34, 53 (1958).
[A detailed and valuable review, if somewhat dated.]

2. Quantum Field Theory of Inelastic Diffraction: I. Low-Order Perturbation Theory
C. B. Duke and G. E. Laramore, Phys. Rev. B3, 3183 (1971);
II. Two-Step Inelastic Diffraction
G. E. Laramore and C. B. Duke, Phys. Rev. B3, 3198 (1971).
[Detailed study of energy loss and diffraction patterns, including predicted new structure in the profiles (v.s. E, v.s. θ) in inelastic diffraction.]

3. An Elementary Theory of Inelastic Scattering of Fast Electrons by Thin Crystals,
Y. Kainuma, J. Phys. Soc. Japan 20, 2263 (1965).
[Typical calculation using dynamical theory.]

4. Theory of Inelastic Processes in Low-Energy Electron-Loss Spectroscopy
J. I. Gersten, Phys. Rev. 188, 774 (1969).
[Formulation of plasmon generation calculations.]

5. Mean Free Path for Discrete Electron Energy Losses in Metallic Foils
A. W. Blackstock, R. H. Ritchie, and R. D. Birkhoff, Phys. Rev. 100, 1078 (1955).
[A fundamental paper which discusses much of the physics of discrete energy losses.]

6. Anregung von Volumen- und Oberflächenplasmaschwingungen in Al und Mg durch Mittelschnelle Elektronen
P. Schmüser, Z. Physik 180, 105 (1964).
[Discussion of energy loss and angular dependence in Al and Mg, including effects of coupling of the two surfaces, giving thickness-dependent effects.]

7. Messung der Energie Verlustspektren von Aluminum- und Silberfolien mit hoher Auflösung
J. Geiger and K. Wittmaack, Z. Physik 195, 44 (1966).
[A high resolution study of the plasmon energy losses at 14.97 eV (Al) and 3.64, 3.78 eV (Ag).]

8. High Resolution Investigation of the Energy Losses of 30 keV Electrons in Aluminum Foils of Various Thicknesses
H. Boersch, J. Geiger, A. Imbush, and N. Niedrig, Phys. Letters 22, 146 (1966).
[Uses double Wien Filters to obtain FWHM $\sim$ 0.07 eV.]

9. High-Resolution Energy-Loss Spectrum of Molecular Oxygen
J. Geiger and B. Schröder, J. Chem. Phys. 49, 740 (1968).
[A study of the molecular spectrum at a resolution of 4 MeV, comparable to optical spectroscopy.]

10. Wechselwirkung von Elektronen mit Gitterschwingungen in Ammoniumchlorid und Ammoniumbromid
H. Boersch, J. Geiger, and A. Bohg, Z. Physik 227, 141 (1969).
[Typical data obtained with spectrometer resolution FWHM = 4 - 10 MeV and $\Delta\theta \sim 1.2 \times 10^{-4}$ rad. Indicates energy losses and gains near 20 MeV.]

11. Observed Radiation from Surface Plasmons in Aluminum
A. J. Braunder, Jr., and E. T. Arakawa, Z. Physik 239, 337 (1970).
[Observation of radiative decay of plasmons at 10.2 and 15 eV.]

12. Information on Excited States of Crystals from Inelastic Electron Diffraction Intensities
J. M. Cowley and S. Kuwabara, Phys. Letters 34A, 135 (1971).
[Crystal electron excitation modifies the inelastic LEED patterns.]

IX. Surface Phenomena

1. Thermionic Emission
   C. Herring and M. H. Nichols, Rev. Mod. Phys. 21, 185 (1949).
   [The classic reference for emission phenomena, especially non-uniform (patchy) surfaces.]

2. Electron Reflection Coefficient at Zero Energy. I. Experiments
   H. Heil and J. V. Hollweg, Phys. Rev. 164, 881 (1967).
   [Special technique measured reflection coefficient as 7% + 39% per eV above zero for Ag.]

3. Electron Reflection Coefficient at Zero Energy. II. Computer Experiments on the Reflection of Slow Electrons in the Electrostatic Field or Surface Patches
   H. Heil, Phys. Rev. 164, 887 (1967).
   [Computer calculated trajectory analysis of reflection from various analytical potentials representing a patchy surface.]

4. Interaction of Slow Electrons with Surfaces
   E. Bauer, J. Vac. Sci. and Tech. 7, 3 (1969).
   [Review of major effects.]

5. Kelvin Device to Scan Large Areas for Variations in Contact Potential
   J. H. Parker, Jr., and R. W. Warren, Rev. Sci. Inst. 33, 948 (1962).
   [Reports contact potentials vary across surface and variations are relatively small for certain materials, including carbon.]

6. Surface Preparation
   J. W. Faust, Jr., in Methods of Experimental Physics, Vol. 6, (Solid State Physics), K. L.-Horovitz, V. A. Johnson, Eds., Academic Press, New York (1959), p. 147.
   [A guide to the preparation and study of clean and smooth surfaces.]

X. Electron Spectrometers

1. Electron Optics (3^{rd} Ed.)
   O. Klemperer, Cambridge Univ. Press, Cambridge (1971).
   [An invaluable intermediate-level reference work on all phases of electron optics.]

2. An Introduction to Electron Optics
L. Jacob, J. Wiley and Sons, New York (1951).
[A somewhat dated and elementary presentation, of value mainly for orientation.]

3. Theory and Design of Electron Beams
J. R. Pierce, D. Van Nostrand and Co., New York (1954).
[A fairly complete and lucid discussion of the physics and engineering of electron guns, lenses, and beams.]

4. Electron Beams, Lenses, and Optics
A. B. El-Kareh and J. C. J. El-Kareh, Academic Press, New York (1970) (Vols. 1,2).
[A design engineering manual with extensive tables for practical design of relatively standard configurations.]

5. Quadrupoles in Electron Lens Design
P. W. Hawkes, Academic Press, New York (1969).
[Detailed study.]

6. Focusing of Charged Particles
A. Septier, Ed., Academic Press, New York (1967) (Vols. 1,2).
[A collection of review articles on various aspects of potential fields, trajectories, lenses, etc.]

7. The Optics of Dipole Magnets
J. J. Livingood, Academic Press, New York (1969).
[A comprehensive treatment of dipole magnets, including especially achromatic systems.]

8. High Resolution Electron Beams and Their Application
L. Kerwin, P. Marmet, and J. D. Carette, in Case Studies in Atomic Collision, Physics I., E. W. McDaniel and M. R. C. McDowell, Eds., North-Holland Pub. Co., Amsterdam (1969).
[A brief review of various spectrometers, and a longer discussion of what they are used for.]

9. Characteristic Energy Losses of Electrons in Solids
O. Klemperer and J. P. G. Shepard, Adv. Phys. 12, 355 (1963).
[A somewhat dated (but still valuable) review of data and their interpretation.]

10. Characteristic Energy Losses of Electrons in Solids
L. Marton, L. B. Leder, and H. Mendlowitz, Adv. Electr. and El. Phys. 7, 183 (1955).
[Review of spectrometers and energy loss measurements.]

11. Electron Beam Spectroscopy
O. Klemperer, Rep. Prog. Phys. 28, 77 (1965).
[An important review of high-resolution electron spectrometers and their use.]

12. Measurement of Momentum [of Charged Particles]
T. R. Gerholm, in Methods of Experimental Physics, Vol. 5, L. C. L. Yuan, C.-S. Wu, Eds., Academic Press, New York (1961), p. 341.
[A review of electric and magnetic deflection analysis, oriented mainly to higher energies.]

13. Das Auflösungsvermögen des Electrostatisch-Magnetischen Energieanalysators für Schnelle Electronen
H. Boersch, J. Geiger, and W. Stickel, Z. Phys. 180, 415 (1964).
[Details of a double Wien filter spectrometer with 17 MeV resolution.]

14. Optimum Adjustment and Correction of the Wien Filter
W. H. J. Anderson, Brit. J. Appl. Phys. 18, 1573 (1967).
[Discusses design and operation for best resolution.]

15. How to Obtain High Resolution with a Wien Filter Spectrometer
J. Geiger, M. Nolting, and B. Schröder, Grenoble Electron Microscopy Conf., Vol. II, p. 111 (1970).
[Uses Wien filter between two immersion lenses and nonaxial injection to achieve resolution of 1.7 MeV at 20 eV.]

16. A Double Wien Filter as a High Resolution, High Transmission Electron Energy Analyzer
W. H. J. Anderson and J. B. Le Poole, J. Phys. E 3, 121 (1970).
[General discussion of double filter.]

17. A Wien Filter for Use as an Energy Analyzer with an Electron Microscope
C. H. Curtis and J. Silcox, Rev. Sci. Inst. 42, 630 (1971).
[An attachment for an electron microscope.]

18. Scanning Electron Diffraction Attachment with Electron Energy Filtering
J. F. Graczyk and S. C. Moss, Rev. Sci. Inst. 40, 424 (1969).
[An instrument with an angular resolution of 2.2×10^{-4} rad and energy resolution of 10^{-5} at 100 keV.]

19. A Parallel Plate Electrostatic Spectrograph
T. S. Green and G. A. Proca, Rev. Sci. Inst. 41, 1409 (1970).

20. An Electrostatic Analyzer with no Fringe Field
F. Mariani, Rev. Sci. Inst. 41, 807 (1970).
[Suggests forming metallic surfaces in the shape of equipotential surfaces surrounding a simple, exactly soluble geometry, e.g. a spherical cap.]

21. Optimized Fields for Double-Focusing β Spectrometers
T. Groth, Nucl. Inst. Meth. 85, 205 (1970).
[Computer calculation of trajectories.]

22. A High Resolution e^- Spectrometer for Use in Transmission Scanning Electron Microscopy
A. V. Crewe, M. Isaacson, and D. Johnson, Rev. Sci. Inst. 42, 411 (1971).
[Design and construction of a magnetic spectrometer with resolution 2 ppm at 20 keV.]

23. An Electron Beam Spectrometer for the Measurement of the Angular Distribution of Plasma Losses in Thin Films
R. S. Cole and J. C. E. Jennings, J. Phys. D 4, 54 (1971).
[A magnetic prism deflection analyzer with 0.7 eV and 0.8 mrad resolution.]

24. Design of a High-Resolution, High-Efficiency Magnetic Spectrometer for Electron Spectroscopy
C. S. Fadley, R. N. Healy, J. M. Hollander, and C. E. Miner, Paper presented at the Photoelectron Spectroscopy Conference, Asilomar (Calif.) September 1971.
[Detailed design of a double-focusing spectrometer capable of resolutions of 10^{-4}.]

25. Methods of Measuring the Performance of an Electrostatic Spectrometer
D. Roy and J.-D. Carette, Rev. Sci. Inst. 42, 1122 (1971).
[Analysis of performance of a 121° cylindrical system.]

26. Improvement of the Resolving Power and Transmission of Electrostatic Spectrometers
D. Roy and J.-D. Carette, Jour. Appl. Phys. 42, 3601 (1971).
[More details about design optimization.]

27. An Energy Modulated High Energy Resol. Electron Spectrometer
D. E. Golden and A. Zecca, Rev. Sci. Inst. 42, 210 (1971).
[Description of a retarded potential difference spectrometer with resolution 8 MeV at 20 eV.]

28. Nuclear Spectroscopy Measurements Employing Modulation of Target Potential
J. Morris and T. R. Ophel, Nucl. Inst. Meth. 40, 245 (1966).
[Techniques for applying high voltage to a target.]

29. Correction of Spherical Aberration by Means of Microwave Lenses
N. C. Vaidya and P. W. Hawkes, Grenoble Electron Microscopy Conf., Vol. II, p. 19 (1970).
[High frequency fields applied to electron optical components to compensate certain aberrations.]

30. A secondary Emission Analog for Improved Auger Spectroscopy with Retarding Potential Analyzers
E. N. Sickafus, Rev. Sci. Inst. 42, 933 (1971).
[Eliminates signal from secondaries by adding simulated secondary spectrum.]

XI. Superconducting Techniques

1. Superconductive Materials and Some of Their Properties
   B. W. Roberts, in Progress in Cryogenics 4, 159 (1964).
   [A complete list of materials, properties, and references through 1963.]

2. Superconducting Resonant Cavities
   E. Maxwell, Progress in Cryogenics 4, 123 (1964).
   [A comprehensive review of the theory and practice of SC cavities. $Q = 2 \times 10^8$ achieved by Fairbank at 2.8 GHz.]

3. A Compendium of the Properties of Materials at Low Temperatures
   R. B. Stewart and V. J. Johnson, WADD Technical Report 60-56 National Bureau of Standards, 1961.
   [Extensive tables and graphs of density, expansivity, thermal conductivity, specific heat, transition heats, phase equilibria, dielectric constants, adsorption, surface tension, and viscosity at low temperatures.]

4. Electron Microscopy at Liquid Helium Temperatures
   H. Fernandez-Moran, Grenoble Electron Microscopy Conf. Vol. II, p. 91 (1970).
   [Design of apparatus.]

5. An Electron Microscope Liquid Helium Stage for Use with Accessories
   J. A. Venables, D. J. Ball, and G. J. Thomas, J. Phys. E 1, 121 (1968).
   [Design.]

6. The Josephson Junction as a Detector of Microwave and Far Infrared Radiation
   P. L. Richards, Lawrence Radiation Laboratory Report UCRL-19035 (196).
   [Experimental results and discussion.]

7. Resonant Nonlinear Response of Point Contact Josephson Junctions
   P. L. Richards, S. A. Sterling, Lawrence Radiation Laboratory Report UCRL-18635 (1968).
   [Microwave feedback of junction to increase sensitivity.]

XII. High Vacuum Techniques

1. The Physical Basis of Ultrahigh Vacuum
   P. A. Redhead, J. P. Hobson, and E. V. Karnelsen, Chapman and Hall, London (1968).
   [The best comprehensive review of the subject.]

2. Handbook of Materials and Techniques for Vacuum Devices
W. H. Knoll, Reinhold Pub. Corp., New York (1967).
[A valuable reference for vacuum properties of glass, ceramics, metals, joining, cathodes, secondary emission, high voltage breakdown, etc.]

3. High Vacuum Engineering
A. E. Barrington, Prentice-Hall, Inc., New Jersey (1963).
[A succinct presentation of high vacuum systems in a readily accessible form.]

4. Ultrahigh Vacuum and Its Applications
R. W. Roberts and T. A. Vanderslice, Prentice-Hall, Inc., New Jersey (1963).
[A brief introductory exposition of typical techniques ca. 1963, with many references.]

5. Cryosorption Pumping of Air on Molecular Sieves at 77°K - The Ultimate Achievable Vacuum
S. A. Stern and F. S. Di Pado, J. Vac. Sci. Tech. 6, 941 (1969).
[General remarks and references relating to best obtainable vacuum.]

6. Ultrahigh Vacuum Bakeable Valves with Integral Spare Seal
R. G. Bernard, J. Vac. Sci. Tech. 7, 267 (1970).
[Short review of techniques.]

7. Selective Pumping of an 800,000 Liter Chamber
L. V. Omelka, J. Vac. Sci. Tech. 7, 257 (1970).
[Techniques (mainly 20°K cryopumping) to achieve 3.5×10^{-7} Torr in a very large volume system.]

8. Pressure Bursts in High-Vacuum Systems
R. A. Fleugge and J. E. Huber, J. Vac. Sci. Tech. 8, 419 (1971).
[Bursts are due to oil dripping; may be initiated by blow to system, continue for days.]

9. The Use of Diffusion Pumps for Obtaining Ultraclean Vacuum Environments
D. J. Santeler, J. Vac. Sci. Tech. 8, 299 (1971).
[Describes techniques for using DP's to the 10^{-14} Torr range.]

10. A Sliding Seal for Ultrahigh Vacuum
R. P. Merrill and D. L. Smith, J. Vac. Sci. Tech. 8, 517 (1971).
[Bakeable rotating feedthru.]

XIII. Other Experimental Techniques

1. Electronic Noise in Detector Systems
J. E. Draper, in Methods of Experimental Physics, Vol. 4, Part A, (Atomic Sources and Detectors), V. W. Hughes, H. L. Schultz, Eds., Academic Press, New York (1967), pp. 319 - 337.
[A quantitative discussion of noise and its limitation in low level electron detection.]

2. An Improved Field Emission Cathode for Use in Storage-Tube and Other Electron-Optical Applications
J. Kelly and C. A. Spindt, Stanford Res. Inst. Preprint, June 1971.
[Structure and properties of the field emitting SRI tips.]

3. Efficient Electron Emission from GaAs - Al_{1-x} Ga_x As Optoelectronic Cold-Cathode Structures
H. Schade, H. Nelson, and H. Kressel, Appl. Phys. Letters 18, 413 (1971).
[CW operation at 0.4 amp/cm^2.]

4. An Electro-optic Tunnel Cathode
R. E. Collins and L. W. Davis, Solid. St. Elect. 7, 445 (1964).
[Performance data.]

5. Experiments on Light Waves in a Thin Tapered Film and a New Light-Wave Coupler
P. K. Tien and R. J. Martin, Appl. Phys. Letters 18, 398 (1971).
[Use of a smooth taper to couple light beams to films.]

6. Heat and Thermodynamics
M. W. Zemansky, McGraw-Hill Book Co., N. Y. (1957).
[Includes an elementary discussion of thermoelectric effects.]

7. Field Theory of Guided Waves
R. E. Collin, McGraw-Hill, (1960).
[The standard reference on the subject.]

8. Light Baffle Attenuation Measurements in the Visible
R. P. Heinisch, C. L. Jolliffe, Appl. Opt. 10, 2016 (1971).
[Experiments on light shielding baffles.]

9. Geometrical Optics in Thin Film Light Guides
R. Ulrich, R. J. Martin, Appl. Opt. 10, 2077 (1971).
[General discussion of effects.]

10. A Solid State Source of Microwaves [Gunn Effect]
R. Bowers, Sci. Amer. 215, 22 (1966).
[Popular presentation of history and theory.]

XIV. Aharanov-Bohm Effect

1. Aharanov-Bohm Effect - Quantum Effects of Charged Particles in Field-Free Regions
   H. Erlichson, Amer. J. Phys. 38, 162 (1970).
   [A review of the Aharanov-Bohm effect with comments.]

2. Experiments Verifying the Aharanov-Bohm Effect
   J. Woodilla and H. Schwarz, Amer. J. Phys. 39, 111 (1971).
   [An addenda to the review by Erlichson.]

3. Classical Electromagnetic Lag Effects and Quantum Interference Pattern Shifts
   T. H. Boyer, Preprint (1971).
   [Proposes an experiment analogous to the electrostatic Aharanov-Bohm effects.]

4. The Classical Electromagnetic Interaction of a Charged Particle with a Solenoid and the Implications for the Aharanov-Bohm Effect
   T. H. Boyer, Preprint (1971).

XV. Gravitational Force

1. Gravitational Properties of Antimatter
   L. I. Schiff, Proc. Nat'l. Acad. Sci. 45, 69 (1959).
   [Considers evidence for equality of gravitation mass of particles and their antiparticles.]

2. Slow Ground State Electrons and the Anomalous Magnetic Moment of the Free Electron
   L. V. Knight, Ph.D. Thesis, Stanford Univ. (1965).
   [Details of experimental technique.]

3. Free Fall Experiments with Negative Ions and Electrons
   F. C. Witteborn, Thesis, Stanford (1965).
   [Details of experimental techniques.]

4. The sign of the Gravitational Force
   S. Deser and F. A. E. Pirani, Ann. Phys. 43, 436 (1967).
   [Theoretical considerations.]

5. Experimental Comparison of the Gravitational Force on Freely Falling Electrons and Metallic Electrons
   F. C. Witteborn and W. M. Fairbank, Phys. Rev. Letters 19, 1049 (1967).
   [Evidence that gravitationally induced electric field in metals exactly equals -mg.]

6. Experiments to Determine the Force of Gravity on Single Electrons and Positrons
   F. C. Witteborn and W. M. Fairbank, Nature 220, 436 (1968).
   [Summary of their work.]

7. On the Measurements of Differences Between the Gravitationally Induced Electric Fields Near Various Metals
   F. C. Michel, Phys. Rev. Letters 21, 104 (1968).
   [Criticism of certain experiments.]

XVI. External Fields

1. The Motion of an Electron Located in an External Field
   G. E. Zil'berman, Sov. Phys. JETP 9, 1040 (1959).
   [Wavefunctions of an electron in a solid with an external magnetic field.]

2. Exact Solution of Dirac's Equation for a Plane Wave of Determined Frequency
   D. M. Volkov, CR Acad. Sci. (USSR) 1, 605 (1935).
   [Exact wavefunctions are derived.]

3. Sondheimer Oscillations in Aluminum
   K. Førsvoll, I. Holwech, Phys. Letters 3, 66 (1962).
   [Observation of periodicity in the conductivity of a thin film as a function of applied magnetic field.]

TECHNICAL INFORMATION DIVISION
LAWRENCE BERKELEY LABORATORY
UNIVERSITY OF CALIFORNIA
BERKELEY, CALIFORNIA 94720